Stony Brook University

Structure-Property Relationships of Polymeric Materials at the Solid-Polymer Melt Interfaces

A Dissertation Presented

by

Naisheng Jiang

to

The Graduate School

in Partial Fulfillment of the

Requirements

for the Degree of

Doctor of Philosophy

in

Materials Science and Engineering

Stony Brook University

August 2014

Stony Brook University

The Graduate School

Naisheng Jiang

We, the dissertation committee for the above candidate for the

Doctor of Philosophy degree, hereby recommend

acceptance of this dissertation.

Tadanori Koga
Associate Professor, Department of Materials Science and Engineering

Jonathan Sokolov
Professor, Department of Materials Science and Engineering

T.A. Venkatesh
Associate Professor, Department of Materials Science and Engineering

Masafumi Fukuto
Condensed Matter Physics and Materials Science Department,
Brookhaven National Laboratory, Upton, NY 11973, USA

This dissertation is accepted by the Graduate School

Charles Taber

Dean of the Graduate School

Abstract of the Dissertation

Structure-Property Relationships of Polymeric Materials at the Solid-Polymer Melt Interfaces

by

Naisheng Jiang

Doctor of Philosophy

in

Materials Science and Engineering

Stony Brook University

2014

In this thesis, by combining various surface and interface characterization techniques, I report the structures, dynamics, and physical and mechanical properties of polymeric materials at the solid-polymer melt interface. Following the introduction, in Chapter 2, I show the experimental evidence of irreversibly adsorbed polymer layers (several nanometers thick) on silicon substrates regardless of the magnitude of attractive polymer-solid interactions. Interestingly, the adsorbed layers are composed of an inner, higher density region (~ 2 nm in thickness regardless of molecular weight (M_w) with a more flattened chain conformation ("flattened layer") and an outer bulk-like density region whose thickness increases with M_w ("loosely adsorbed layer")). In Chapter 3, I show the impact of the adsorbed layer on the local viscosity of single polystyrene (PS) thin films, overcoming the effects of a surface mobile layer at the air/polymer interface. In Chapter 4, I reveal the novel adhesive properties of the two adsorbed PS layers (i.e., flattened layer and loosely adsorbed layer), which have contrasting roles in thermodynamic stability of a polymer film when

prepared on the two adsorbed layers. In chapter 5, I further examine the swelling behavior of the adsorbed PS layer in supercritical CO_2. The neutron reflectivity results demonstrate that the loosely adsorbed PS layer, which is found to be immobile even at temperatures far above the glass transition temperature, swells in CO_2. Further interdiffusion experiments using bilayers of PS and deuterated PS in CO_2 indicate that swollen PS thin films have a mobility gradient in the direction normal to the film surface associated with the adsorbed layer. In Chapter 6, I exhibit work related to polymer structures and dynamics at the polymer-"curved" solid surface. For this purpose, I use polybutadiene (PB) chains bound to carbon black (CB) filler surfaces, known as "bound rubber" in the rubber industry, by extracting with solvent leaching. Small-angle neutron scattering and neutron spin echo experiments for the "bound rubber-coated" CB fillers dispersed in deuterated toluene reveal similar heterogeneous chain conformations on the curved surface: flattened chains constitute the inner unswollen region of the bound rubber layer and loosely adsorbed polymer chains form the outer swollen region. In addition, results show that the outer loosely adsorbed chains display similar collective relaxation to the "breathing" dynamics that have been reported in end-grafted polymer chains in a good solvent.

Dedication Page

To my wife and my parents and all my best friends.

Table of Contents

List of Figures

List of Tables

Acknowledgments

Foremost, I would like to express my sincere gratitude to my thesis advisor Dr. Tadanori Koga for his excellent guidance, patience, friendship, continuous inspiration and support during my 4 years of PhD studies. He has provided deep understanding and insightful discussions related to my research and also the development of my personal career. His encouragement and moral support have been incredibly helpful, especially during the most difficult times in my studies. I could not imagine having a better advisor and mentor for my Ph.D studies. It would not have been possible to complete this doctoral thesis without his mentorship and support.

I would like to thank Dr. Maya Endoh for her guidance and assistance during my years in Koga's group. I also would like to thank my committee members, Dr. Jonathan Sokolov, Dr. T.A. Venkatesh and Dr. Masafumi Fukuto for their helpful suggestions and insightful comments on my thesis. I am also indebted to Dr. Jonathan Sokolov and Dr. Masafumi Fukuto for their strong technical support on various laboratory instruments and x-ray scattering measurements Stony Brook University and Brookhaven National Laboratory.

Furthermore, I would like to thank Dr. Atsushi Takahara, my gracious host and research supervisor at Kyushu University, in addition to the faculties and students in Takahara Laboratory who helped me with my research. I would like to credit Dr. Michihiro Nagao, Dr. Sushil Satija, Dr. Bulent Akgun and Dr. Michael Dimitriou for their invaluable insights on various neutron scattering experiments at the National Institute of Standards and Technology, Center for Neutron Research. I would further like to acknowledge Dr. Lin Yang, Dr. Steve Bennett and Dr. Jean Jordan-Sweet for their technical support at the National Synchrotron Light Source, Brookhaven National Laboratory. Additionally, I would like to thank Dr. Miriam Rafailovich and her students, including Dr. Chung-Chueh Chang, Dr. Ying Liu, Dr. Cheng Pan, Yingjie Yu, Hongfei Li,

Zhenhua Yang, Ke Zhu, Linxi Zhang and others, in Garcia MRSEC for their support and help with various laboratory instruments, especially the AFM measurements.

Special thanks must be extended to all the members in the Koga Research Group for their strong support and many fruitful discussions throughout the years: Dr. Peter Gin, Dr. Mitsunori Asada, Dr. Shotaro Nishitsuji, Levent Sendogdular, So-King Lam, Fen Chen, Zexi Han, Chen Liang, Xiameng Chen, Yuxuan Ruan, Mani Sen, Jun Shang, Xiaoyu Di, Jiaxun Wang, Wenduo Zeng, Justin Veren, Justin Cheung, Alexander Saeboe and Deborah Barkley. In particular, I would like to thank Levent Sendogdular, Fen Chen, Jun Shang, Xiaoyu Di and Jiaxun Wang for their continuous encouragement and support during my most difficult times.

Many thanks to my best friends in United States, China, Japan and elsewhere for their support and encouragement throughout: Xiaofei Liang, Wei Nan, Zhemin Zhang, Tan Li, Tao Ni, Rui Lv, Lunpeng Ma, Nan Li, Guanyu Guo, Da Yang, Crystal Yu, Shan He, Dongye Zhang, Kai Yang, Yunlong Wang, Fangzhen Wu, Guang Cheng, Xue Liang, Yichen Guo, Mengjia Gaowei, Huanhuan Wang, Yu Ji, Wei Ma, Ya-Ting Hsieh and many others, including some of whom have already been named. Without them, this journey would be a lonely and difficult undertaking.

I would like to thank my parents for their unwavering love and support throughout my life. Distance has kept us apart for many years as we live in two different countries, but they have always stood by my side through trials and adversity. Their love has helped me see through clouds of uncertainty that lay in my path und ultimately kept me focused on my goals.

Finally, from the bottom of my heart I would like to say “thank you” to my wife Cici for always cheering me up and standing by my side through the good times and the bad. I owe her my eternal gratitude for her love, understanding and support during my PhD study.

Chapter 1: Introduction

1.1 Goals and objectives

Thin polymer films have become increasingly important to our daily lives. They can be found in anti-stick coatings for cookware, adhesive sealing in food packaging and screen protectors on cell phones, laptops and televisions. They can also be found in electronics, optics, sensors and other hi-tech devices. As many components in sophisticated devices are moving toward to the nanometer scale, the thickness of the polymer films used in their construction must decrease to dimensions comparable to the size of the polymer chains themselves in order to meet technological demands. However, it is well know that many fundamental characteristics of polymeric materials, including structure, conformation, dynamics and other physical and mechanical properties, differ substantially from those of the bulk due to the so-called "nanoconfinement" effect. Hence, a more thorough understanding of structure-property relationships under nanoconfinement is of great importance in the development of new nanotechnologies.

Polymer film deposition on inorganic substrates via spin-casting has been widely used in both scientific research and industrial applications. Through rapid solvent evaporation, smooth and uniform polymer films of tunable thickness can be formed on various planar solid substrates. Generally, the as-cast films are then thermally annealed at temperatures above the glass transition temperature T_g of the polymer in order to equilibrate. The resulting confined polymer films have two interfaces. One is the polymer-air interface where the polymer chains are in contact with vacuum or air. The other is the polymer-solid or polymer-substrate interface where the polymer chains are in contact with a solid phase such as silicon, carbon, mica, glass, metals or steels. In the latter case, the polymer cannot diffuse into the solid surface but may instead bond to it by

adsorption of polymer chains. Through intensive studies of thin polymer films in the last 20 years, there is now growing evidence that the polymer-air interface and polymer-solid interface play crucial roles in the effects of nanoconfinement. The nature of the polymer, however, becomes substantially complex due to the presence of the two interfaces which cannot be well explained by a single unified model.[1] Although numerous observations have found that many physical and mechanical properties of thin films vary significantly from those of the bulk, the current understanding of how this deviation depends upon the structure of the polymers involved and the specific nature of their surface and interface features is rudimentary.

This dissertation will mainly focus on understanding the structure-property relationships of polymeric materials at the polymer-solid interface using various laboratory methods and surface/interface characterization techniques. The primary goal is to understand the formation mechanism of irreversibly adsorbed polymer layers on solid substrates from the melt. Previous studies by Koga's group[2] have shown that the polymer adsorbed layers formed from the melt are composed of the two different nanoarchitectures: flattened chains that constitute the inner, higher density region of the adsorbed layers, and the loosely adsorbed polymer chains that form the outer bulk-like density region. The inner, high density flattened layer, which is independent of molecular weight, can be extracted from the loosely adsorbed layer by using an enhanced solvent leaching process.[2] While many experiments have been focused on understanding the formation of the adsorbed layer (which is in fact composed of both flattened chains and loosely adsorbed chains) on the solid surface,[3-5] the detailed formation mechanism of the isolated flattened layer still lacks necessary study. Furthermore, the relationship between the formation of flattened chains and loosely adsorbed chains remains unexplored. In Chapter 2, we aim to answer the following questions: (i) what are the formation kinetics of the flattened chains at solid-polymer melt interface?

(ii) What is the relationship between the growth of the flattened layer and the loosely adsorbed layer? (iii) What are the effects of polymer/substrate interactions on the structure and adsorption kinetics of the flattened layer and (iv) what are the thermal properties of the flattened layer compared to the bulk? To achieve these goals, high temperature X-ray reflectivity in conjunction with the Fourier transformation (FT) method and atomic force microscopy were utilized in order to characterize flattened layers on the nanometer scale. Three different homopolymers, polystyrene (PS), poly-(methyl methacrylate) (PMMA), and poly(2-vinylpyridine) (P2VP) were used as models since these polymers have similar chain stiffnesses and bulk glass transition temperatures (Tg)[6], but different interactions with Si substrates.

Having characterized the formation mechanism of the adsorbed layer on solid substrates, the second goal of this dissertation is to identify the local viscosity of thin polymer films near the solid polymer melt (SPM) interface using the state-of-the-art marker grazing incidence x-ray photon correlation spectroscopy (GIXPCS) technique with gold nanoparticles embedded in the polystyrene (PS) films prepared on silicon substrates. At the end of this chapter (Section 1.5), we will introduce the basic principles of marker GIXPCS, which involve the random drifting (Brownian motion) of individual markers which adequately track the local viscosity of entangled polymer chains in the regions of interest within individual PS thin films. In Chapter 3, we aim to answer the following questions regarding the local viscosity in thin PS films: (i) what is the local viscosity as a function of the distance from the polymer-substrate interface? (ii) What is the impact of the very thin adsorbed layer on the local viscosity? (iii) What is the mobility of the adsorbed chains? (iv) What is the relationship between the local viscosity and the T_g of polymer thin films reported in the literature? The marker GIXPCS experiments were carried out to measure the local viscosity as a function of distance from the polymer-solid melt interface. Formation of the

adsorbed layer was identified using X-ray reflectivity combined with the well-established Guiselin approach. To study the mobility of the adsorbed layer, the interdiffusion behavior between adsorbed chains and free chains is further investigated using neutron reflectivity. The obtained temperature dependent local viscosity by GIXPCS is also extrapolated back to T_g via the Williams-Landel-Ferry (WLF) equation in order to compare with T_g measurements in the literature.

The next objective of this dissertation is to investigate how the difference in the adsorbed chain conformations at the polymer-solid interface affect the stability of thin polymer films on solid substrates. It is known that solid surfaces can be either non-slippery (wettable) or slippery (nonwettable) to a thin polymer film depending on the several factors, such as effective interface potential[7, 8], polarity[9], film thickness[10, 11] and non-equilibrium nature due to spin coating[12]. However, the role of the chain conformations near the polymer-solid interface in determining the wetting/dewetting of thin polymer films from a substrate is still not well understood. In Chapter 4, we aim to investigate (i) the relation between the dewetting of thin polymer films and the irreversible adsorption of polymer chains on solid substrates, (ii) how the difference in the conformation of adsorbed chains on solid surfaces affect the stability of thin polymer films and (iii) the possible surface modifications induced by adsorbed chains that have ramifications in tuning the wettability of thin polymer films on solid substrates. PS and P2VP spun-cast films on silicon substrates of different thickness and molecular weight were thermally annealed at $T > T_g$ and characterized by polarized optical microscopy, atomic force microscopy and X-ray reflectivity. Dewetted and non-dewetted films were further leached with different solvents in order to investigate the adsorption of flattened chains or loosely adsorbed chains at the polymer-solid melt interface. Water contact angle and thermally-based adhesion measurements were also carried out

to improve our understanding of the surface features of flattened layers or adsorbed layers on solid substrates.

The fourth objective of this dissertation is to outline polymer interdiffusion between free chains and the loosely adsorbed chains in CO_2. Based on the results from Chapter 3, no interdiffusion between free chains and the loosely adsorbed chains was observed even after thermal annealing at temperatures far above the T_g of the polymer. Previous studies also indicate that there is no thermal expansion of the adsorbed layer within a wide range of temperatures. Hence, the adsorbed layer has been regarded as an immobile layer in air or under vacuum. The question is whether the adsorbed layer is still immobile even in solvent conditions. Supercritical CO_2 was selected as the plasticization agent for the adsorbed layer since it can be used as a non-destructive solvent in processing thin polymer films, and the swelling behavior and dynamics of thin PS films on silicon substrates in CO_2 have been largely reported in the literature[13-19]. It has been found that the excess sorption of CO_2 molecules takes place within the narrow temperature and pressure regime near the critical point of CO_2, known as the "density fluctuation ridge"[20], resulting in the anomalous swelling of supported polymer thin films[13-16, 18, 21-24] and the enhanced polymer interdiffusion at miscible polymer interfaces.[14] In Chapter 5, we aim to investigate (i) the swelling and interdiffusion of the adsorbed layer in $scCO_2$ and (ii) the effect of the adsorbed layer on the interdiffusion process. The swelling behavior of the adsorbed deuterated polystyrene (d-PS) layer and the interdiffusion between the adsorbed hydrogenous polystyrene (h-PS) chains and free d-PS chains in an overlayer were studied by using a high-pressure neutron reflectivity technique with a custom-built high-pressure cell.[15] At the same time, h-PS bottom layers with thicknesses ranging from 0.6 R_g to 4 R_g were also used in the bilayers in order to understand the long range effect of the adsorbed layer on the interdiffusion dynamics in CO_2.

The last part of this dissertation will explore the nano-architectures and dynamics of polymer chains strongly adsorbed onto nanofiller surfaces. The so-called bound polymer layer (BPL layer), which represents a thin polymer layer irreversibly adsorbed on the surface of a nanoparticle, has long been thought an important factor in the mechanical reinforcement of polymer-filler systems. However, the detailed structure and corresponding dynamical properties of the BPL layer are still unclear mainly due to the lack of experimental techniques that allow us to measure the chain statistics of bound polymer chains separately from those of free chains in bulk. In Chapter 6, we aim to (i) investigate nano-architectures and nanosecond dynamics of the bound polybutadiene (PB) chains on the surface of carbon black (CB) fillers in toluene and (ii) compare the nano-architectures from part (i) with those of a PB brush grafted on the same CB. The combined use of small-angle neutron scattering (SANS) and neutron spin echo (NSE) in conjunction with the selective deuteration of either the polymer or the solvent enable us to elucidate the structure and dynamics information of the BPL exclusively. Transmission electron microscopy was also used to determine the thickness of the BPL layer in the dry state.

The entirety of this thesis has covered the structure and formation of irreversibly adsorbed polymer layers on solid substrates or nanoparticles and how these layers play a role in determining physical, mechanical and dynamical properties of thin polymer films or polymer nanocomposites on the nanometer scale. Various surface and interface characterization techniques were employed in this thesis. We believe these exciting experimental findings will not only shed light on the structure-property relationships of nanoconfined polymeric materials at the solid-polymer-melt interface, but will also prove greatly important in the development of new nanostructures and nanotechnological devices over a wide range of applications.

1.2 Dynamics of Thin Polymer Films Prepared on planar Solid Substrates

Thin polymer films prepared on inorganic solid substrate have gained enormous interest since 1990's due to their wide range of applications in cutting-edge technologies including organic coatings, photovoltaics, electronics, sensors and solar cells.[25] Polymers in a solid-supported thin film geometry have their surfaces in contact with two different media: the free surface (air or vacuum) and the solid surface. Since the early elegant studies on the glass transition behavior of thin polymer films by Keddie, Jones and Cory,[26, 27] various techniques have been employed to investigate the dynamics of thin polymer films prepared on solid substrates, including in-situ spectroscopic ellipsometry,[26-32] temperature-dependent X-ray photoelectron spectroscopy,[33] Brillouin light scattering,[34-36] atomic force microscopy (AFM),[37-42] scanning force microscopy (SFM),[43] positronium annihilation lifetime spectroscopy,[44] fluorescence labeling/multilayer technique,[45-47] dielectric relaxation spectroscopy,[5, 48-56] X-ray reflectivity[57-59] and X-ray photon correlation spectroscopy (XPCS).[60-62] There has been growing evidence that the physical and mechanical properties of polymer chains nanoconfined in thin films, including glass transition temperature (T_g),[45, 63-65] viscoelastic property,[66-70] self-diffusion/interdiffusion[71, 72] and physical aging[73], vary significantly from the bulk properties. These unusual properties in thin films have been greatly attributed to the effects of the free surface and the substrate interface. It has been proposed that at the free surface, there is a surface-mobile polymer layer in which segmental mobility is significantly enhanced[26, 27]. Several experimental and theoretical studies [28, 29, 33, 35, 47, 74-80] support this idea. On the other hand, it has been suggested that the molecular motion could be either enhanced or suppressed near the solid surface, depending on the interaction between the polymer and substrate.[57-59, 81-83] Interestingly, both the free surface and the substrate interfacial

effects can propagate into the film interior to a degree larger than the length scale of the radius of gyration of a polymer, resulting in a large dynamical heterogeneity across the film.

The central question is which interfacial effect is more dominant in determining the dynamics of polymer in thin films, the free surface effect or the substrate effect? The local T_g measurements by fluorescence labeling/multilayer method suggest that the surface enhanced mobility layer in polystyrene films on glass substrates could extend into the film interior to a distance at least 36 nm from the surface and overwhelm any possible effect from the substrate.[45, 47, 84] However, very recent dielectric spectroscopy studies[5, 49] show that different thermal annealing procedures yield a range of different T_g values for thin PS films prepared on aluminum or other substrates, and such deviation in T_g is directly linked to the growth of a thin irreversibly adsorbed layer, as shown in Figure 1-1, instead of the free surface effect. Such an irreversibly adsorbed layer, formed upon thermal annealing at a temperature far above bulk T_g, cannot be removed even after extensive rinsing with a good solvent.[2, 3, 5, 85] Moreover, several studies have shown that the irreversible adsorption of polymers from the melt onto solid surfaces is a very general phenomenon in thin polymer films that undergo thermal annealing and can be found even when the polymer-substrate interaction is weak.[3]

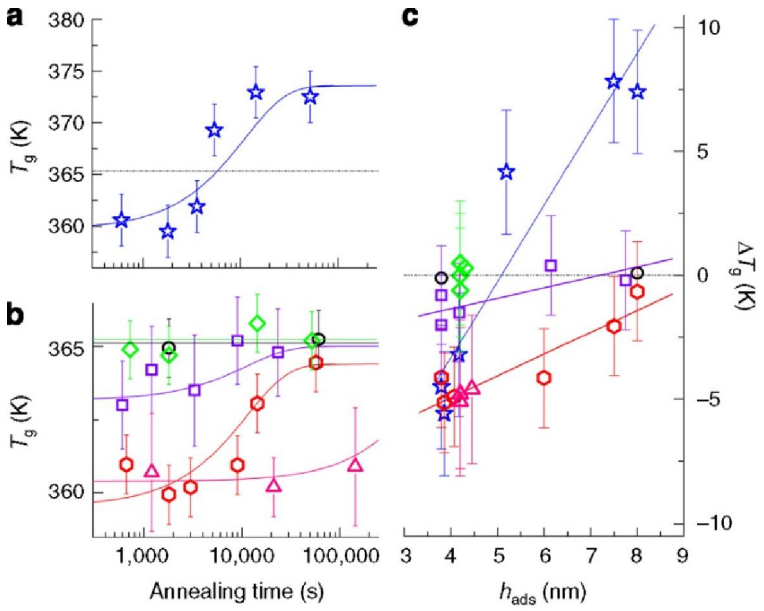

Figure 1 - 1. (a) The increase in T_g of residual films of PS97 prepared at different annealing times follows the same kinetics as the irreversible adsorption process: the solid lines are obtained by normalization of the traces of $\Delta\varepsilon_{high}(t)$ collected during isothermal experiments. At short annealing times ($t < t_{on}$), T_g is 5 K lower than in bulk (dash-dotted line) and increases till saturating at T_g^{BULK} + 7 K at $t >> t_{ads}$. (b) A similar correlation is observed for ultrathin films of different thickness and molecular weight: PS97, 18 nm (red hexagons), 35 nm (violet squares), 300 nm (black circles); PS160, 20 nm (pink triangles) and 44 nm (green diamonds). (c) The difference between the T_g of the films (same symbols as in a, b were used) and the bulk value, ΔT_g, is plotted versus the thickness of the interfacial layer adsorbed in the same annealing conditions; straight lines are linear fits of the different data sets. Although for ultrathin films bulk T_g is recovered at $t >> t_{ads}$, for residual films of PS97 $\Delta T_g = 0$ is achieved at much shorter times. Error bars take into account the width of the glass-transition temperature as determined by capacitive dilatometry in cooling. Figure reproduced from ref. 5.

Despite many exciting experimental findings, the dynamical properties of thin polymer films prepared on solid substrates still remain controversial and the underlying mechanism of many anomalous behaviors is still not fully understood. One of the major reasons is that many techniques are only able to measure the "average" properties of the entire surface, while the local behavior might be heterogeneous, depending on the interplay between the free surface and the substrate interface. At the same time, many experiments have focused on the free surface effect while only

a few studies regarding the substrate effect have been reported in the literature. Hence, it is crucial to develop an advanced nanoscale tool to determine the in situ local properties of polymeric nanomaterials as a function of the distance from the interfaces, especially from the substrate interface.

Another important issue is that the majority of dynamical studies of thin polymer films in the past 20 years have focused on the thickness dependence of T_g[86]. However, the relationship between various dynamical properties in bulk polymers may not be valid in thin films, as implied by many recent experimental studies. For example, in bulk polymers, the value of T_g is largely correlated with the time scale for segmental dynamics and the temperature dependences of the viscosity. However, in contrast to the significant reduction of T_g with decreasing film thickness of thin PS films, large decreases in the tracer diffusion and interdiffusion rate in both in-plane and out-of-plane directions have been observed.[87, 88] At the same time, recent studies by Koga's group have shown that the surface reduced viscosity of PS thin film does not imply any deviation of T_g from the bulk value. Hence, the correlation between large shifts in the observed T_g in thin polymer films and the change in the other dynamical properties still remains mysterious. Therefore, other physical and mechanical properties of thin films, such as the modulus, viscosity and diffusion/interdiffusion behavior, are of great importance in improving understanding of polymer dynamics in thin films at the nanoscale level.

In Chapter 3, we investigate the local viscosity of thin PS films on silicon substrates using marker grazing incidence X-ray photon correlation spectroscopy (GIXPCS). In chapter 5, we study the interdiffusion of PS as a function of the distance from the substrate in the presence of supercritical CO_2 using neutron reflectivity. The basic principles of these two techniques are briefly described at the end of this chapter (Section 1.5). With the help of both techniques, we will

show how these dynamical properties of thin polymer films are affected by the solid substrate, or in other words, the formation of irreversibly adsorbed layers at the polymer-solid interface.

1.3 Polymer Adsorption on Solids

Adsorption of polymer chains on solid surfaces is a fundamental but highly complex phenomenon in polymer physics. Unlike small molecules, the adsorption of macromolecules involves a great number of possible chain configurations at the solid-polymer interface. From a thermodynamic point of view, the adsorption process of polymers can be described as a counterbalance between the high loss in the conformational entropy of chains during the transition from a randomly coiled state to an adsorbed state, and a large reduction in free energy due to the enthalpic gain achieved upon the increase in the number of solid/segment points.[89] Therefore, the way polymer chains are adsorbed to the solid substrate is governed by many factors, such as polymer-solid interaction, molar weight, chain stiffness, chemical composition of the polymer, surface properties, solvent interaction etc.

1.3.1 Irreversible adsorption

Depending on the specific interaction forces that are involved in the adsorption process, there are two kinds of adsorption mainly reported in the literature. The first is when polymer chains are attached to the substrate due to covalent or chemical bonding forces generated by a chemical reaction between the substrate surface and the chains, namely chemisorption. The second is when no significant chemical reactions are involved but the chains are adsorbed to the substrate surface via dispersion, dipolar forces or van der Waals interactions, which is called physisorption. For chemisorption, the surface sticking energy per monomer, ε, is one to two orders of magnitude

greater than kT. Hence, a chemisorption process, such as chemically grafted polymer chains on solids, is generally irreversible. Unlike strong chemisorption, the sticking energy of physisorption is only of the same order as kT. However, irreversible physisorption of polymer chains is still largely observed even when the polymer-solid interaction is weak possibly due to the fact that desorption kinetics is often much slower than the kinetics of adsorption.[90-93] Especially when multiple surface-segment contacts are formed, the energy required to desorb one chain is not just the sum of all the bonding energy per contact, it requires all the contacts to detach at the same time. Since this thesis mainly focuses on the adsorbed layer formed via physisorption, the terms "adsorb" refers to the physisorption of polymer chains hereafter, unless otherwise stated.

1.3.2 Conformations of Adsorbed Polymer Chains on Planar Solids

The early theoretical picture given by Simah and co-workers[94] shows that the equilibrium physisorbed polymer chain on a solid surface consists of three types of segment sequences: trains, loops and tails. For trains, all segments are fully adsorbed to the substrate. Loops constitute unbound segments that connect trains, and tails are the nonadsorbed chain ends. Other concepts and models[89, 95-97] include additional parameters, such as chain intramolecular architectures, interactions between different segments and molecules, interactions between segments and solid surfaces, and the concentration of the polymer to describe thermodynamic equilibrium of the chain conformation at the solid surface, including the amount of adsorbed polymers and the density profile at equilibrium. However, a fundamental problem arises when applying these classic models to real situations: the equilibration of chains at the solid surface may take too long such that the theoretical conformational equilibrium may not be achieved within the experimental time scale. Therefore, as many authors point out, the detailed growth of the adsorbed layer on a solid surface

should play a more essential role than the equilibrium theory in determining the structure of the adsorbed chains at the solid-polymer interface.[91-93, 98-101]

Considering polymer chains adsorbing onto an unoccupied solid surface from a dilute solution, the early arrived chains could easily adsorb onto the empty surface and maximize the number of segment-surface contacts per chain without interference with each other. However, the later arrived chains will sooner or later encounter a space issue, or a parking problem, which results in a decrease in the number of segment-surface contacts per chain, or the size of the "footprint" on the solid surface.[90, 92, 93, 98, 102] Recent studies by Koga's group have shown that polymer adsorption from the melt is also governed by the history of piecemeal deposition, similar to adsorption from a dilute solution. This finding is fundamentally important in practical applications since most nano-devices are based on polymer melts. As depicted in Fig. 1-2, the early arriving polymer chains adopt a flat conformation on the substrate, forming the inner high density region, while the late arriving chains adsorb loosely onto the substrate, developing the outer bulk-like density region. Due to the flattening of chains, the inner flattened layer is almost independent of molecular weight, contrasting sharply with the molecular weight dependence of the loosely adsorbed layer. Moreover, the selective extraction of the loosely adsorbed layer and flattened layer in a thin polymer film using Guiselin's approach can be easily controlled by tuning the desorption energy, which is proportional to the number of segment-surface contacts per chain.

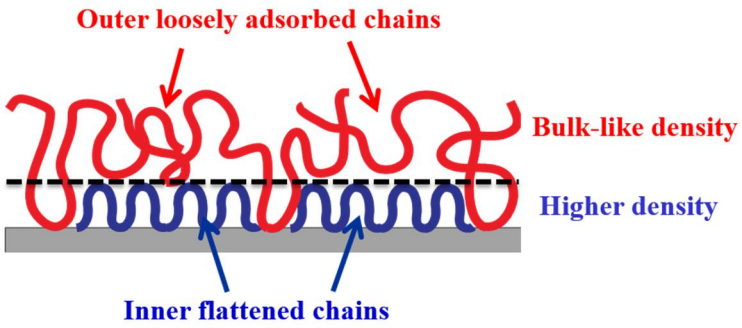

Figure 1 - 2. Schematic view of the two different chain conformations at the solid-polymer melt interface. Figure reproduced from ref. 2.

1.3.3 Kinetics of Polymer Adsorption onto planar solids

Early reports on the kinetics of irreversible chain adsorption from dilute solution by Ligoure and Leibler[103] suggest that the time evolution of the thickness of the adsorbed layer consists of two stages: at low surface coverage, the adsorption process is diffusion controlled and the anchored chains do not overlap or interfere with their neighbors; after surface coverage has reached a critical value, the adsorption slows down due to the energy barrier caused by the presence of previously adsorbed chains and limited available empty surface area. Monte Carlo simulations and Brownian dynamic simulation studies[104, 105] also suggest that adsorption time and the adsorbed amount of polymers on solid surfaces strongly depends on specific polymer-substrate interactions and chain stiffnesses. With increasing polymer-substrate interaction, the total amount of adsorbed polymer increases, but the time for polymers to be fully integrated into the adsorbed layer also increases due to the slow relaxation and rearrangement of adsorbed chains. Besides, recent dielectric spectroscopy studies[4, 106-108] show that the overall adsorption kinetics from the melt follow almost the same trend as that from the dilute solution. The thickness of the adsorbed layer h_{ads} as a function of annealing time t can be described as:[107]

$$h_{ads} = \begin{cases} h_{t=0} + vt^{\alpha}, & t < t_{cross} \\ h_{t_{cross}} + \Pi \log t, & t > t_{cross} \end{cases}$$

where t_{cross} is the crossover time, v and Π express the respect growth rates in the different regimes and the power α indicates the type of adsorption mechanism involved. Hence, the crossover time t_{cross} can be used to describe the time of transition from the faster power-law growth of early stage adsorption to the slower logarithmic growth before reaching the equilibrium of adsorption. However, due to the presence of chain entanglements, friction, and incomplete equilibration, the polymer adsorption onto solids from the melt is expected to be a much more complicated process compared to that from the dilute solution. In Chapter 2, we will discuss the formation mechanism of the adsorbed chains from the melt in more detail, including the effect of polymer substrate interaction on the adsorbed structure and adsorption kinetics.

1.4 Stability/Instability of Thin Polymer Films on Solid Substrates

Thermodynamic stability (wetting) or instability (dewetting) of a polymer film on top of a solid is of vital importance in many technologies (e.g., coating, adhesion and corrosion) as well as new emerging nanotechnologies such as organic photovoltaics, semiconductor chips, and biosensors[25]. A homogeneous thin polymer film may completely wet to a solid substrate without any deformation in an equilibrium situation. Otherwise, the film will deform from the substrate and encounter a dewetting process in order to lower the total free energy of the system. As shown in Figure 1-3, the dewetting process can be separated into different stages: initial rupture, expansion and growth of holes, coalescence into polygonal network and formation of dewetting droplets with clear three phase contact lines and a non-zero contact angle with respect to the solid substrate.[109-

[112] From the thermodynamic point of view, two key factors determine whether a thin polymer film will wet or dewet from the solid substrate: effective interface potential (Φ) and film thickness (h). The effective interface potential which is used to describe the total excess free energy of the film system consists of both short-range repulsion and long-range Van der Waals interactions. Based on the curve of the effective interface potential (ϕ) as a function of film thickness (h), one can tell whether the system is stable, metastable or unstable.[8] However, in real systems, the film stability could also be affected by many other factors, such as the residual stress induced by film preparation[12], surface contamination[113] and the polarity of the substrate[9].

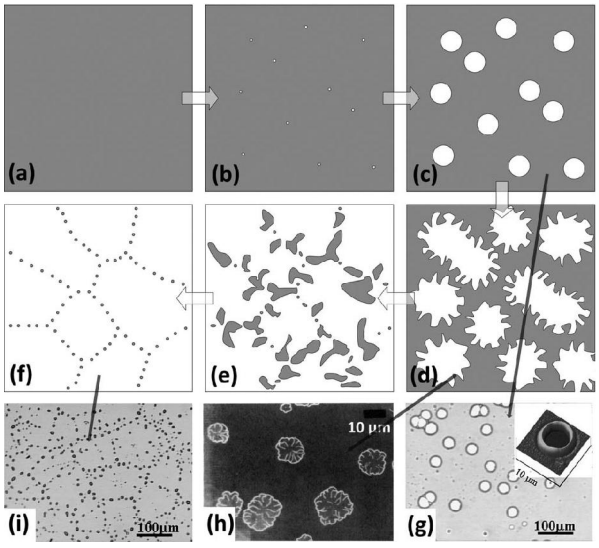

Figure 1 - 3. (a–f) Schematics showing various stages of the dewetting process. (g–i) Representative micrographs of several stages of dewetting: holes, rims and cellular patterns. Figure reproduced from ref. 109.

A spin coated polystyrene (PS) thin film on a silicon substrate covered by a natural silicon oxide layer is the most commonly used system for dewetting studies. PS has infinitesimally low vapor pressure in the melt, so the total mass of the polymer film can be safely conserved during the dewetting process. The relatively low mobility of the PS and its glassy nature at room temperature

also make the dewetting structure and kinetics easy to observe. The effective interface potential, which determines the film stability, can be easily tuned by changing the thickness of the oxide layer on the Si.[8, 112] For a non-wettable substrate, dewetting of thin PS films can be induced by thermal annealing at temperatures above the T_g of PS. Optical microscopy and atomic force microscopy are the most common techniques used to investigate the dewetting scenario both ex-situ or in-situ.

Generally, there are three types of dewetting depending on rupture mechanism: spinodal dewetting, homogeneous nucleation or thermal nucleation, and heterogeneous nucleation. Spinodal dewetting is a spontaneous self-destruction process for unstable systems in which the 2nd derivative of the effective interfacial potential, $\phi''(h)$, is negative. The resultant spinodal dewetting patterns clearly exhibit a film thickness dependent characteristic spinodal wavelength, $\lambda(h)$. Said wavelength also depends on the surface tension of the polymer and the Hamaker constant for the polymer–air interface. Thermal nucleation, by definition, is the dewetting nucleated by thermal activation. However, in most cases, a nucleus formed via thermal activation can only be seen when $\phi''(h) = 0$, where no interfacial potential barrier exists in the system. Dewetting via heterogeneous nucleation is induced by defects in the film such as dust or the local stress induced by the fast solvent evaporation over the course of spin-casting. This type of dewetting is often seen in metastable cases ($\phi''(h) > 0$) where a certain potential barrier needs to be overcome by the existence of localized defects. For PS, films are metastable when thick PS films ($h > 5$ nm) are prepared on silicon substrates with an approximate 1-3 nm thick oxide layer on the surface.

For thin polymer films on solid substrates that are metastable or unstable, thermal annealing at a temperature above the T_g of the polymer may cause rupture and dewetting of the film, which in

most cases is undesirable for coating, adhesion and other processes related to high-tech nano-devices. Therefore, many strategies have been developed to improve the stability of thin polymer films against dewetting from the substrate. Some strategies focus on the modification of the solid substrate by pre-coating a very thin polymer brush layer or nanoparticle interfacial layer on the solid surface.[114-117] Other strategies focus on changing the film composition by adding a small amount of a different component to the film,[118-123] such as end-functionalized polymer chains, different homopolymer chains, dendrimers or nanoparticles. The underlying mechanism for suppressing the dewetting of thin polymer films by introducing a polymer brush layer or other polymer layer is that these chains can be adsorbed to the solid substrate and act as "connectors" that cause a resistance force at the dewetting front.[124]

1.5 Research Approach and Main Characterization Techniques

In this dissertation, thin polymer films with thicknesses less than 150 nm were generally prepared on silicon substrates via spin-casting from polymer solutions with a rotation speed of ~ 2500 rpm. The thickness of the films were controlled based on the concentrations of the polymer solutions. Different surface treatments on the 100 Si wafers were applied in order to change the hydrophobicity of the silicon surface as well as the silicon oxide layer. Thermal annealing or CO_2 annealing with different temperatures or pressures were applied for different purposes. To investigate the adsorption of polymer chains on solid substrates, the pre-annealed films were carefully leached with different solvents, depending on the target desorption energy to be applied. The residual flattened layers or loosely adsorbed layers were then annealed at high temperatures above the T_g of the polymers under vacuum to equilibrate the layers and remove any excess solvent.

The entire process is schematically shown in Figure 1-4. Non-contact mode atomic force microscopy, ellipsometry and x-ray reflectivity techniques were further used to characterize these layers in detail.

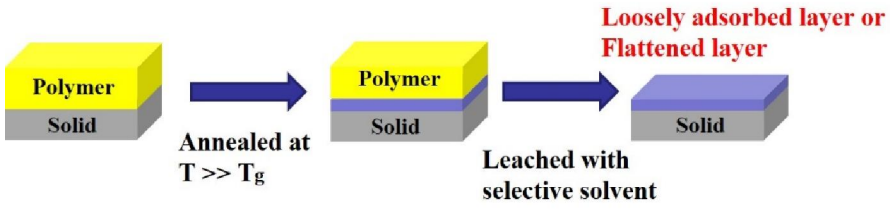

Figure 1 - 4. Schematics showing the preparation of adsorbed layers on solid substrate from the melt using the Guiselin's approach.

In most of the studies we present, the structures and properties of thin polymer films or adsorbed layers were characterized using various X-ray/neutron scattering and microscopy techniques. In the following section, we will briefly introduce the basic principles of the main scattering techniques applied in this thesis.

1.5.1 Marker Grazing-Incidence X-ray Photon Correlation Spectroscopy

Photon correlation spectroscopy using laser light is a well-established tool[125] which probes the dynamic properties of matter by analyzing the temporal correlations among photons scattered by the matter. During the last decade, the development of third generation synchrotron radiation sources has made it possible to extend photon correlation spectroscopy (PCS) from the optical region into the x-ray domain. This enables us to probe the dynamic properties of systems on molecular length scales as well as use optically dense samples that are not accessible for conventional PCS. XPCS has currently been extended into the sub-microsecond range of temporal

resolution, and the advent of an x-ray free-electron laser would further provide a unique opportunity to identify chemical and biological phenomena with unprecedented temporal resolution (femtosecond regime). Thus, XPCS has great potential to impact the study of a variety of nonequilibrium phenomena. Since this thesis focuses on the use of GIXPCS, the reader is referred to some recent reviews[126-128] for coverage of (transmission) XPCS including the basics and other promising fields of application.

Recently, Sinha and co-workers have demonstrated that the GIXPCS technique is the most direct and unambiguous way to study the lateral dynamics of polymer thin films prepared on solid substrates based on surface capillary wave fluctuations.[60, 61, 129-133] Using the normal hydrodynamic theory for capillary wave fluctuations on viscous (homogeneous) liquid films, they have shown that the viscosity of individual PS films several tens of nanometers in thickness are in good agreement with the bulk.[60] However, it should be emphasized that the viscosity obtained by this concept corresponds to the "average" over entire PS films,[60] since the capillary fluctuations propagate into the film interior. Thus, as aforementioned, another strategy is required to determine the local rheological property of polymer thin films, clarifying to what extent the two interfacial effects propagate into the film interior.

There is an earlier transmission XPCS result, showing that the viscosity of surrounding glycerol can be reasonably determined by the Brownian motion of gold particles embedded in the liquid as markers.[134] This type of strategy is the so-called passive microrheology approach or tracer diffusion approach which takes advantage of inherently strong X-ray contrasts of markers. For GIXPCS, the normalized intensity–intensity time autocorrelation function $g_2(q_{//}, t)$ which is measured as a function of the in-plane wave vector transfer ($q_{//}$) and delay time (t) can be obtained by the following equation:

$$g_2(q_{//},t) = < I(q_{//},t')I(q_{//},t'+t) > / < I(q_{//},t') >^2, \quad (1)$$

where I ($q_{//}$, t') refers to the scattering intensity at $q_{//}$ and at time t'. The brackets < > refer to averages over time t'. $g_2(q_{//},t)$ is related to the normalized intermediate structure factor [$f(q_{//},t)$] via $g_2(q_{//},t) = 1 + A[f(q_{//},t)]^2$, where A is a speckle contrast ($0 < A < 1$) which is determined by the angular size of the coherent x-ray source. In the case of the aforementioned passive microrheology strategy, the $f(q_{//},t)$ function contains the dynamical information for Brownian motion of the embedded markers in the equilibrium. To apply the strategy to a complex fluid system, the concentration of the markers should be sufficiently low and the markers should be neutral to surrounding materials. By satisfying these conditions, the complications due to particle-fluid interactions and the interference among the markers can be ruled out. If the motions of the markers obey Gaussian statistics, the mean square displacement of the markers in the given time domain, $<\Delta r^2(t)>$, is related to $g(q_{//},t)$ by:[126]

$$g_2(q_{//},t) = 1 + A\exp[-\left\langle \Delta r^2(t) \right\rangle q_{//}^2/3]. \quad (2)$$

For pure diffusive particle motion, the mean square displacement of the markers over t exhibit the relation of $<\Delta r^2(t)> = 6Dt$, where D is the diffusion constant. The normalized intensity–intensity time autocorrelation function is then: $g_2(q_{//},t) = 1 + A\exp[-2Dq_{//}^2 t]$. Thus, by measuring the $g_2(q_{//},t)$, one can determine the viscosity (η) of the surrounding material via the well-known Stoke-Einstein relation,

$$D = \frac{k_B T}{6\pi\eta R}, \quad (3)$$

where R is the radius of the markers, k_B is the Boltzmann constant, T is the absolute temperature. Here we adopt this concept for GIXPCS, assigning it the "marker GIXPCS" hereafter. In a recent study, we successfully employed the marker GIXPCS to show the effect of free surface on the local viscosity distributions in thin PS films.[135] The corresponding experimental geometry is shown schematically in Figure 1-5. We found that the marker dynamics agreeably correlate to the viscosity of the polymer matrix via the known Stoke-Einstein relation (eq. (3)). In Chapter 3, we apply the same strategy to investigate the characteristic of the adsorbed polymer layer and its

impact on the local viscosity distributions near the solid surface. The marker GIXPCS experiments were performed at beam line 8-ID at the Advanced Photon Source (APS), Argonne National Laboratory. The detail experimental setup will be further described in Chapter 3.

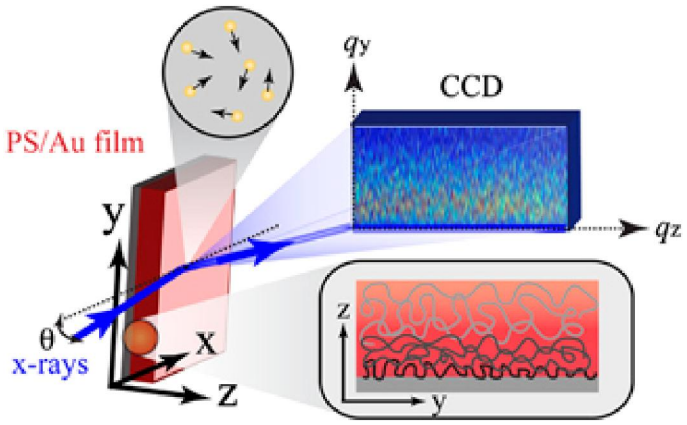

Figure 1 - 5. Schematic diagram of the marker GIXPCS experiments. The use of resonance enhanced X-ray scattering for marker GIXPCS enables the probing electrical field to be intensified by more than one order of magnitude in the regions of interest within single polymer films.

1.5.2 X-ray/Neutron Reflectivity

X-ray and neutron reflectivity are famous and well-known techniques for the investigation of the surface and interface of thin polymer films due to their excellent spatial resolution and penetration depth.[136] Both techniques can provide valuable information for thin polymer films prepared on planar solid substrates with nanometer scale resolution, including layer density, film thickness, surface and interface roughness, etc.

For X-ray reflectivity, the intensity contrast comes from variation in electron density between different materials or media. A major advantage of X-ray reflectivity over neutron reflectivity is the higher intensity and out-of-plane spatial resolution given by synchrotron radiation sources.

Hence, X-ray reflectivity can be used as an ideal tool in investigating a silicon substrate supported thin polymer layer in air or under vacuum with high experimental efficiency. However, in practical cases, the difference in electron density could be very small, yielding "small-contrast" layer systems, such as single polymer films that constitute two different density layers with density differences of only ~ 10 %. As a result, interpretation of the data based merely on the reflection curve of intensity as a function of q_z turns out to be difficult. Hence, the Fourier transformation (FT) method is introduced to analyze the data with the reflection curve simultaneously in order to overcome the problem of small contrast.[137] In previous studies, we have successfully utilized X-ray reflectivity in conjunction with the FT method to analyze the adsorbed PS layer, which consists of two different-density PS layers, at the solid-polymer-melt interface.[2] The reader is referred to the article by Seeck and coworkers[137] for more details regarding the FT method on the X-ray reflectivity data analysis.

Neutron reflectivity is also a powerful tool for studying the surface and interface of thin polymer films. Due to the relatively low brilliance of the neutron source, the reflection of neutrons does not provide as high an intensity or resolution as that of synchrotron X-ray. However, neutron source has major advantages for structural characterization of thin polymer films in several aspects. One of the biggest advantages is the strong contrast variation achieved by using different isotopes. Deuterium labeling by replacing hydrogen (H) atoms with deuterium (D) atoms is the most commonly used method for enhancing the scattering contrast at surfaces or interfaces due to the large scattering difference between the two isotopes. This method is of great advantage in investigating a polymer-polymer interface by deuterating one of the two polymers. Another major advantage of neutron is high transmissivity, and less absorption into materials which allows neutrons to penetrate neutral bulk materials, such as thick silicon wafers, or various sample

environments, such as liquids or high pressure gas. This enables us to investigate the deeply buried polymer/liquid interfaces in solvents or supercritical fluids.

In this thesis, the structure and thermal property of various adsorbed polymer layers on silicon substrates are investigated using x-ray reflectivity measurements carried out at the X10B and X20A beamlines at the National Synchrotron Light Source, Brookhaven National Laboratory (NSLS, BNL). In situ high temperature experiments were performed under vacuum (~ 10^{-5} Torr with the use of turbo molecular pump) by using a custom-built vacuum furnace with Kapton windows.

In situ neutron reflectivity experiments were performed at the National Institute of Standards and Technology Center for Neutron Research (NCNR) NG-7 reflectometry in order to investigate the swelling and interdiffusion behavior of adsorbed polymer chains in CO_2. A specially designed high-pressure cell was mounted along the beam path with two cylindrical sapphire windows (2.4 cm in thick, o.d. 5 cm) installed at each side for transmitting the incident beams and receiving the reflected beams, as shown schematically in Figure 1-6. Sealing was achieved by a combination of Teflon and a nylon gasket placed between the sapphire windows. The cell had a volume of about 10 mL and a maximum pressure rating of 140.0 MPa. Previous works by Koga's group[138-144] have shown the capability of such an in situ neutron reflectivity setup in investigating the structure and properties of thin polymer films in CO_2 within a wide range of pressures and temperatures. The detailed design and setup of the high pressure cell has been described elsewhere in the literature.[140] It is worth mentioning that due to high absorption of neutrons in compressed CO_2, the incident and reflected beams passed through the Si wafer with a transmission of 0.90 relative to air.

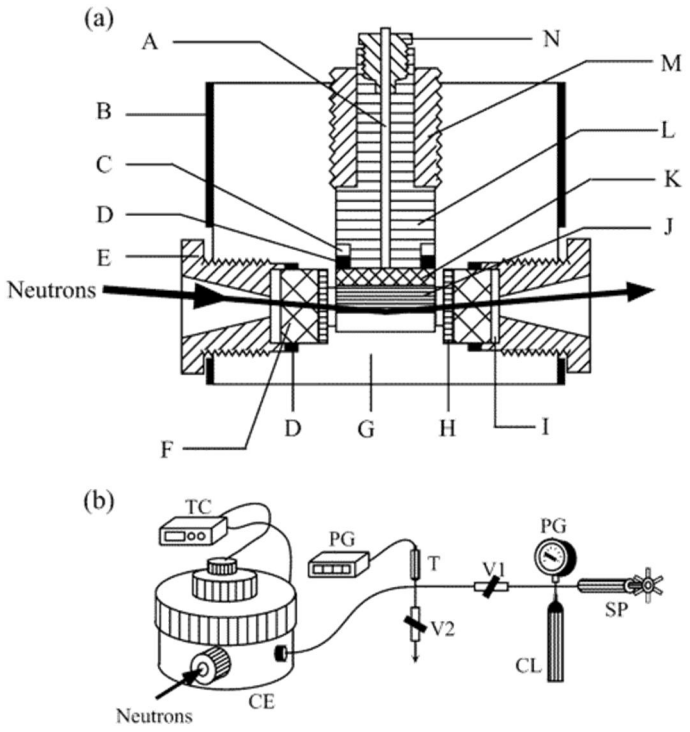

Figure 1 - 6. Schematic diagram of (a) high-pressure cell and (b) experimental configuration for NR experiments: (A) thermocouple, (B) heater, (C) backup ring, (D) Teflon O-ring, (E) retainer, (F) sapphire windows, (G) chamber, (H) Teflon gasket (I) nylon gasket, (J) Si wafer (K) Al spacer, (L) cover, (M) main nut, (N) HF4 connection, (CL) CO2 cylinder, (SP) hand-operated syringe pump, (PG) pressure gauge, (V1) inlet valve, (V2) release valve, (T) pressure transducer, (TC) temperature controller, (CE) high-pressure chamber. Figure reproduced from ref. 129.

1.5.3 Neutron Spin Echo Spectrometry

Neutron spin echo (NSE) spectrometry is an ideal technique that provides unique a opportunity to observe the molecular dynamics of macromolecules simultaneously in space and time.[145] It possesses a much higher energy resolution compared to the conventional inelastic/quasi-elastic neutron scattering techniques, such as triple (three) axis spectrometry and time-of-flight (TOF) spectrometry, due to the use of the Larmor precession of the neutron spin in a preparation zone with a magnetic field to measure the energy transfer of neutrons. Figure 1-7 shows the accessible regions of the length-time space of the NSE compared to other dynamical investigation

methods. It can be seen that NSE covers the largest time scale (0.01 – 100 ns) and length scale (1 – 100 Å) among all inelastic/quasi-elastic neutron scattering techniques. Hence, various modes of motions present in polymer systems can be detected within the unique time length-time space provided by NSE, including segmental motions described by the Rouse and Zimm models, cooperative diffusion motion in polymer networks and even the very slow reptation motions in entangled polymer melts or concentrated polymer solutions.[146]

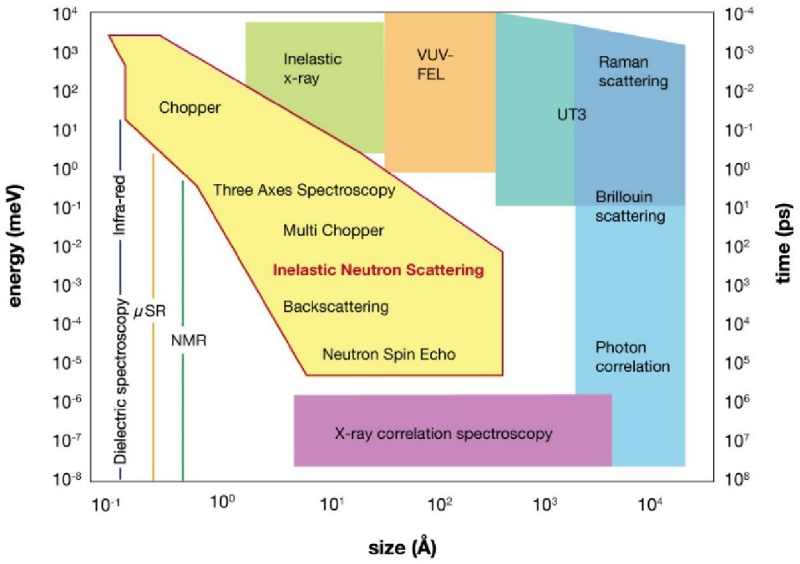

Figure 1 - 7. Length and time domains available with neutron spin echo compared to other investigation methods. Figure reproduced from The Heinz Maier-Leibnitz Zentrum website at http://www.mlz-garching.de/.)

Through the polarization of neutron beam, NSE measures the Fourier transform of the dynamic structure factor $S(q,\omega)$, i.e. the Normalized Intermediate Scattering Function: $I(q,t)/I(q,0)$. If no typical finite energy transfer of neutrons exists in the system (quasi-elastic scattering regime),

the relaxation dynamics of polymer chains at a certain q value can be obtained from the decay of $I(q,t)/I(q,0)$ as a function of time. While coherent dynamics with large scale objectives (slower dynamics) can be well measured by NSE, incoherent dynamics at high q are often difficult mainly due to the low incoherent scattering intensity and the limited q coverage of the instrument.[147]

In Chapter 6, we utilize NSE to investigate the dynamics of bound (adsorbed) polybutadiene (PB) chains in toluene. The NSE measurements were performed at the National Institute of Standards and Technology Center for Neutron Research (NCNR). The deuterium labeling method, as previous described, was used to enhance the scattering contrast. Since the scattering length density (SLD) of carbon black ($SLD_{CB} = 6.0\times10^{-4}$ nm^{-2}) and d-toluene ($SLD_{\text{d-toluene}} = 5.7\times10^{-4}$ nm^{-2}) is nearly the same, the bound h-PB layer which appears as a "shell" structure in the systems can be easily identified under neutron scattering.

1.6 References

1. Tsui, O. K. C.; Russell, T. P., *Polymer thin films*. World Scientific: Singapore; Hackensack, NJ, 2008.

2. Gin, P.; Jiang, N.; Liang, C.; Taniguchi, T.; Akgun, B.; Satija, S. K.; Endoh, M. K.; Koga, T. *Phys Rev Lett* **2012,** 109, (26), 265501.

3. Fujii, Y.; Yang, Z. H.; Leach, J.; Atarashi, H.; Tanaka, K.; Tsui, O. K. C. *Macromolecules* **2009,** 42, (19), 7418-7422.

4. Rotella, C.; Napolitano, S.; Vandendriessche, S.; Valev, V. K.; Verbiest, T.; Larkowska, M.; Kucharski, S.; Wubbenhorst, M. *Langmuir* **2011,** 27, (22), 13533-13538.

5. Napolitano, S.; Wubbenhorst, M. *Nat Commun* **2011,** 2.

6. *Polymer Handbook 4th Ed.* John Wiley & Sons, Inc.: NY, 1999.

7. Reiter, G.; Sharma, A.; Casoli, A.; David, M. O.; Khanna, R.; Auroy, P. *Langmuir* **1999,** 15, (7), 2551-2558.

8. Seemann, R.; Herminghaus, S.; Jacobs, K. *Phys Rev Lett* **2001,** 86, (24), 5534-5537.

9. Sharma, A. *Langmuir* **1993,** 9, (3), 861-869.

10. Reiter, G. *Phys Rev Lett* **1992,** 68, (1), 75-78.

11. Reiter, G. *Europhys Lett* **1993,** 23, (8), 579-584.

12. Reiter, G.; Hamieh, M.; Damman, P.; Sclavons, S.; Gabriele, S.; Vilmin, T.; Raphael, E. *Nat Mater* **2005,** 4, (10), 754-758.

13. Koga, T.; Seo, Y. S.; Zhang, Y.; Sin, K.; Kusano, K.; Nishikawa, K.; Rafailovich, M. H.; Sokolov, J. C.; Chu, B.; Peiffer, D.; Occhiogrosso, R.; Satija, S. K. *Phys. Rev. Lett.* **2002,** 89, 125506.

14. Koga, T.; Seo, Y. S.; Hu, X.; Kwanwoo, S.; Zhang, Y.; Rafailovich, M. H.; Sokolov, J. C.; Chu, B.; Satija, S. K. *Europhys. Lett.* **2002,** 60, 559.

15. Koga, T.; Seo, Y. S.; Shin, K.; Zhang, Y.; Rafailovich, M. H.; Sokolov, J. C.; Chu, B.; Peiffeer, D.; Satija, S. K. *Macromolecules* **2003,** 36, 5236.

16. Koga, T.; Ji, Y.; Seo, Y. S.; Rafailovich, M. H.; Sokolov, J. C.; Satija, S. K. *J. Polym. Sci., Part B:Polym. Phys.* **2004,** 42, 3282.

17. Meli, L.; Pham, J. Q.; Johnston, K. P.; Green, P. F. *Physical Review E* **2004,** 69, (5), 8.

18. Li, Y.; park, E.; Lim, K.; Johnston, K. P.; Green, P. F. *J. Polym. Sci., Part B:Polym. Phys.* **2007,** 45, 1313-1324.

19. Chebil, M. S.; Vignaud, G.; Grohens, Y.; Konovalov, O.; Sanyal, M. K.; Beuvier, T.; Gibaud, A. *Macromolecules* **2012,** 45, (16), 6611-6617.

20. Nishikawa, K.; Tanaka, I.; Amemiya, Y. *J. Phys. Chem.* **1996,** 100, 418-421.

21. Sirard, S. M.; J., Z. K.; Sanchez, L. C.; Green, P. F.; Johnston, K. P. *Macromolecules* **2002,** 35, 1928.

22. Li, X. X.; Vogt, B. D. *Polymer* **2009,** 50, (17), 4182-4188.

23. Koga, T.; Gin, P.; Yamaguchi, H.; Endoh, M.; Sendogdular, L.; Kobayashi, M.; Takahara, A.; Akgun, B.; Satija, S. K.; Sumi, T. *Polymer* **2011,** 52, 4331-4336.

24. Mendoza-Galvan, A.; Trejo-Cruz, C.; Solis-Canto, O.; Luna-Barcenas, G. *J. Supercrit. Fluids* **2012,** 64, 25-31.

25. Geoghegan, M.; Krausch, G. *Prog. Polym. Sci.* **2003,** 28, (2), 261-302.

26. Keddie, J. L.; Jones, R. A. L.; Cory, R. A. *Faraday Discussions* **1994,** 98, 219-230.

27. Keddie, J. L.; Jones, R. A. L.; Cory, R. A. *Europhys Lett* **1994,** 27, (1), 59-64.

28. Kim, J. H.; Jang, J.; Zin, W. C. *Langmuir* **2000,** 16, (9), 4064-4067.

29. Kawana, S.; Jones, R. A. L. *Phys Rev E* **2001,** 63, (2).

30. Xie, F. C.; Zhang, H. F.; Lee, F. K.; Du, B. Y.; Tsui, O. K. C.; Yokoe, Y.; Tanaka, K.; Takahara, A.; Kajiyama, T.; He, T. B. *Macromolecules* **2002,** 35, (5), 1491-1492.

31. Fakhraai, Z.; Valadkhan, S.; Forrest, J. A. *Eur Phys J E* **2005,** 18, (2), 143-148.

32. Fakhraai, Z.; Forrest, J. A. *Phys Rev Lett* **2005,** 95, (2).

33. Kajiyama, T.; Tanaka, K.; Takahara, A. *Macromolecules* **1995,** 28, (9), 3482-3484.

34. Mattsson, J.; Forrest, J. A.; Borjesson, L. *Phys Rev E* **2000,** 62, (4), 5187-5200.

35. Forrest, J. A.; DalnokiVeress, K.; Dutcher, J. R. *Phys Rev E* **1997,** 56, (5), 5705-5716.

36. Forrest, J. A.; DalnokiVeress, K.; Stevens, J. R.; Dutcher, J. R. *Phys Rev Lett* **1996,** 77, (10), 2002-2005.

37. Teichroeb, J. H.; Forrest, J. A. *Phys Rev Lett* **2003,** 91, (1).

38. Qi, D.; Ilton, M.; Forrest, J. A. *Eur Phys J E* **2011,** 34, (6).

39. Ilton, M.; Qi, D.; Forrest, J. A. *Macromolecules* **2009,** 42, (18), 6851-6854.

40. Qi, D.; Fakhraai, Z.; Forrest, J. A. *Phys Rev Lett* **2008,** 101, (9).

41. Fakhraai, Z.; Forrest, J. A. *Science* **2008,** 319, (5863), 600-604.

42. Sharp, J. S.; Teichroeb, J. H.; Forrest, J. A. *Eur Phys J E* **2004,** 15, (4), 473-487.

43. Tanaka, K.; Takahara, A.; Kajiyama, T. *Macromolecules* **1997,** 30, (21), 6626-6632.

44. DeMaggio, G. B.; Frieze, W. E.; Gidley, D. W.; Zhu, M.; Hristov, H. A.; Yee, A. F. *Phys Rev Lett* **1997,** 78, (8), 1524-1527.

45. Roth, C. B.; McNerny, K. L.; Jager, W. F.; Torkelson, J. M. *Macromolecules* **2007,** 40, (7), 2568-2574.

46. Priestley, R. D.; Ellison, C. J.; Broadbelt, L. J.; Torkelson, J. M. *Science* **2005,** 309, (5733), 456-459.

47. Ellison, C. J.; Torkelson, J. M. *Nat Mater* **2003,** 2, (10), 695-700.

48. Rotella, C.; Wubbenhorst, M.; Napolitano, S. *Soft Matter* **2011,** 7, (11), 5260-5266.

49. Rotella, C.; Napolitano, S.; De Cremer, L.; Koeckelberghs, G.; Wubbenhorst, M. *Macromolecules* **2010,** 43, (20), 8686-8691.

50. Napolitano, S.; Wubbenhorst, M. *Polymer* **2010,** 51, (23), 5309-5312.

51. Rotella, C.; Napolitano, S.; Wuebbenhorst, M. *Macromolecules* **2009,** 42, (5), 1415-1417.

52. Peter, S.; Napolitano, S.; Meyer, H.; Wubbenhorst, M.; Baschnagel, J. *Macromolecules* **2008,** 41, (20), 7729-7743.

53. Napolitano, S.; Lupascu, V.; Wubbenhorst, M. *Macromolecules* **2008,** 41, (4), 1061-1063.

54. Napolitano, S.; Wubbenhorst, M. *J Phys Chem B* **2007,** 111, (21), 5775-5780.

55. Napolitano, S.; Prevosto, D.; Lucchesi, M.; Pingue, P.; D'Acunto, M.; Rolla, P. *Langmuir* **2007,** 23, (4), 2103-2109.

56. Kessairi, K.; Napolitano, S.; Capaccioli, S.; Rolla, P.; Wubbenhorst, M. *Macromolecules* **2007,** 40, (6), 1786-1788.

57. Wallace, W. E.; Vanzanten, J. H.; Wu, W. L. *Phys Rev E* **1995,** 52, (4), R3329-R3332.

58. vanZanten, J. H.; Wallace, W. E.; Wu, W. L. *Phys Rev E* **1996,** 53, (3), R2053-R2056.

59. Fryer, D. S.; Peters, R. D.; Kim, E. J.; Tomaszewski, J. E.; de Pablo, J. J.; Nealey, P. F.; White, C. C.; Wu, W. L. *Macromolecules* **2001,** 34, (16), 5627-5634.

60. Kim, H.; Ruhm, A.; Lurio, L. B.; Basu, J. K.; Lal, J.; Lumma, D.; Mochrie, S. G. J.; Sinha, S. K. *Phys Rev Lett* **2003,** 90, (6).

61. Kim, H.; Ruhm, A.; Lurio, L. B.; Basu, J. K.; Lal, J.; Mochrie, S. G. J.; Sinha, S. K. *Physica B* **2003,** 336, (1-2), 211-215.

62. Li, C. H.; Koga, T.; Jiang, J.; Sharma, S.; Narayanan, S.; Lurio, L. B.; Hu, Y.; Jiao, X.; Sinha, S. K.; Billet, S.; Sosnowik, D.; Kim, H.; Sokolov, J. C.; Rafailovich, M. H. *Macromolecules* **2005,** 38, (12), 5144-5151.

63. Ellison, C. J.; Torkelson, J. M. *Nature Mater.* **2003,** 2, 695-700.

64. Fakhraai, Z.; Forrest, J. A. *Phys. Rev. Lett.* **2005,** 95, 025701.

65. Yang, Z. H.; Fujii, Y.; Lee, F. K.; Lam, C. H.; Tsui, O. K. C. *Science* **2010,** 328, (5986), 1676-1679.

66. Bodiguel, H.; Fretigny, C. *Macromolecules* **2007,** 40, (20), 7291-7298.

67. Li, C. H.; Kim, H. J.; Jiang, J.; Li, C.; Koga, T.; Lurio, L.; Schwarz, S.; Narayanan, S.; Lee, H. J.; Lee, Y. J.; Jiang, Z.; Sinha, S.; Rafailovich, M. H.; Sokolov, J. C. *Europhys Lett* **2006,** 73, (6), 899-905.

68. Bodiguel, H.; Fretigny, C. *Phys Rev Lett* **2006,** 97, (26).

69. O'Connell, P. A.; McKenna, G. B. *Science* **2005,** 307, (5716), 1760-1763.

70. Masson, J. L.; Green, P. F. *Phys Rev E* **2002,** 65, (3).

71. Zheng, X.; Sauer, B. B.; Vanalsten, J. G.; Schwarz, S. A.; Rafailovich, M. H.; Sokolov, J.; Rubinstein, M. *Phys Rev Lett* **1995,** 74, (3), 407-410.

72. Zheng, X.; Rafailovich, M. H.; Sokolov, J.; Strzhemechny, Y.; Schwarz, S. A.; Sauer, B., B.; Rubinstein, M. *Phys Rev Lett* **1997,** 79, 241-244.

73. Priestley, R. D.; Ellison, C.; Broadbelt, L. J.; Torkelson, J. M. *Science* **2005,** 309, 456-459.

74. Herminghaus, S. *Eur Phys J E* **2002,** 8, (2), 237-243.

75. Long, D.; Lequeux, F. *Eur Phys J E* **2001,** 4, (3), 371-387.

76. Kim, J. H.; Jang, J.; Zin, W. C. *Langmuir* **2001,** 17, (9), 2703-2710.

77. Sharp, J. S.; Forrest, J. A. *Phys Rev Lett* **2003,** 91, (23).

78. Forrest, J. A.; Dalnoki-Veress, K. *Adv Colloid Interfac* **2001,** 94, (1-3), 167-196.

79. Forrest, J. A.; Dalnoki-Veress, K.; Dutcher, J. R. *Phys Rev E* **1998,** 58, (5), 6109-6114.

80. Forrest, J. A.; DalnokiVeress, K.; Stevens, J. R.; Dutcher, J. R. *Phys Rev Lett* **1996,** 77, (19), 4108-4108.

81. Tsui, O. K. C.; Russell, T. P.; Hawker, C. J. *Macromolecules* **2001,** 34, (16), 5535-5539.

82. Frank, C. W.; Rao, V.; Despotopoulou, M. M.; Pease, R. F. W.; Hinsberg, W. D.; Miller, R. D.; Rabolt, J. F. *Science* **1996,** 273, (5277), 912-915.

83. Sharp, J. S.; Forrest, J. A. *Phys Rev E* **2003,** 67, (3).

84. Priestley, R. D.; Mundra, M. K.; Barnett, N. J.; Broadbelt, L. J.; Torkelson, J. M. *Aust J Chem* **2007,** 60, (10), 765-771.

85. Durning, C. J.; O'Shaughness, B.; Sawhney, U.; Nguyen, D.; Majewski, J.; Smith, G. S. *Macromolecules* **1999,** 32, (20), 6772-6781.

86. Ediger, M. D.; Forrest, J. A. *Macromolecules* **2014,** 47, (2), 471-478.

87. Frank, B.; Gast, A. P.; Russell, T. P.; Brown, H. R.; Hawker, C. J. *Macromolecules* **1996,** 29, (20), 6531-6534.

88. Zheng, X.; Rafailovich, M. H.; Sokolov, J.; Strzhemechny, Y.; Schwarz, S. A.; Sauer, B. B.; Rubinstein, M. *Phys Rev Lett* **1997,** 79, (2), 241-244.

89. Scheutjens, J. M. H. M.; Fleer, G. J. *The Journal of Physical Chemistry* **1980,** 84, (2), 178-190.

90. Schneider, H. M.; Frantz, P.; Granick, S. *Langmuir* **1996,** 12, (4), 994-996.

91. Douglas, J. F.; Schneider, H. M.; Frantz, P.; Lipman, R.; Granick, S. *Journal of Physics: Condensed Matter* **1997,** 9, (37), 7699.

92. O'Shaughnessy, B.; Vavylonis, D. *J Phys-Condens Mat* **2005,** 17, (2), R63-R99.

93. O'Shaughnessy, B.; Vavylonis, D. *Eur Phys J E* **2003,** 11, (3), 213-230.

94. Simha, R.; Frisch, H. L.; Eirich, F. R. *The Journal of Physical Chemistry* **1953,** 57, (6), 584-589.

95. Scheutjens, J. M. H. M.; Fleer, G. J. *Macromolecules* **1985,** 18, (10), 1882-1900.

96. Scheutjens, J. M. H. M.; Fleer, G. J. *The Journal of Physical Chemistry* **1979,** 83, (12), 1619-1635.

97. Papirer, E., *Adsorption on silica surfaces*. CRC Press: 2000.

98. Granick, S. *Eur. Phys. J. E* **2002,** 9, (1), 421-424.

99. Santore, M. M. *Curr Opin Colloid In* **2005,** 10, (3–4), 176-183.

100. Sommer, J.-U. *Eur. Phys. J. E* **2002,** 9, (1), 417-419.

101. Fu, Z.; Santore, M. *Macromolecules* **1999,** 32, (6), 1939-1948.

102. Fu, Z.; Santore, M. M. *Langmuir* **1997,** 13, (21), 5779-5781.

103. Ligoure, C.; Leibler, L. *J. Phys. France* **1990,** 51, (12), 1313-1328.

104. Linse, P. *Soft Matter* **2012,** 8, (19), 5140-5150.

105. Linse, P.; Källrot, N. *Macromolecules* **2010,** 43, (4), 2054-2068.

106. Housmans, C.; Sferrazza, M.; Napolitano, S. *Macromolecules* **2014,** 47, (10), 3390-3393.

107. Napolitano, S.; Capponi, S.; Vanroy, B. *Eur. Phys. J. E* **2013,** 36, (6), 1-37.

108. Napolitano, S.; Rotella, C.; Wübbenhorst, M. *Acs Macro Lett* **2012,** 1, (10), 1189-1193.

109. Ramanathan, M.; Darling, S. B. *Progress in Polymer Science* **2011,** 36, (6), 793-812.

110. Reiter, G. *Langmuir* **1993,** 9, (5), 1344-1351.

111. Zhai, X. W.; Weiss, R. A. *Langmuir* **2008,** 24, (22), 12928-12935.

112. Seemann, R.; Herminghaus, S.; Neto, C.; Schlagowski, S.; Podzimek, D.; Konrad, R.; Mantz, H.; Jacobs, K. *J Phys-Condens Mat* **2005,** 17, (9), S267-S290.

113. Muller-Buschbaum, P. *Eur Phys J E* **2003,** 12, (3), 443-448.

114. Suh, H. S.; Kang, H. M.; Liu, C. C.; Nealey, P. F.; Char, K. *Macromolecules* **2010,** 43, (1), 461-466.

115. Kargupta, K.; Sharma, A. *Langmuir* **2003,** 19, (12), 5153-5163.

116. Renger, C.; Muller-Buschbaum, P.; Stamm, M.; Hinrichsen, G. *Macromolecules* **2000,** 33, (22), 8388-8398.

117. Mansky, P.; Liu, Y.; Huang, E.; Russell, T. P.; Hawker, C. J. *Science* **1997,** 275, (5305), 1458-1460.

118. Yerushalmi-Rozen, R.; Klein, J.; Fetters, L. J. *Science-AAAS-Weekly Paper Edition-including Guide to Scientific Information* **1994,** 263, (5148), 793-795.

119. Costa, A. C.; Composto, R. J.; Vlcek, P.; Morera, S. *J Adhesion* **2005,** 81, (7-8), 683-698.

120. Costa, A. C.; Composto, R. J.; Vlcek, P. *Macromolecules* **2003,** 36, (9), 3254-3260.

121. Oslanec, R.; Costa, A. C.; Composto, R. J.; Vlcek, P. *Macromolecules* **2000,** 33, (15), 5505-5512.

122. Krishnan, R. S.; Mackay, M. E.; Duxbury, P. M.; Hawker, C. J.; Asokan, S.; Wong, M. S.; Goyette, R.; Thiyagarajan, P. *J Phys-Condens Mat* **2007,** 19, (35).

123. Henn, G.; Bucknall, D. G.; Stamm, M.; Vanhoorne, P.; Jerome, R. *Macromolecules* **1996,** 29, (12), 4305-4313.

124. Reiter, G.; Schultz, J.; Auroy, P.; Auvray, L. *Europhys Lett* **1996,** 33, (1), 29-34.

125. Chu, B., *Dynamic Light Scattering, 2nd Ed.* Academic Press: New York, 1991.

126. Leheny, R. L. *Curr Opin Colloid In* **2012,** 17, (1), 3-12.

127. Sutton, M. *Cr Phys* **2008,** 9, (5-6), 657-667.

128. Livet, F. *Acta Crystallogr A* **2007,** 63, 87-107.

129. Mochrie, S. G. J.; Lurio, L. B.; Ruhm, A.; Lumma, D.; Borthwick, M.; Falus, P.; Kim, H. J.; Basu, J. K.; Lal, J.; Sinha, S. K. *Physica B* **2003,** 336, (1-2), 173-180.

130. Kim, H.; Ruhm, A.; Lurio, L. B.; Basu, J. K.; Lal, J.; Mochrie, S. G. J.; Sinha, S. K. *J Phys-Condens Mat* **2004,** 16, (33), S3491-S3497.

131. Jiang, Z.; Kim, H.; Jiao, X.; Lee, H.; Lee, Y. J.; Byun, Y.; Song, S.; Eom, D.; Li, C.; Rafailovich, M. H.; Lurio, L. B.; Sinha, S. K. *Phys Rev Lett* **2007,** 98, (22).

132. Kim, H.; Jiang, Z.; Lee, H.; Lee, Y. J.; Jiao, X. S.; Li, C. H.; Lurio, L.; Rafailovich, M.; Sinha, S. K. *Thin Solid Films* **2007,** 515, (14), 5536-5540.

133. Jiang, Z.; Mukhopadhyay, M. K.; Song, S.; Narayanan, S.; Lurio, L. B.; Kim, H.; Sinha, S. K. *Phys Rev Lett* **2008,** 101, (24).

134. Dierker, S. B.; Pindak, R.; Fleming, R. M.; Robinson, I. K.; Berman, L. *Phys Rev Lett* **1995,** 75, (3), 449-452.

135. Koga, T.; Li, C.; Endoh, M. K.; Koo, J.; Rafailovich, M.; Narayanan, S.; Lee, D. R.; Lurio, L. B.; Sinha, S. K. *Phys Rev Lett* **2010,** 104, (6).

136. Russell, T. P. *Materials Science Reports* **1990,** 5, (4), 171-271.

137. Seeck, O. H.; Kaendler, I. D.; Tolan, M.; Shin, K.; Rafailovich, M. H.; Sokolov, J.; Kolb, R. *Appl Phys Lett* **2000,** 76, (19), 2713-2715.

138. Koga, T.; Seo, Y. S.; Zhang, Y. M.; Shin, K.; Kusano, K.; Nishikawa, K.; Rafailovich, M. H.; Sokolov, J. C.; Chu, B.; Peiffer, D.; Occhiogrosso, R.; Satija, S. K. *Physical Review Letters* **2002,** 89, (12).

139. Koga, T.; Seo, Y.-S.; Hu, X.; Shin, K.; Zhang, Y.; Rafailovich, M. H.; Sokolov, J. C.; Chu, B.; Satija, S. K. *EPL (Europhysics Letters)* **2002,** 60, (4), 559.

140. Koga, T.; Seo, Y. S.; Shin, K.; Zhang, Y.; Rafailovich, M. H.; Sokolov, J. C.; Chu, B.; Satija, S. K. *Macromolecules* **2003,** 36, (14), 5236-5243.

141. Koga, T.; Ji, Y.; Seo, Y. S.; Gordon, C.; Qu, F.; Rafailovich, M. H.; Sokolov, J. C.; Satija, S. K. *J Polym Sci Pol Phys* **2004,** 42, (17), 3282-3289.

142. Koga, T.; Jerome, J. L.; Seo, Y. S.; Rafailovich, M. H.; Sokolov, J. C.; Satija, S. K. *Langmuir* **2005,** 21, (14), 6157-6160.

143. Koga, T.; Li, C.; Sun, Y.; Brazin, A.; Rafailovich, M. H.; Sokolov, J. C.; Douglas, J. F.; Mahajan, D. *Top Catal* **2005,** 32, (3-4), 257-262.

144. Koga, T.; Kugler, B.; Loewenstein, J.; Jerome, J.; Rafailovich, M. H. *J Appl Crystallogr* **2007,** 40, S684-S686.

145. Richter, D.; Fetters, L. J.; Huang, J. S.; Farago, B.; Ewen, B. *J Non-Cryst Solids* **1991,** 131, 604-611.

146. Imae, T.; Kanaya, T.; Furusaka, M.; Torikai, N., *Neutrons in soft matter*. John Wiley & Sons: 2011.

147. Richter, D.; Monkenbusch, M.; Arbe, A.; Colmenero, J., Neutron Spin Echo in Polymer Systems. In *Advances in Polymer Science*, Springer Berlin Heidelberg: 2005; Vol. 174, pp 1-221.

Chapter 2: Formation Mechanism of High-Density, Flattened Polymer Nanolayers Adsorbed on Planar Solids

2.1 Introduction

A spin-coating process (i.e., a rapid solvent-cast process) is a well-established technique to prepare homogenous polymer thin films on planar substrates in a well-controlled manner. But, it is also known that this rapid solvent evaporation process results in non-equilibrium stressed conformations of polymer chains on substrates and such residual stress causes film instability[1-3] and changes in properties of polymer thin films[4-6]. In order to achieve full relaxation of the residual stress and equilibration of the chain conformations, prolong thermal annealing (at temperatures far above the bulk T_g) compared to bulk reputation times[7] is typically required[3, 8, 9]. On the other hand, prolong thermal annealing expedites polymer adsorption from the melt onto solid substrates[10]. Based on the established protocol combined thermal annealing at a temperature far above T_g and subsequent rinsing with a good solvent, several research groups have shown the formation of irreversibly adsorbed polymer layers with thickness of several nanometers to a few tens of nanometers even onto weakly attractive surfaces[11-19]. The vital points of such adsorbed layers (known as Guiselin brushes[20]) are to (i) create an "interphase" with the properties between those of the adsorbed layer and bulk even for weakly interactive systems[21-23] and (ii) control the structures[24, 25], dynamics[18, 26] and other physical properties[27-32] of polymer thin films. Recently, our group has demonstrated that polystyrene (PS) adsorbed layers on planar Si substrates are composed of an inner higher density region (~ 2 nm in thickness regardless of molecular weights (M_w)) with a more flattened chain conformation and an outer bulk-like density region whose thickness increases with M_w[19]. Hereafter, we assign the inner high-density layer and outer bulk-like density layer as the "flattened layer" and "loosely adsorbed layer", respectively. It is postulated

that this two-layer formation is attributed to piecemeal deposition with differential spreading dictated by the still-uncovered surface area, as reported in polymer adsorption from dilute solutions[33-36]. The formation of the flattened layer on planar substrates is consistent with the Brownian dynamic simulation results reported by Linse and co-workers[37]: Flexible homopolymer adsorbed chains tend to orient their conformations parallel to the surface and form a compact, higher density layer relative to the bulk in equilibrium. The flattened chain conformation can be in principle drawn by a counterbalance between the conformational entropy of chains and the energy gain of attached segments to the surface in the total free energy[19, 38].

In this chapter, we aim to understand the formation process of the flattened layer from the melt by distinguishing from that of the loosely adsorbed polymer layer on planar substrates. In contrast to irreversible adsorption from dilute polymer solutions, the kinetics from the melt is more sluggish and complicated due to chain entanglements, friction, and incomplete equilibration[39, 40]. Yet, several recent dielectric spectroscopy studies reported by Napolitano and coworkers[31, 41, 42] showed that the growth of the polymer adsorbed layers (which should be composed of the flattened and loosely adsorbed layers, while they never clarified it) on planar solids exhibit power-law growth at the early stage of adsorption and gives way to a slower logarithmic growth before reaching the final chain conformations. This overall behavior is similar to irreversible polymer adsorption from dilute solution[33-36, 43, 44]. However, the kinetics of the inner two-layer formation still lacks study so far. Here, we use three different homopolymers, polystyrene (PS), poly (2-vinylpyridine) (P2VP), and poly(methyl methacrylate) (PMMA) as models since these polymers have similar inherent stiffness and bulk glass transition temperature (T_g), but different affinities with Si substrates. We have optimized the thermal annealing and solvent leaching conditions to extract the lone flatten layers on planar substrates. X-ray reflectivity and atomic force microscopy techniques allow

detailed characterization of the flattened layers at the nanometer scale. A series of the experimental findings shed light on the importance of polymer/substrate interactions in the final structures and formation kinetics of the flattened chains at the solid-polymer melt interface.

2.2 Materials and Methods

2.2.1 Sample Preparation

PS, P2VP, and PMMA were purchased from Pressure Chemical Co., Polysciences Inc., and Scientific Polymer Products Inc., respectively. The characteristics are tabulated in Table 2-1. The polymers were dissolved in a good solvent (toluene (Sigma-Aldrich, HPLC grade, > 99.9%) for PS and PMMA, and dimethylformamide (DMF, Sigma-Aldrich, ACS reagent, > 99.8%) for P2VP) with polymer concentrations of about 2.5 wt%. Si substrates were cleaned by immersion in a hot piranha solution (i.e., a mixture of H_2SO_4 and H_2O_2, *caution: a* piranha solution *is highly corrosive upon contact with skin or eyes and is an explosion hazard when mixed with organic chemicals/materials; Extreme care should be taken when handing it*) for 30 min, and subsequently rinsed with deionized water thoroughly. Then, only for preparation of PS thin films, we used an aqueous solution of hydrogen fluoride (HF) to remove a native oxide layer on Si substrates. Hereafter, we assign hydrogen passivated Si substrates and Si without the HF treatment as H-Si and B-Si, respectively. It should be noted that a SiO_2 layer of about 1 nm in thickness was reproduced even just after HF etching due to atmospheric oxygen and moisture[45]. However, the surface tension (γ) of the H-Si is quite different (48.71 mJ/m^2 for the dispersion part (γ_d) and 3.98 mJ/m^2 for the polar part (γ_p) [46]) from that of the B-Si (γ_d = 25.8 mJ/m^2 and γ_p = 25.8 mJ/m^2 [47]). As

summarized in Table 2-1, the interfacial energy (γ_{ls}) between the polymer and the substrate were calculated based on the Owens-Wendt-Kaelble equation[48, 49] with the respective surface tension.

Table 2-1. Characteristics of the polymers used in the study

Polymer	M_w (kDa)	M_w/M_n	$T_{g,\,bulk}$ (°C)	Surface tension (mJ/m^2)			γ_{ls} (mJ/m^2)[%]	l (nm)[$]
				γ	γ_D	γ_P		
PS	50	1.04	100	40.6	34.5	6.1	5.6	0.9
	290	1.04						
	650	1.07						
PMMA	97	1.05	105	41.1	29.6	11.5	3	0.85
P2VP	200	1.5	98		-[&]		Strongest[50, 51#]	0.9

[%]: Interfacial energy

[$]: Persistence length[52]

[&]: No data available

[#]: Strongest interactions among the three polymers according to the references.

To prepare the final flattened layer, we reproduced the established protocol[19]: Approximately 50 nm-thick spin cast films prepared on either H-Si or B-Si substrates were annealed at high temperatures (~ T_g + 50 °C) for long time (typically several days) under vacuum below 10^{-3} Torr; the films were then leached in baths of a fresh good solvent at room temperature until the resultant film thickness remained constant. In the case of P2VP, the T_g of supported P2VP thin films is reported to increase significantly compared to the bulk value[50, 51]. Hence, we chose further higher

temperature (~ T_g + 90 °C) as the annealing temperature. As will be discussed later, the leaching conditions used (type of a solvent, leaching time, leaching temperature etc.) should be optimized; otherwise we might end up with the formation along with the loosely adsorbed layers. This selective extraction of the two adsorbed layers is possible owing to the large difference in the desorption energy between the outer loosely adsorbed chains and the flattened chains, which is proportional to the number of segment-surface contacts.[53, 54] We have also validated that the flattened layer is formed before the solvent leaching process. The resultant polymer flattened layers were dried in a vacuum oven at 150 - 190 °C, depending on the polymers, for 24 h to remove any excess solvent trapped in the films before further experiments.

2.2.2 X-ray Reflectivity (XR)

XR experiments were performed under vacuum (approximately 10^{-4} - 10^{-5} Torr) at the X10B and X20A beam lines of the National Synchrotron Light Source, Brookhaven National Laboratory. The specular reflectivity was measured as a function of the scattering vector in the direction perpendicular to the surface, $q_z = 4\pi sin\theta/\lambda$, where θ is the incident angle and λ is the X-ray wavelength (λ = 0.087 nm at X10B and λ = 0.118 nm at X20A, which are equivalent to the X-ray energy of 14.2 keV and 10.5 keV, respectively). The XR data was fit by using a standard multilayer fitting routine for a dispersion value (δ in the X-ray refractive index) in conjunction with a Fourier transformation (FT) method, a powerful tool to obtain detailed structures for low X-ray contrast polymer multilayers[55, 56]. In order to study the thermal stability of the flattened layers, we also performed high temperature XR under vacuum by using a custom-built vacuum furnace with Kapton windows. The films were first heated to high temperature (150 °C - 200 °C), and XR measurements were initiated from the cooling process at a temperature interval of 10 °C. Heating

and re-cooling experiments were also performed to ensure reproducibility. At given temperatures, we stabilized the films for approximately 1 h before data collection.

2.2.3 Atomic Force Microscopy (AFM) measurements

Surface morphologies of the flattened and loosely adsorbed layers were studied by using atomic force microscopy (AFM) (Bruker Bioscope Catalyst and Digital Nanoscope III). A standard tapping mode was conducted in air by using a cantilever with a spring constant of about 40 N/m and a resonant frequency of about 300 kHz. The scan rate was 1.0 Hz with a scanning density of 256 or 512 lines per frame.

2.3 Results

2.3.1 Formation kinetics: Loosely adsorbed chains vs. flattened chains.

Before moving into the main topics, it would be useful to describe the terminology to be used in this chapter. Granick and co-workers pointed out that when the surface sticking energy per monomer reaches values of only a few k_BT, polymer relaxation times become so large that equilibrium adsorbed layers may not be attained even from dilute solutions[34, 57-63]. In addition, Napolitano and Wübbenhorst proposed that polymer chains adsorbed from the melt on solid substrates reach only a "metastable" state with an extremely long relaxation time[17]. Hence, we define the final adsorbed layers, whose thickness remains unchanged against annealing time, as a "quasiequilibrium" state[64], unless otherwise stated. In addition, we assign the entire adsorbed layer composed of the inner flattened chains and outer loosely adsorbed chains as an "interfacial sublayer"[65].

Firstly, we aim to differentiate the formation kinetics of the lone flattened layer from the interfacial sublayer by using PS since the formation protocols for both layers have been established[15, 17, 19, 31, 42]. A monodisperse PS (weight-average molecular mass (M_w) =290 kDa) was used for this purpose. For the formation of the interfacial sublayer, spin cast PS films (~ 50 nm in thickness) prepared on H-Si substrates were annealed at 150 °C for up to 200 h and then solvent leached at minimum of 5 times in baths of fresh toluene at room temperature[19]. In the case of the flattened layer, we previously demonstrated that a further intensive leaching process (~ 120 days) with toluene at room temperature enables us to remove the outer loosely adsorbed layer preferentially[19]. However, as will be discussed below, we here adopted an alternative leaching process with chloroform at room temperature that allows us to more effectively uncover the lone flattened layer within a total leaching time of a couple of days. Here we show how the two different solvent leaching processes work to prepare the two different chain conformations on H-Si substrates. Figure 2-1 shows the XR profiles of the interfacial sublayer and the flattened PS layer at annealing time (t_{an}) of 100 h. The corresponding best fits (shown in the solid lines in Figure 2-1) to the XR data were obtained by using a three-layer (a Si substrate, a SiO_2 layer, and a PS layer) dispersion model for the flattened layer and a four-layer (a Si substrate, a SiO_2 layer, and two PS layers with different densities) for the interfacial sublayer, respectively (the inset of Figure 2-1). The choices of these layer models were determined by the corresponding FT profiles of the XR profiles and the details have been described elsewhere[19]. Note that the δ value of the bulk PS with the X-ray energy of 14.2 keV is $\delta_{bulk}=1.14\times10^{-6}$. From independent XR measurements using a H-Si substrate, the thickness of the SiO_2 layer was determined to be 1.3 nm (2.4 nm for a bare B-Si layer). Hence, the XR results clearly show that the interfacial sublayer is composed of the inner higher-density layer (~ 15 % higher than the bulk) and the outer bulk-like density layer, and the

thickness of the lone flattened layer after the chloroform leaching is in good agreement with that of the inner high-density region of the interfacial sublayer. Hence, the results validate that we have successfully extracted the lone flattened layer by the chloroform rinsing. Note that the δ value of the lone flattened layer is smaller than that within the interfacial sublayer due to the empty (air) spaces of the film, as discussed below.

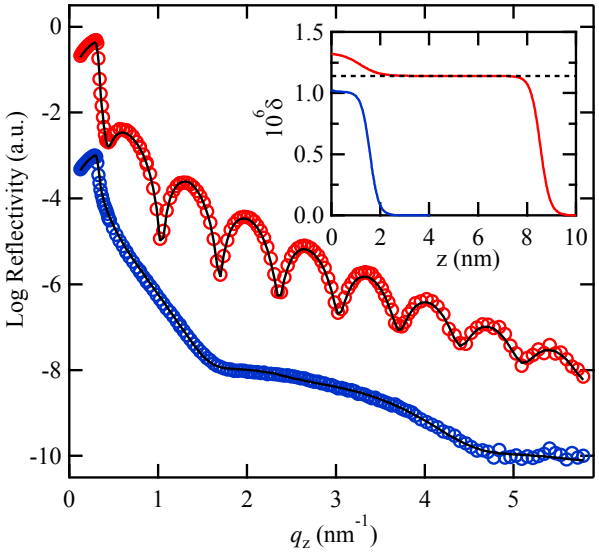

Figure 2 - 1. XR curves of the quasiequilibrium PS (M_w=290 kDa) interfacial sublayer (red circles) and flattened layer (blue circles) at t_{an}=100 h. The solid lines correspond to the best-fits to the data based on the dispersion (δ) profiles against the distance (z) from the SiO_2 surface shown in the inset: red line: the interfacial sublayer; blue line: the flattened layer. The dotted line in the inset corresponds to the δ value of bulk PS.

As shown in Figure 2-2 (a), the flattened layer has microscopic "textures" with the characteristic length of about 100 nm, while the surface of the interfacial sublayer is homogeneous (Figure 2-2 (b)) at t_{an} = 100 h. As shown in Figure 2-2 (c), the average height of the surface textures from the SiO_2 surface is estimated to be about 3 nm, which is in reasonably agreement with the XR result.

In order to estimate the surface coverage (ϕ_p) of the flattened polymer chains, we applied bearing area analysis using the NanoScope Analysis software (version 1.40, Bruker). A bearing area gives a percentage of the surface above a critical threshold. For this analysis, the AFM height images were used and we set the critical threshold to 0 nm at the polymer/SiO_2 interface. Figure 2-2 (d) shows a representative bearing analysis result using the AFM image shown in Figure 2-2 (a). The average ϕ_p value of 75% (± 5 %) was estimated based on several AFM images at different spots of the film. Since the loosely adsorbed chains cover the substrate homogeneously at t_{an} = 100 h (Figure 2-2 (b)), it is reasonable to suppose that the empty regions (~ 25%) of the flattened layer correspond to the sites where the loosely adsorbed chains grew and were then removed by the chloroform leaching. These results are consistent with a set of polymer adsorption experiments from dilute solutions reported by Granick and coworkers,[61, 66] who proved that the flattened chain conformations have much higher fractions than the loosely adsorbed chains. This problem is similar to random sequential adsorption for colloids and proteins[67-73]. The present surface coverage of 75% is much larger than the "jamming limit" (54.7% of surface sites) predicted for rigid disks[67], suggesting that flexible polymer chains can adsorb more effectively and compactly by taking advantage of their flexibility to accommodate the limited surface sites.

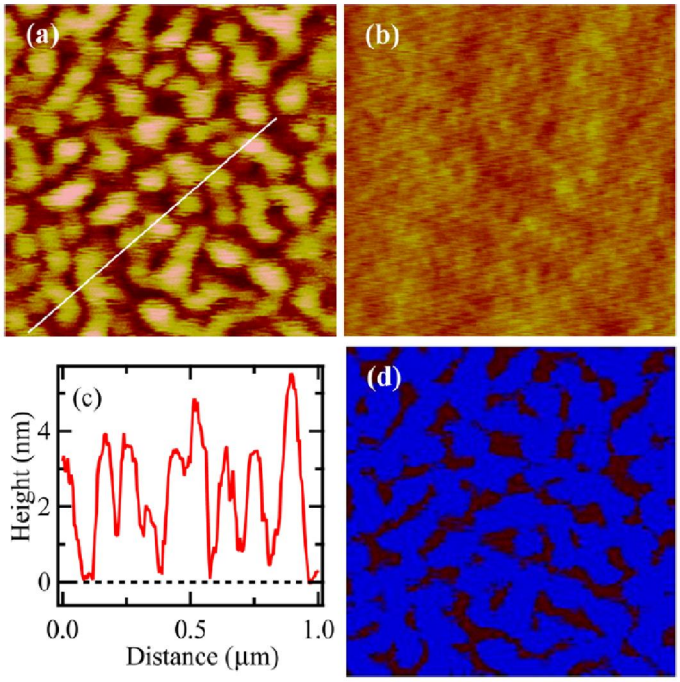

Figure 2 - 2. AFM height images of (a) the PS (M_w = 290 kDa) flattened layer surface and (b) interfacial sublayer surface at t_{an} = 100 h. The scan sizes and height scales of the images are 1 μm × 1 μm and 0 - 6 nm, respectively. The corresponding height profile along the white line in (a) is plotted in (c). The dotted line corresponds to the SiO_2 surface. (d) Corresponding bearing area analysis result for the AFM image shown in (a). The areas occupied by the polymer (bearing areas) are colored in blue.

Figure 2-3 shows the thickness of the PS flattened layer (h_f) measured by XR against t_{an}. From the figure we can see the flattened layer (red circles) exhibits a power-law growth ($h_f \propto t_{an}^{\alpha}$) with $\alpha = 0.50 \pm 0.05$ at the early stage of the kinetics and reached the quasiequilibrium conformation with the thickness of 2.1 nm after $t_{an} > 4$h. Figure 2-3 also plots the time evolution of the thickness of the PS interfacial sublayer. We can see that the interfacial sublayer exhibits similar power-law growth with $\alpha = 0.36 \pm 0.04$ at the early stage kinetics, which is slower than that for the flattened layer due to the limited space issues, and there is a crossover time (t_c) at around 4 h, where the power-law behavior gives way to a slower logarithmic growth, followed by a plateau region at $t_{an} >$ 96 h. The overall adsorption kinetics of the interfacial sublayer is in good agreement with previous

experimental results on the adsorbed PS monolayers on Al substrates[31, 42]. Interestingly, the crossover time (t_c = 4 h) for the interfacial sublayer is nearly equivalent to that of the flattened layer. Thus, the important conclusion is that the two different chain architectures emerge and grow independently on the solid surface.

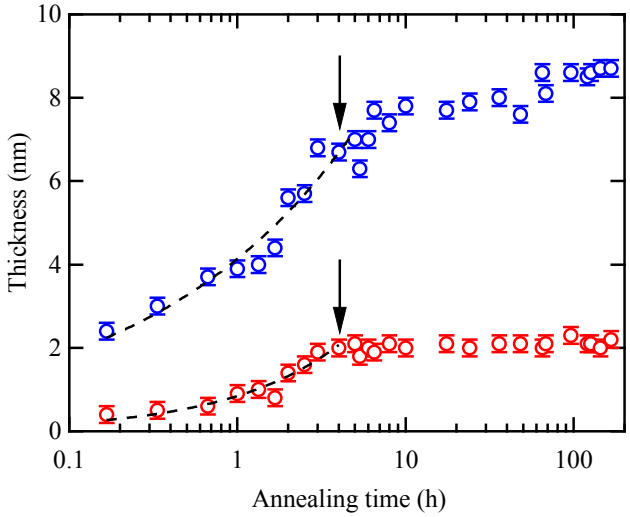

Figure 2 - 3. Growth of the PS (M_w = 290 kDa) interfacial sublayer (blue circles) and flattened layer (red circles) against t_{an} at 150 °C. The dotted lines correspond to the best-fits of the power-law growth described in the text. The crossover times from the power-law growth to logarithmic growth for the interfacial sublayer and from the power-law growth to the quasiequilibrium state for the flatten layer are indicated in the arrows.

2.3.2 The effect of the interactions on the flattened layer formation

We next focus on the effect of the solid-segment interactions on the flattened layer formation. For this purpose, we compare P2VP, PMMA and PS flattened layers. Figure 2-4 (a) shows the adsorption kinetics of these flattened layers. The PMMA and P2VP flattened layers on B-Si substrates were extracted by intensive toluene and DMF leaching, respectively. From the figure we can see power-law growth of the P2VP and PMMA flattened layers before reaching the plateau

regions (i.e., the quasiequilibrium state), but the exponents (~ 0.3) are slightly smaller than that of the PS flattened layer. In addition, it is likely that the final thickness and the t_c values increase with increasing the magnitude of the solid-segment interactions: P2VP > PMMA > PS (see, Table 2-1).

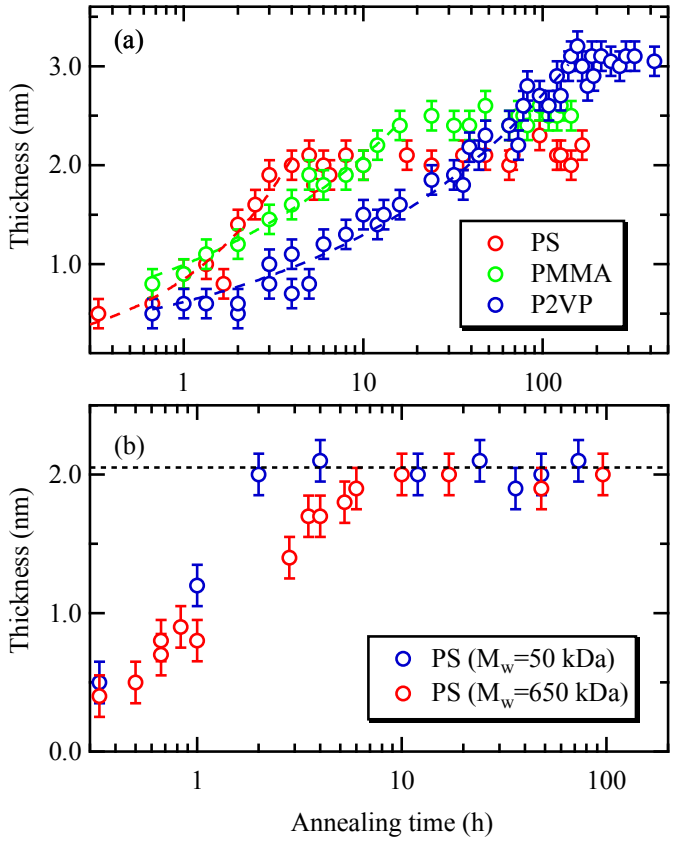

Figure 2 - 4. (a) Film thickness of the PS (Mw = 290 kDa), PMMA, and P2VP flattened layers against tan. (b) Comparison of the growth of the two different PS (Mw =50 kDa and 650 kDa) flattened layers. The final thicknesses of the two PS flattened layers at the quasiequilibrium state (indicated in the dotted line) are equivalent.

To further consider the effect of the viscosity, which also affects the adsorption kinetics of entangled polymers, we investigated the adsorption kinetics of two other PS with different

molecular weights (M_w = 50 kDa and 650 kDa). As shown in Figure 2-4 (b), it was found that t_c increases with increasing M_w, while the final thickness remained constant, as previously reported[19]. However, the difference in t_c between the two PS flattened layers is at most 5 times, while the difference in the viscosity is more than three order of magnitude based on the well-known relationship, $\eta \propto M_w^{3.4}$.[7] Hence, the effect of the viscosity alone cannot explain the large difference (more than two orders of magnitude) in t_c between the PS (M_w = 290 kDa) and P2VP (M_w = 200 kDa). Hence, we may conclude that the magnitude of the interactions controls not only the final thickness but also the kinetics of the flattened layer formation. This can be qualitatively explained by simulation results that the number of polymer chains adsorbed on solids increase with increasing the solid-segment interaction[37].

In order to further illuminate the difference in the adsorption kinetics among the three flattened layers, the detailed surface morphologies of the flattened layers were characterized by AFM. Figure 2-5 (a) and (b) show the AFM height images of the PMMA and P2VP flattened layers after reaching the quasiequilibrium states. Hence, similar dimple structures are seen in the PMMA flattened layer and the surface coverage remains nearly identical (~75 %) to that of the PS flattened layer (Figure 2-5 (a)). On the other hand, we found that the P2VP flattened layer surface is reasonably uniform (ϕ_p ~ 90 %) (Figure 2-5 (b)). To further understand the effect of the solid-segment interaction on the dimple structures, we used polybutadiene (M_w=100 kDa, M_w/M_n=1.06, Polymer Source Inc.) that has a much weaker interaction with H-Si (γ_{ls} = 22.1 (mJ/m^2)). As a result, we found similar dimple structures with a surface coverage of ~ 70 % and a relatively broad distribution of the characteristic lengths (30 nm ~ 140 nm) at the surface of the quasiequilibrium PB flattened layer (see, Supporting Information). Hence, it is not conclusive yet whether the polymer/solid interaction is the main factor to control the size of the dimple structures, while the

surface coverage tends to increase with increasing the interaction. On the other hand, it is noteworthy to point out that the dimple structures resemble of phase-separated structures (i.e., polymer-rich and polymer-poor regions) of end-grafted polymer brushes in a poor solvent regime[74-82]. We are currently studying whether the dimple structures are related to phase separation induced by the leaching process, i.e., immersing in the good solvent and subsequently exposing the flattened chains to air (a poor solvent).

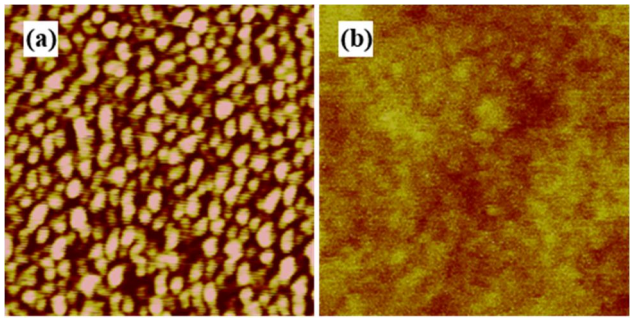

Figure 2 - 5. AFM height images of the (a) PMMA and (b) P2VP flattened layers at the quasiequilibrium state. The scan sizes and height scales of the images are 1 μm × 1 μm and 0 - 6 nm, respectively.

2.4 Discussion

The polymer-polymer interactions become crucial when more polymers are adsorbed on solids. In the case of end-grafted polymer chains, as the grafting density increases, they will interact with one another and start to stretch in the direction normal to the surface due to excluded volume interactions between neighboring chains[83]. Here we may adopt the mechanism of end-grafting chains in order to explain the increase in the film thickness of the flattened layer. According to Aubouy and co-workers[84], end-tethered polymer chains with large grafting density in polymer

melts correspond to "dry (stretched) brushes", i.e., brush layers are substantially unpenetrated by matrix polymer chains, and the brush height proportionally increases with grafting density. As mentioned above, the irreversibly adsorbed polymer chains on solids are considered as the "Guiselin" brushes with many solid/segment contacts ($N^{1/2}$ contacts per chain)[20]. Additionally, we have previously validated that the PS interfacial sublayer does not allow interpenetration of free polymer melt chains even at 170 °C (>> T_g of PS)[18]. It is hence postulated that the inner flattened chains and the outer loosely adsorbed chains composed of the interfacial sublayer can be regarded as dry brushes. If this would be the case, the increases in the film thicknesses of the flattened layers shown in Figure 2-3 and Figure 2-4 indicate the increases in the effective grafting density (i.e., the number of chain attachments per area in irreversible physisorption) of the flattened chains. The increase in the effective grafting density would be the driving force for flattening that is achieved by the energy gain of attached segments to the surface greater than the conformational entropy loss of the adsorbed chains in the total free energy[19,38]. At this point, it is not conclusive yet that the increase in the effective grafting density is correlated to the increase in ϕ_p.

The question arises: When is the formation of the flattened chains initiated on the substrate surface? According to previous simulation results, the time scale for early arriving polymer chains to lie flat on solids is only a few hundred nanoseconds[37, 85-88], which is way beyond our experimental time scale. In fact, we found the formation of a very thin PS adsorbed layer (less than 1 nm in thickness) resulted from spin-casting alone without subsequent thermal annealing, as previously reported[15, 17, 31, 42]. Hence, we expect that the initial (non-equilibrium) flattened chains emerge under solution conditions rather than under melt conditions[11], and the adsorption kinetics of the flattened layer at $t < t_c$ corresponds to a "collapse and zipping-down" process onto solids[53, 54] and the succeeding relaxation and re-arrangement of the flattened conformations toward their

quasiequilibrium states in the melt.

On the other hand, as shown in Figure 2-3, diffusion-controlled adsorption of late arriving chains (i.e., the origin of the loosely adsorbed polymer chains) also takes place at $t < t_c$, but it is retarded due to screening by the flattened chains already present at the surface. As a consequence, the late arriving chains form bridges jointing up nearby empty sites[53]. The competition between the zipping down of the flattened chains and the diffusion-controlled adsorption of the late coming chains continues until $t = t_c$ when the substrate surface is fully covered. At $t > t_c$, the zipping down of the flattened layer formation is over and a "reeling-in" process of the partially adsorbed (late arriving) chains[64] governs. This reeling-in process in the melt is more sluggish due to excluded-volume repulsion of the already existing adsorbed chains and chain entanglements with unadsorbed chains, resulting in the very slow logarithmic growth of the film thickness before achieving the final state (Figure 2-3). As a consequence, the resultant two chain architectures composed of the interfacial sublayer is analogous to those formed via polymer adsorption from a dilute solution[33-36, 43, 44].

In order to further understand the formation mechanism of the flattened layer, we studied the time evolution of the surface morphologies of the P2VP flattened layer by AFM. As shown in Figure 2-6 (a), we clarified that the transient P2VP flattened layer at t_{an} = 65 h and subsequent DMF leaching also shows dimple structures with h_f = 2.3 nm and ϕ_p ~75 % that are nearly identical to those of the PS and PMMA quasiequilibrium flattened layers. As discussed above, the empty spaces of the transient P2VP flattened layer should be the sites where the loosely adsorbed chains grow. Hence, owing to the very strong solid-segment interaction, it is likely that the loosely adsorbed P2VP chains can further collapse and zip down onto the substrate surface[37, 85], transforming into the quasiequilibrium flattened chains (Figure 2-5 (b)). At the same time, this would suggest that the transient flattened chains are still able to move or slide in the lateral

direction in order to accommodate the further zipping down chains. To verify this homogenization process of the flattened layer surface, we used the patchy P2VP flattened layer as a "substrate" for a spin-cast P2VP (50 nm-thick) film. The "bilayer" film of the bottom transient flattened layer and top spin-cast layer was then subject to high temperature annealing at 190 °C for 168 h, which is beyond t_c (= 96 h) for P2VP, and subsequent leaching with DMF. As shown in Figure 2-6 (b), the resultant P2VP flattened layer extracted from the annealed bilayer is found to be homogenous and somewhat thicker (3.9 nm in thickness) than that of the quasiequilibrium P2VP flattened layer shown in Figure 2-5 (b) (3.1 nm in thickness), possibly owing to a further increase in the effective grafting density. It should be noted that we confirmed that the heterogeneous surfaces of the PS and PMMA quasiequilibrium flattened layers shown in Figure 2-2 (a) & Figure 2-5 (a) remain nearly unchanged even after similar bilayer experiments.

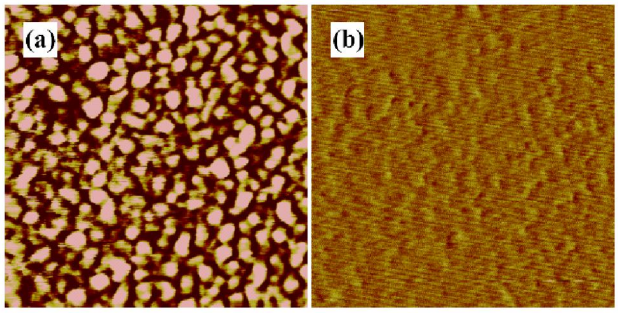

Figure 2 - 6. The AFM phase image of the transient P2VP flattened layer at t_{an} = 65 h is shown in (c). A 50 nm-thick P2VP layer was directly spun cast on top of the transient flattened layer and then subject to thermal annealing at 190 °C for 168 h and subsequent DMF leaching. The surface morphology of the flattened layer resulted from the bilayer is shown in (d). The scan sizes of the images are 1 μm × 1 μm.

Finally, we show the thermal stability of the quasiequilibrium flattened layers. Based on high temperature XR experiments, we found that the quasiequilibrium P2VP flattened layer shows no

significant changes in the thickness up to 200 °C (Figure 2-7). If we use the same definition of T_g as bulk (i.e., a change in a slope in a plot of specific volume against temperature[89]), the XR data indicates that there is no T_g of the P2VP quasiequilibrium flattened layer up to 200 °C, which is far above the bulk T_g (= 98 °C). The same conclusion can be drawn for the PS and PMMA quasiequilibrium flattened layers (Figure 2-7) as well as the transient P2VP flattened layer at t_{an} = 65 h. These findings may be consistent with previous differential scanning calorimetry experiments: No evidence of T_g of intercalated PS chains confined between clay particles within the domain spacing of 3 nm[90]. Hence, the long-range segmental mobility is entirely restricted on the solid surface, while the flattened chains (at least at the transient state) are still able to move laterally, as discussed above. Further experiments on the global chain dynamics of the flattened chains deserve future work.

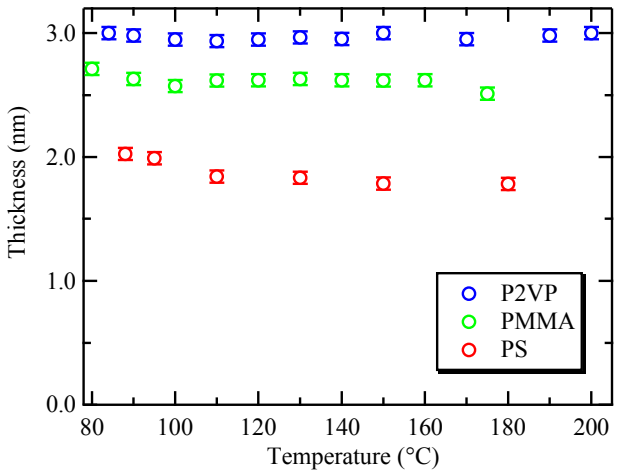

Figure 2 - 7. Film thicknesses of the three polymer flattened layers against temperature determined by the in-situ XR measurements. The XR data was collected during the cooling process and heating processes, and we confirmed that all the temperature dependences of the film thicknesses are independent of the thermal processes.

2.5 Conclusion

We have revealed the effects of solid/segment interactions on the formation of the high-density polymer flattened layers on planar Si substrates via thermal annealing of spin-cast polymer thin films. PS, P2VP, and PMMA homopolymers that have nearly identical stiffness and bulk T_g were chosen as models. The optimization of the thermal annealing and subsequent solvent leaching processes allowed us to unveil the lone flattened layer separately from the loosely adsorbed layer formed at the polymer melt/substrate interface simultaneously. X-ray reflectivity experiments have elucidated that the time growth of the flattened layers composed of the three different polymers exhibit similar power-law growth before reaching the quasiequilibrium state. Since the initial flattened chains are expected to be formed under solution conditions rather than under melt conditions[11,37,84-87], the adsorption kinetics corresponds to the collapse and zipping-down process of the non-equilibrium flattened chains toward the quasiequilibrium state in the melt. The increase in the film thickness indicates that the transient flattened chains prefer to increase attaching points to the substrate so as to overcome the conformational entropy loss at the polymer melt-solid interface[19, 38]. It was also found that as the solid-segment interaction becomes stronger, the thickness of the quasiequilibrium flattened layer increases, while the quasiequilibrium process becomes more sluggish. We are currently investigating the effect of chain stiffness, another crucial factor to control the adsorption kinetics[88], on the formation process of the flattened layer. The details will be published elsewhere.

2.6 References

1. Richardson, H.; Carelli, C.; Keddie, J. L.; Sferrazza, M. *Eur Phys J E* **2003,** 12, (3), 437-440.

2. Reiter, G.; Hamieh, M.; Damman, P.; Sclavons, S.; Gabriele, S.; Vilmin, T.; Raphael, E. *Nat Mater* **2005,** 4, (10), 754-758.

3. Damman, P.; Gabriele, S.; Coppée, S.; Desprez, S.; Villers, D.; Vilmin, T.; Raphaël, E.; Hamieh, M.; Al Akhrass, S.; Reiter, G. *Phys Rev Lett* **2007,** 99, (3), 036101.

4. Ziebert, F.; Raphael, E. *Phys Rev E* **2009,** 79, (3), 10.

5. Thomas, K. R.; Chenneviere, A.; Reiter, G.; Steiner, U. *Phys Rev E* **2011,** 83, (2), 8.

6. Barbero, D. R.; Steiner, U. *Phys Rev Lett* **2009,** 102, (24), 248303.

7. Doi, M.; Edwards, S. F., *The Theory of Polymer Dynamics*. Oxford Science: Oxford, 1986.

8. Thomas, K. R.; Chenneviere, A.; Reiter, G.; Steiner, U. *Phys Rev E* **2011,** 83, (2), 021804.

9. Chung, J. Y.; Chastek, T. Q.; Fasolka, M. J.; Ro, H. W.; Stafford, C. M. *ACS Nano* **2009,** 3, (4), 844-852.

10. Fleer, G. J.; Cohen Stuart, M. A.; Scheutjens, J. M. H. M.; Cosgrove, T.; Vincent, B., *Polymers at Interfaces*. Chapman and Hall: London, 1993.

11. Durning, C. J.; O'Shaughness, B.; Sawhney, U.; Nguyen, D.; Majewski, J.; Smith, G. S. *Macromolecules* **1999,** 32, (20), 6772-6781.

12. Napolitano, S.; Prevosto, D.; Lucchesi, M.; Pingue, P.; D'Acunto, M.; Rolla, P. *Langmuir* **2007,** 23, (4), 2103-2109.

13. Napolitano, S.; Wübbenhorst, M. *J. Phys. Chem. B* **2007,** 111, 9197-9199.

14. Napolitano, S.; Lupascu, V.; Wubbenhorst, M. *Macromolecules* **2008,** 41, (4), 1061-1063.

15. Fujii, Y.; Yang, Z. H.; Leach, J.; Atarashi, H.; Tanaka, K.; Tsui, O. K. C. *Macromolecules* **2009,** 42, (19), 7418-7422.

16. Napolitano, S.; Pilleri, A.; Rolla, P.; Wübbenhorst, M. *Acs Nano* **2010,** 4, (2), 841-848.

17. Napolitano, S.; Wubbenhorst, M. *Nat Commun* **2011,** 2.

18. Koga, T.; Jiang, N.; Gin, P.; Endoh, M. K.; Narayanan, S.; Lurio, L. B.; Sinha, S. K. *Phys Rev Lett* **2011,** 107, (22).

19. Gin, P.; Jiang, N.; Liang, C.; Taniguchi, T.; Akgun, B.; Satija, S. K.; Endoh, M. K.; Koga, T. *Phys Rev Lett* **2012,** 109, (26), 265501.

20. Guiselin, O. *Europhys. Lett.* **1992,** 17, (3), 225-230.

21. Wallace, W. E.; van Zanten, J. H.; Wu, W. L. *Phys. Rev. E* **1995,** 52, R3329-3332.

22. van Zanten, J. H.; Wallace, W. E.; Wu, W. L. *Phys. Rev. E* **1996,** 53, R2053-2056.

23. Zhang, Y.; Ge, S.; Tang, B.; Koga, T.; Rafailovich, M. H.; Sokolov, J. C.; Peiffer, D. G.; Li, Z.; Dias, A. J.; McElrath, K. O.; Lin, M. Y.; Satija, S. K.; Urquhart, S. G.; Ade, H.; Nguyen, D. *Macromolecules* **2001,** 34, (20), 7056-7065.

24. Asada, M.; Jiang, N.; Sendogdular, L.; Gin, P.; Wang, Y.; Endoh, M. K.; Koga, T.; Fukuto, M.; Schultz, D.; Lee, M.; Li, X.; Wang, J.; Kikuchi, M.; Takahara, A. *Macromolecules* **2012,** 45, 7098-7106.

25. Vanroy, B.; Wübbenhorst, M.; Napolitano, S. *ACS Macro Letters* **2013,** 2, (2), 168-172.

26. Zheng, X.; Rafailovich, M. H.; Sokolov, J.; Strzhemechny, Y.; Schwarz, S. A.; Sauer, B. B.; Rubinstein, M. *Phys Rev Lett* **1997,** 79, (2), 241-244.

27. Hu, X.-W.; Granick, S. *Science* **1992,** 258, 1339.

28. Orts, W. J.; Vanzanten, J. H.; Wu, W. L.; Satija, S. K. *Phys Rev Lett* **1993,** 71, (6), 867-870.

29. Zheng, X.; Rafailovich, M. H.; Sokolov, J.; Strzhemechny, Y.; Schwarz, S. A.; Sauer, B., B.; Rubinstein, M. *Phys Rev Lett* **1997,** 79, 241-244.

30. Napolitano, S.; Wubbenhorst, M. *Nat. Commun.* **2011,** 2.

31. Napolitano, S.; Rotella, C.; Wübbenhorst, M. *ACS Macro Letters* **2012,** 1, (10), 1189-1193.

32. Labahn, D.; Mix, R.; Schönhals, A. *Phys Rev E* **2009,** 79, (1), 011801.

33. Johnson, H. E.; Granick, S. *Science* **1992,** 255, (5047), 966-968.

34. Schneider, H. M.; Frantz, P.; Granick, S. *Langmuir* **1996,** 12, (4), 994-996.

35. Soga, I.; Granick, S. *Langmuir* **1998,** 14, (15), 4266-4271.

36. Douglas, J. F.; Johnson, H. E.; Granick, S. *Science* **1993,** 262, (5142), 2010-2012.

37. Linse, P.; Källrot, N. *Macromolecules* **2010,** 43, (4), 2054-2068.

38. Schuetjens, M. H. M.; Fleer, G. J. *J. Phys. Chem.* **1980,** 84, 178.

39. Granick, S. *Eur. Phys. J. E* **2002,** 9, (1), 421-424.

40. Santore, M. M. *Curr Opin Colloid In* **2005,** 10, (3–4), 176-183.

41. Napolitano, S.; Capponi, S.; Vanroy, B. *Eur. Phys. J. E* **2013,** 36, (6), 1-37.

42. Rotella, C.; Napolitano, S.; Vandendriessche, S.; Valev, V. K.; Verbiest, T.; Larkowska, M.; Kucharski, S.; Wubbenhorst, M. *Langmuir* **2011,** 27, (22), 13533-13538.

43. Fu, Z. L.; Santore, M. *Macromolecules* **1999,** 32, (6), 1939-1948.

44. Fu, Z.; Santore, M. M. *Langmuir* **1997,** 13, (21), 5779-5781.

45. Shin, K.; Hu, X.; Zheng, X.; Rafailovich, M. H.; Sokolov, J.; Zaitsev, V.; Schwarz, S. A. *Macromolecules* **2001,** 34, 4993-4998.

46. Wang, Y.; Rafailovich, M.; Sokolov, J.; Gersappe, D.; Araki, T.; Zou, Y.; Kilcoyne, A. D. L.; Ade, H.; Marom, G.; Lustiger, A. *Phys Rev Lett* **2006,** 96, (2), 028303.

47. Kawai, A.; Kawakami, J.; Sasazaki, H. *J Photopolym Sci Tec* **2008,** 21, (6), 739-740.

48. Israelachvili, J. N., *Intermolecular and surface forces: revised third edition*. Academic press: 2011.

49. Kwok, D. Y.; Neumann, A. W. *Adv. Colloid Interface Sci.* **1999,** 81, (3), 167-249.

50. vanZanten, J. H.; Wallace, W. E.; Wu, W. L. *Phys Rev E* **1996,** 53, (3), R2053-R2056.

51. Roth, C. B.; McNerny, K. L.; Jager, W. F.; Torkelson, J. M. *Macromolecules* **2007,** 40, (7), 2568-2574.

52. *Polymer Handbook 4th Ed.* John Wiley & Sons, Inc.: NY, 1999.

53. O'Shaughnessy, B.; Vavylonis, D. *Eur Phys J E* **2003,** 11, (3), 213-230.

54. O'Shaughnessy, B.; Vavylonis, D. *Phys Rev Lett* **2003,** 90, (5), 056103.

55. Seeck, O. H.; Kaendler, I. D.; Tolan, M.; Shin, K.; Rafailovich, M. H.; Sokolov, J.; Kolb, R. *Appl. Phys. Lett.* **2000,** 76, (19), 2713-2715.

56. Koga, T.; Seo, Y. S.; Jerome, J. L.; Ge, S.; Rafailovich, M. H.; Sokolov, J. C.; Chu, B.; Seeck, O. H.; Tolan, M.; Kolb, R. *Appl. Phys. Lett.* **2003,** 83, (21), 4309-4311.

57. Johnson, H. E.; Granick, S. *Macromolecules* **1990,** 23, (13), 3367-3374.

58. Frantz, P.; Granick, S. *Phys Rev Lett* **1991,** 66, (7), 899-902.

59. Frantz, P.; Granick, S. *Macromolecules* **1994,** 27, (9), 2553-2558.

60. Frantz, P.; Granick, S. *Macromolecules* **1995,** 28, (20), 6915-6925.

61. Jack, F. D.; Hildegard, M. S.; Peter, F.; Robert, L.; Steve, G. *Journal of Physics: Condensed Matter* **1997,** 9, (37), 7699.

62. Soga, I.; Granick, S. *Macromolecules* **1998,** 31, (16), 5450-5455.

63. Zhao, J.; Granick, S. *Macromolecules* **2007,** 40, (4), 1243-1247.

64. Zajac, R.; Chakrabarti, A. *Phys Rev E* **1995,** 52, (6), 6536-6549.

65. Buenviaje, C.; Ge, S. R.; Rafailovich, M.; Sokolov, J.; Drake, J. M.; Overney, R. M. *Langmuir* **1999,** 15, (19), 6446-6450.

66. Schneider, H. M.; Granick, S. *Macromolecules* **1992,** 25, (19), 5054-5059.

67. Feder, J.; Giaever, I. *J Colloid Interf Sci* **1980,** 78, (1), 144-154.

68. Onoda, G. Y.; Liniger, E. G. *Phys Rev A* **1986,** 33, (1), 715-716.

69. Adamczyk, Z.; Siwek, B.; Zembala, M. *J Colloid Interf Sci* **1992,** 151, (2), 351-369.

70. Ramsden, J. J. *J Stat Phys* **1993,** 73, (5-6), 853-877.

71. Ramsden, J. J. *Phys Rev Lett* **1993,** 71, (2), 295-298.

72. Adamczyk, Z.; Siwek, B.; Zembala, M.; Belouschek, P. *Adv Colloid Interfac* **1994,** 48, (0), 151-280.

73. Van Tassel, P. R.; Viot, P.; Tarjus, G.; Talbot, J. *The Journal of Chemical Physics* **1994,** 101, (8), 7064-7073.

74. Lai, P. Y.; Binder, K. *The Journal of chemical physics* **1992,** 97, 586.

75. Grest, G. S.; Murat, M. *Macromolecules* **1993,** 26, (12), 3108-3117.

76. O'shea, S.; Welland, M.; Rayment, T. *Langmuir* **1993,** 9, (7), 1826-1835.

77. Yeung, C.; Balazs, A. C.; Jasnow, D. *Macromolecules* **1993,** 26, (8), 1914-1921.

78. Zhao, W.; Krausch, G.; Rafailovich, M.; Sokolov, J. *Macromolecules* **1994,** 27, (11), 2933-2935.

79. Choi, B. C.; Choi, S.; Leckband, D. E. *Langmuir* **2013,** 29, (19), 5841-5850.

80. Ishida, N.; Biggs, S. *Macromolecules* **2010,** 43, (17), 7269-7276.

81. Ishida, N.; Biggs, S. *Langmuir* **2007,** 23, (22), 11083-11088.

82. Carignano, M. A.; Szleifer, I. *The Journal of Chemical Physics* **1994,** 100, (4), 3210-3223.

83. Jones, R. A.; Richards, R. W., *Polymers at Surfaces and Interfaces*. Cambridge University Press: 1999.

84. Aubouy, M.; Fredrickson, G. H.; Pincus, P.; Raphaeel, E. *Macromolecules* **1995,** 28, (8), 2979-2981.

85. Linse, P. *Soft Matter* **2012,** 8, (19), 5140-5150.

86. Källrot, N.; Linse, P. *The Journal of Physical Chemistry B* **2010,** 114, (11), 3741-3753.

87. Källrot, N.; Dahlqvist, M.; Linse, P. *Macromolecules* **2009,** 42, (10), 3641-3649.

88. Källrot, N.; Linse, P. *Macromolecules* **2007,** 40, (13), 4669-4679.

89. Kovacs, A. J. *Adv. Polym. Sci.* **1964,** 3, 394–508.

90. Li, Y.; Ishida, H. *Macromolecules* **2005,** 38, (15), 6513-6519.

Chapter 3: Impact of an Irreversibly Adsorbed Layer on Local Viscosity of Nanoconfined Polymer Melts

3.1 Introduction

It is well known that various properties of polymers confined on a nanometer length scale differ substantially from bulk values. Most of the previous studies have focused on glass transition temperature (T_g), which has been found to be reduced relative to the bulk (see for instance, review [1] and references cited therein). Specifically, Torkelson and co-workers have shown that the decrease in T_g depends on the length scale over which perturbations to T_g originating at the air/polymer interface propagate into a film (the so-called "free-surface effect") [2-4]. In contrast to this concept, Napolitano et al. have recently reported that a very thin irreversibly adsorbed layer at the substrate interface is responsible for the T_g-confinement effect even for very weak polymer-substrate interaction systems [5, 6]. Thus, the effects of these interfacial layers on polymer characteristics still remain a controversial area of research. One of the main reasons for this is due to the lack of experimental techniques that allow us to identify these interfacial layers in single nanoconfined polymer films simultaneously and to further decouple these interfacial effects as a function of the distance from the interfaces. In this Letter, we show that the irreversibly adsorbed layer play a crucial role in determination of the local viscosity of entangled nanoconfined polystyrene (PS) films at temperatures far above the bulk T_g. We use x-ray photon correlation spectroscopy (XPCS) with gold nanoparticles as markers embedded in supported PS thin films which provides the viscosity of polymer chains in the regions of interest [7]. The results reveal that while a surface mobile layer having reduced viscosity exists at the air/polymer interface, the long-range perturbations (~ 60 nm in thickness) associated with the irreversibly adsorbed layer formed onto the weakly interactive substrates result in the significant increase in the viscosity with decreasing the distance from the substrate. Since the formation of the surface mobile layer [7-16] and

irreversibly adsorbed layer [5, 6, 17-23] is rather general, the present experimental findings would shed new light on the impact of the irreversibly adsorbed layer on the local rheological property of polymer chains confined on a nanometer length scale.

3.2 Materials and Methods

3.2.1 Sample Preparation

Hydrogenated polystyrene (hPS, molecular weight (M_w) =123 × 10^3, Pressure Chemical Co.) with a narrow polydispersity (M_w/M_n=1.02) was investigated. Thiol-functionalized (octadecanethiol ($C_{18}H_{37}SH$)) Au nanoparticles were prepared by using the one phase synthesis method [24]. The average radius of the Au particles was 1.5 ± 0.2 nm and the thickness of the $C_{18}H_{37}SH$ layer was approximated to be 1.3 nm [7]. A series of hPS/Au films (the volume fraction of the Au nanoparticles was fixed to be 0.2%) with four different thicknesses (h =32, 57, 128 and 235 nm) were prepared onto hydrogen-passivated silicon (H-Si) substrates [25]. For the present study, all the films were annealed at 170 °C for 90 h under vacuum to ensure the equilibrium. According to a previous report [26], the index of refraction and the film thickness of spin cast PS thin films (thicknesses ranging from 13 nm to 130 nm) decreased by ~ 0.2 (measured by a spectroscopic ellipsometer equipped with a He-Ne laser) and ~ 2 nm , respectively, relative to those of the annealed films at T=160 °C for 2 h after spin-coating. Therefore, we have defined the equilibrium time as the time when these parameters remain unchanged in the course of the annealing process. It is found that the annealing time of about 30 h at T=170°C is needed for the PS/Au thin films to achieve the equilibrium. In addition, it should be noted that this long annealing time is much longer than the "adsorption time" (~ 6.5 h for the PS/Au films used in this study) which has been defined independently to reach a steady state for the conformation of polymer thin films [6]. We also

confirmed that the Au particles were dispersed well in all the films before and after the XPCS experiments using transmission electron microscopy[7, 25] .

3.2.2 Marker grazing incidence XPCS measurements

The marker XPCS experiments were performed at the beam line 8-ID at the Advanced Photon Source, Argonne National Laboratory. We have previously shown [7] that (i) the PS/Au system used in this study has the weak polymer/nanoparticle interaction whereby, the Brownian motion of the markers adequately tracks the viscosity of the polymer matrix via the Stokes-Einstein relationship and (ii) the marker motion is primarily probing entangled dynamics of polymer chains in the regions of interest, although the diameter of the Au nanoparticles (5.6 nm) is somewhat smaller than the tube diameter for entangled PS (about 9 nm) [27]. Hence, the marker XPCS technique enables us to provide the local viscosity of polymer chains governed by chain entanglements. In this study, we explore the in-situ marker dynamics at the topmost surface and the rest of a film (preferentially the near-center region) independently by using the two illuminated modes with different incident angles (θ): (i) $\theta = 0.15^{o}$, which is just below the critical angle (θ_c) of the total external reflection for PS ($\theta_c = 0.16^{o}$ with x-ray energy of 7.5 keV used in this study) such that the electric field intensity (EFI) decays exponentially into the film and thereby scattering intensity is dominated by the surface area of about 9 nm [28]. We assign this experimental configuration as the "surface-mode" hereafter. (ii) With the incident angle just above θ_c known as "the first resonance mode [29]", where resonance enhancement of EFI in a polymer film takes place, and resonance-enhanced x-rays (REX) are intensified at the position close to the center of the film, as shown in Figure 3-1. At the same time, scattering signals from the air/polymer interface can be completely eliminated (Fig.1), improving the sensitivity of using REX to probe the dynamics of the markers. We assign this experimental configuration as the "center-mode" hereafter. All the grazing

incidence XPCS measurements were performed at high temperatures (156°C ≤ T ≤ 186°C) under vacuum so that the so-called "hyperdiffusive dynamic behavior"[30, 31] observed near T_g can be avoided.

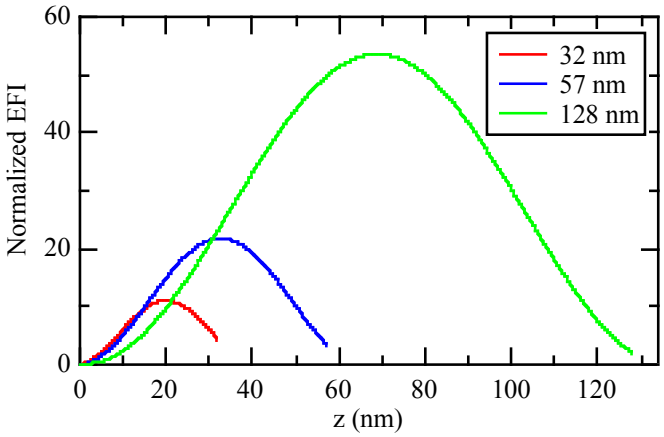

Figure 3 - 1. Calculated REX EFI profiles in the center-mode as a function of the distance (z) from the air/polymer interface for the three film thicknesses. The resonance intensity is normalized by the incident beam intensity.

3.3 Results and Discussions

Representative normalized intensity-intensity time autocorrelation (g_2) functions obtained at four different in-plane scattering vector ($q_{//}$) values for the 57 nm thickness measured at 156°C are shown in Figure 3-2. All the experimental data for the 32 nm and 57 nm films could be fitted by stretched exponential decaying functions (i.e., $g_2(q_{//},t) = 1 + \exp[-2(t/\tau)^{\alpha}]$) with the range of α = 0.4-0.8, where τ and α $(0 < \alpha < 1)$ are the characteristic relaxation time and the stretching exponent that characterizes the shape, respectively. On the other hand, single exponential functions ($\alpha = 1$) were well fitted with all the g_2 functions for the 128 nm [7] and 235 nm films. As will be

discussed later, the differences in α are attributed to the presence of heterogeneous environments within the two thinner films, thereby leading to a wider spectrum of relaxation times.

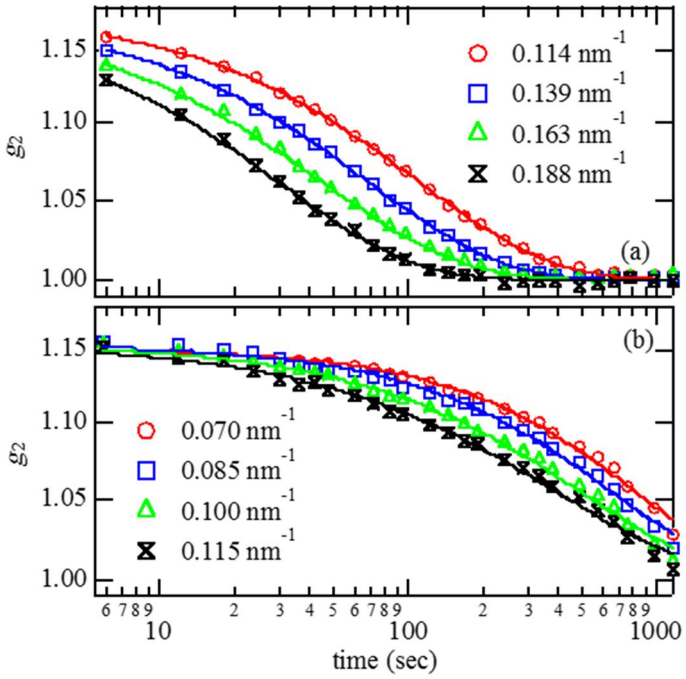

Figure 3 - 2. Measured g_2 functions for the 57 nm film (a) in the surface-mode and (b) center-mode at 156 ºC. The solid lines are the best-fitted functions described in the text.

Figure 3-3 shows the $q_{//}$ dependences of τ for the 57 nm film at 186 °C where we can see the power-law behavior of $\tau \propto q_{//}^{-2}$ for both modes, which is a characteristic of translational diffusive motions of particles and is true for all the temperatures used in this study. As shown in Fig.3, the same power law can be seen in the surface-mode for the 32 nm film, but the τ values are more than two orders of magnitude larger than those for the 57 nm film at the given temperatures. It should be noted that the marker dynamics in the center-mode for the 32 nm film has been observed as

well, but because the correlation times (~ 5000 s) are very close to the resolution of the measurements, quantitative analysis may not be appropriate. Although the relationship of $\tau = 1/(2Dq_{//}^2)$, where D is the diffusion constant, is not strictly valid when the decay of a g_2 function is nonexponential, we use it for the purpose of comparison to other data. From the best-fits to the data (the solid lines in Figure 3-3) with the relationship, the "effective" D values for the surface-mode (D_{sur}) and center-mode (D_{cen}) are calculated. Table 3-1 summarizes the results along with the D values for the 128 nm and 235 nm films where the exponential decay is observed at both modes. From the table we can see that both D_{sur} and D_{cen} values for the 235 nm film are in good agreement with those for the 128 nm film where the difference in these D values is attributed to the reduced viscosity layer at the topmost surface at $T>>T_g$ [7]. Despite some controversy, there is growing experimental evidence of a surface mobile layer [7-16] and recent simulations also support this concept [32]. Hence, our experimental results support these previous studies and further elucidate that the surface reduced viscosity layer exists regardless of film thickness (at least more than 57 nm in thickness) at $T>>T_g$, as discussed below.

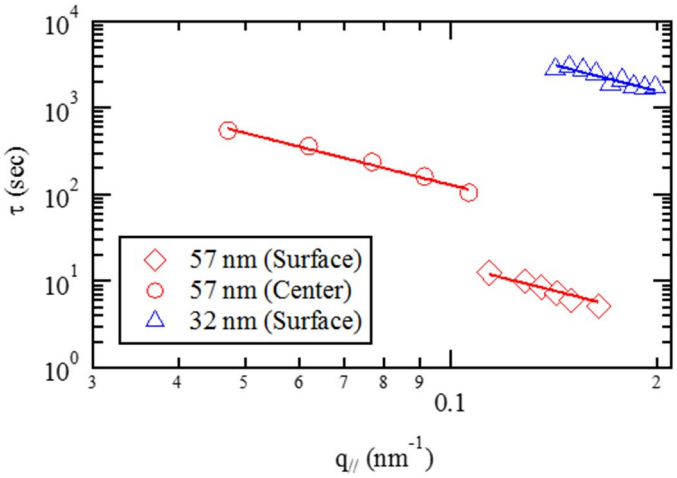

Figure 3 - 3. Log-log plot of τ vs. $q_{//}$ for h = 32 nm and 57 nm in the surface-mode and center-mode at 186 ºC. The solid lines correspond to the best fits of the power law relationship of $\tau \propto q_{//}^{-2}$ to the data.

Table 3 - 1. Measured diffusion coefficients of the Au nanoparticles and calculated viscosities based on the SE law at the surface and the near-center of the films at 186 ºC.

h(nm)	D_{sur}(nm^2/s)	D_{cen}(nm^2/s)	τ_{sur}(Ns/m^2)	τ_{cen}(Ns/m^2)
32	0.016	-#	7.7×10^6	-#
57	6.58	0.76	1.8×10^4	1.6×10^5
128	7.80	5.30	1.5×10^4	2.2×10^4
235	7.84	5.42	1.5×10^4	2.2×10^4

Ultraslow dynamics (the very weak q// dependence of τ)

In order to explore the mechanism for the slowing dynamics of the markers embedded in the 32 and 57 nm films, we next focus on the substrate interface. According to a recent report [20], hPS thin films, which were spun cast on H-Si substrates and then annealed for several hours at 150 °C, showed a very thin residual film even after thoroughly rinsing them with toluene (a good solvent

for PS). In fact, our x-ray reflectivity experiments have proved the presence of the residual layer of about 7 nm in thickness after rinsing all the hPS/Au films with toluene. Furthermore, by using neutron reflectivity, we have measured the interdiffusion process for a bilayer composed of deuterated PS (dPS, M_w=334×10^3, 51 nm in thick) floated onto the residual layer. As shown in Figure 3-4, no interdiffusion was observed for at least 3 days at 170°C. Hence, these experimental results elucidate the existence of the very thin irreversibly adsorbed layer in which no dynamics of the polymer chains is favorable even at T>>T_g.

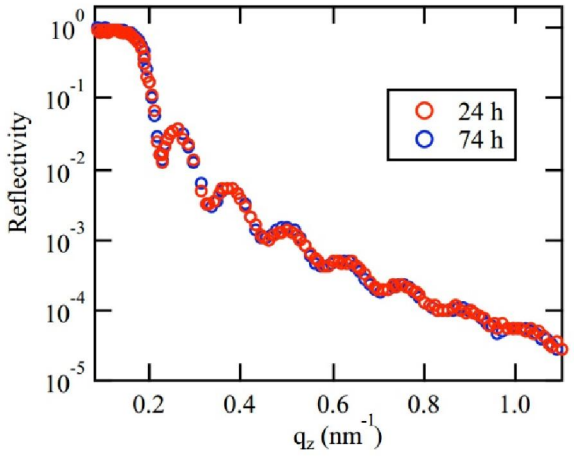

Figure 3 - 4. NR profiles for the bilayer of the bottom hPS dead layer and the dPS overlayer (51 nm in thickness) annealed at 170 ºC in vacuum for the given times, indicating no interdiffusion for at least 3 days at T>>T_g.

Having attained the irreversibly adsorbed layer and established the surface reduced viscosity layer, we further illuminate the effects of the adsorbed layer that plays a dominant role in the slow dynamics. At the distance of approximately 20 nm from the substrate, which is intensified by the center-mode for the 32 nm film, there is almost no dynamics of the markers within the time and

wave vector domains used for XPCS. Since the irreversibly adsorbed layer is only 7 nm in thickness and the contribution to the total scattering signals obtained by the center-mode XPCS is a small portion (see, Figure 3-1), the ultraslow dynamics may not be directly linked to the adsorbed layer. Rather it would arise from the so-called "reduced mobility interface layer" [17, 33, 34], which would be entangled through the network of the adsorbed layer [35], thereby propagating the effect of the irreversibly adsorbed layer even at the distance over the coil size away from the substrate. In addition, as seen in the surface-mode for the 32 nm film, the substrate effect propagates to the surface probed region thoroughly and overwhelms the effect of the surface reduced viscosity layer (if any), giving rise to the very small D_{sur} value (about two orders of magnitude smaller than those of the other thicker films, see Table 3-1). Moreover, we should notice that the marker dynamics in the surface probed region of the 57 nm film is to some extent perturbed by the substrate effect as well, judging from the slight decrease in D_{sur} relative to D_{sur} for the 128 and 235 nm films (Table 3-1). We shall discuss the critical threshold of the long-range perturbations later. It is also important to point out that the present results are quite different from the T_g distributions within PS thin films reported [2-4]: the surface enhanced layer with a large T_g reduction relative to the bulk mainly controls the distributions depending on the extent of nanoconfinement. Hence, the effect of T_g on the heterogeneous dynamics would be ruled out.

Then the question is: what is the origin of the slow dynamics of the markers? As reported previously for PS thin films of about 130 nm in thickness [7], one might expect the dynamics of the markers embedded in the 57 nm film to follow the temperature dependence of the local viscosity in the probed regions, motivated by the Stokes-Einstein (SE) law, i.e., $D = k_B T / (6\pi R_E \eta)$, where k_B is the Boltzmann constant, T is the absolute temperature, and R_E is the effective radius of the Au nanoparticles. Figure 3-5 shows the temperature dependences of the effective local viscosity

values at the surface (η_{sur}) and the near-center (η_{cen}) for the 57 nm film calculated from the SE law with the calculated D values. At the same time, the "average" film viscosity of the hPS/Au film, which is independently determined from thermally driven capillary waves at the air/polymer interface using another XPCS mode ("capillary-mode") [28], is also plotted for comparison. Using the normal hydrodynamic theory for capillary wave fluctuations on viscous (homogeneous) liquid films, Kim et al. have demonstrated that the film viscosity of single PS films, several tens of nanometers in thickness, is in good agreement with the bulk [28]. As seen in Figure 3-5, the η_{sur} values are comparable to the η_{cap} values, while the η_{cen} values are by a factor of about 10 larger. The correspondence between the η_{sur} and η_{cap} values would support the recent experimental report [16] that the surface mobile layer can modify the overall dynamics of ultrathin PS supported films. In other words, this confirms that the marker dynamics in the 57 nm film also tracks the local viscosity reasonably. Moreover, we found that the η_{cap} values for the 57, 128, and 235 nm films remain constant at all the temperatures used, indicating that the same surface mobile layer exists at the topmost surface of the three films. Given this and the somewhat perturbed marker dynamics at the surface of the 57 nm film, we may draw the conclusion that the long-range perturbations associated with the irreversibly adsorbed layer are limited to less than 57 nm from the substrate, resulting in the heterogeneous environment over the surface probed region of the 57 nm film and thereby the nonexponential decay of the g_2 functions (Figure 3-2(a)).

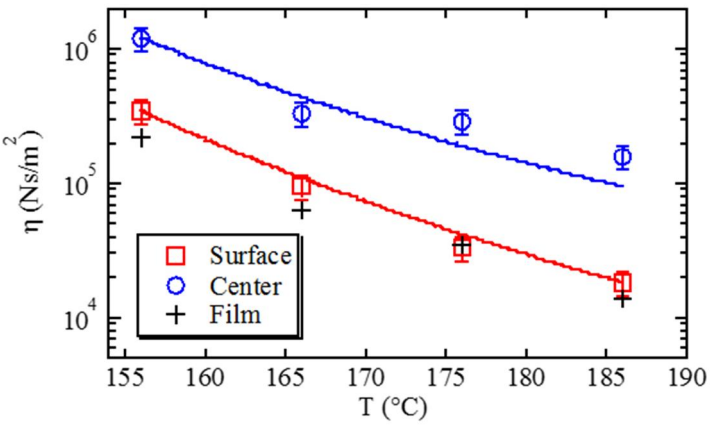

Figure 3 - 5. Temperature dependences of the local viscosity at the surface and near-center of the 57 nm film. The average film viscosity determined from the thermally capillary fluctuations is also plotted (cross symbols). The solid lines correspond to the best-fits of the WLF equation to the data with $c_1 = 4.0 \pm 0.5$ and $T_\infty = 48 \pm 2$ ºC for the surface-mode, and $c_1 = 4.0 \pm 0.5$ and $T_\infty = 65 \pm 2$ ºC for the center-mode, respectively.

The effective η_{sur} and η_{cen} values for each film at 186 ºC are also summarized in Table 1. Hence, we can see that the local viscosity in the different probed regions increases by at least two orders of magnitude with decreasing distance from the substrate interface, which is valid for all the temperatures. In order to interpret this phenomenon, we introduce previous interdiffusion experiments for PS multilayers where a labeled layer of dPS was placed in a matrix of hPS at varying distances from the H-Si substrate interface [36]. Zheng et al. have shown that the diffusion coefficient near the substrate is on the order of 100 times smaller than the bulk and is scaled as $N^{-3/2}$ (N is the degree of polymerization) compared to N^{-2} in the bulk. They conclude that this unusual scaling behavior can be still explained by the reptation theory [37] considering monomer-substrate contacts (~ $N^{1/2}$ per chain) that restrict the chain mobility and modify the friction force from the bulk. Their model may be applicable here with the fact that the $N^{1/2}$ contacts are characteristic of the PS irreversibly adsorbed layer [20] and the viscosity of entangled polymer chains is inversely

proportional to the diffusion coefficient [38]. However, more experimental and theoretical work needs to be done to validate the scaling behavior as well as chain entanglements in terms of the adsorbed layer.

Finally, the above results would remind us of the "percolation transition" in supercooled polymer thin films near T_g [39]. To estimate the local T_g, which may be different from the bulk, we utilized the temperature scaling of the local viscosity. The solid lines in Figure 3-5 correspond to the best-fits to the data with the Williams-Landel-Ferry (WLF) equation [40], $\log(\eta(T)/\eta(T_0)) = -c(T-T_0)/(T-T_\infty)$, where T_0 is a reference temperature chosen, c is a numerical constant, and T_∞ is a fixed temperature at which, regardless of the arbitrary choice of T_0, $\log(\eta(T)/\eta(T_0))$ being infinite. The best-fits of the WLF equation to the data gave us $c = 4.0 \pm 0.5$ and $T_\infty = 48 \pm 2$ ºC for η_{sur}, and $c = 4.0 \pm 0.5$ and $T_\infty = 65 \pm 2$ ºC for η_{cen}, respectively. Hence the T_g values (50 ºC above T_∞ for PS [41]) at the surface and near-center of the 57 nm film are bulk-like (~100 ºC) and 115 ºC, respectively, while a slight decrease in T_g near the center of a supported PS film of about 60 nm thickness was reported by fluorescence label experiments [2]. Although the determination of the full distribution of the T_g values is beyond the scope of this study, it is reasonable to deduce that the phenomenon found in this study occurs at $T >> T_g$.

3.4 Conclusion

The present chapter in this thesis hence points to new physics in our understanding of the effect of confinements on the local viscosity of polymer chains: a very thin irreversibly adsorbed layer plays a vital role even without specific interactions of the polymer with the substrate interface, in contrast to the free-surface effect on T_g. This incongruity may lead to the important conclusion that

the viscosity-confinement effect is not simply linked to the T_g-confinement effect. On the other hand, it is important to address that the critical threshold (~ 60 nm in thickness) for the long-range perturbations associated with the irreversibly adsorbed layer is in good agreement with that for the free-surface effect on T_g (~ 60 nm in thickness for supported PS films regardless of molecular weights [2, 3, 42]). Further XPCS experiments for different polymers (molecular weights, rigidity) and substrates will be carried out to illuminate generalities and/or differences between the viscosity-confinement effect and T_g-confinement effect, providing a better understanding of the global dynamics of polymer chains confined on a nanometer length scale.

3.5 References

1. Forrest, J. A. *Eur. Phys. J. E* **2002,** 8, 261-266.

2. Ellison, C. J.; Torkelson, J. M. *Nature Mater.* **2003,** 2, 695-700.

3. Ellison, C. J.; Mundra, M. K.; Torkelson, J. M. *Macromolecules* **2005,** 38, 1767-1778.

4. Roth, C. B.; McNerny, K. L.; Jager, W. F.; Torkelson, J. M. *Macromolecules* **2007,** 40, 2568-2574.

5. Napolitano, S.; Pilleri, A.; Rolla, P.; Wubbenhorst, M. *ACS Nano* **2010,** 4, 841-848.

6. Napolitano, S.; Wübbenhorst, M. *Nat. Commun.* **2011,** 2, 1259-1266.

7. Koga, T.; Li, C.; Endoh, M.; Koo, J.; Rafailovich, M. H.; Narayanan, S.; Lee, D. R.; Lurio, L.; Sinha, S. K. *Phys. Rev. Lett.* **2010,** 104, 066101.

8. Rudoy, V. M.; Dement'eva, O. V.; Yaminskii, I. V.; Sukhov, V. M.; Kartseva, M. E.; Ogarev, V. A. *Colloid J.* **2002,** 64, 746-754.

9. Teichroeb, J. H.; Forrest, J., A. *Phys. Rev. Lett.* **2003,** 91, 016104.

10. Gasemjit, P.; Johannsmann, D. *J. Polym. Sci., Polym. Phys.* **2006,** 44, 3031-3036.

11. Papaleo, R. M.; Leal, R.; Carreira, W. H.; Barbosa, L. G.; Bello, I.; Bulla, A. *Phys. Rev. B* **2006,** 74, 094203.

12. Sharp, J. S.; Forrest, J. A.; Fakhraai, Z.; Khomenko, M.; Teichroeb, J. H.; Dalnoki-Veress, K. *Eur. Phys. J. E* **2007,** 22, 287-291.

13. Qi, D.; Fakhraai, Z.; Forrest, J. A. *Phys. Rev. Lett.* **2008,** 101, 096101.

14. Fakhraai, Z.; Forrest, J. A. *Science* **2008,** 319, 600-604.

15. Ilton, M.; Qi, D.; Forrest, J. A. *Macromolecules* **2009,** 42, 6851-6854.

16. Yang, Z.; Fujii, Y.; Lee, F. K.; Lam, C.-H.; Tsui, O. *Science* **2010,** 328, 1676-1679.

17. Napolitano, S.; Wubbenhorst, M. *J. Phys. Chem. B* **2007,** 111, 9197-9199.

18. Napolitano, S.; Prevosto, D.; Lucchesi, M.; Pingue, P.; D'Acunto, M.; Rolla, P. *Langmuir* **2007,** 23, 2103-2109.

19. Napolitano, S.; Lupascu, V.; Wubbenhorst, M. *Macromolecules* **2008,** 41, 1061-1063.

20. Fujii, Y.; Yang, Z.; Leach, J.; Atarashi, H.; Tanaka, K.; Tsui, O. *Macromolecules* **2009,** 42, 7418-7422.

21. Rotella, C.; Napolitano, S.; De Cremer, L.; Koeckelberghs, G.; Wubbenhorst, M. *Macromolecules* **2010,** 43, 8686-8691.

22. Rotella, C.; Wubbenhorst, M.; Napolitano, S. *Soft Matter* **2011,** 7, 5260-5266.

23. Napolitano, S.; Rotella, C.; Wubbenhorst, M. *Macromol. Rapid Commun.* **2011,** 32, 844-848.

24. Yee, C. K.; R., J.; A., U.; H., W.; A., K.; M., R.; J., S. *Langmuir* **1999,** 15, 3486-3491.

25. Koga, T. *See supplementary materials for additional references and the details of the materials, methods, NR results.*

26. Hu, X.; Shin, K.; Rafailovich, M.; Sokolov, J.; Stein, R.; Chan, Y.; Williams, K.; Wu, W.; Kolb, R. *High Perform. Polym.* **2000,** 12, 621-629.

27. Graessley, W. W. *J. Polym. Sci. Part B. Polym. Phys.* **1980,** 18, 27-34.

28. Kim, H.; Ruhm, A.; Lurio, L. B.; Basu, J. K.; Lal, J.; Lumma, D.; Mochrie, S. G. J.; Sinha, S. K. *Phys. Rev. Lett.* **2003,** 90, 068302.

29. Wang, J.; Bedzyk, M.; Caffrey, M. *Science* **1992,** 258, 775-778.

30. Guo, H. Y.; Bourret, G.; Corbierre, M. K.; Rucareanu, S.; Lennox, R. B.; Laaziri, K.; Piche, L.; Sutton, M.; Harden, J. L.; Leheny, R. L. *Phys Rev Lett* **2009,** 102, (7).

31. Narayanan, S.; Lee, D. R.; Hagman, A.; Li, X. F.; Wang, J. *Phys Rev Lett* **2007,** 98, (18).

32. Peter, S.; Meyer, H.; Baschnagel, J.; Seemann, R. *J. Phys. Condens. Matter* **2007,** 19, 205119.

33. Wallace, W. E.; van Zanten, J. H.; Wu, W. L. *Phys. Rev. E* **1995,** 52, R3329-3332.

34. van Zanten, J. H.; Wallace, W. E.; Wu, W. L. *Phys. Rev. E* **1996,** 53, R2053-2056.

35. Bruinsma, R. *Macromolecules* **1990,** 23, 276-280.

36. Zheng, X.; Rafailovich, M. H.; Sokolov, J.; Strzhemechny, Y.; Schwarz, S. A.; Sauer, B., B.; Rubinstein, M. *Phys Rev Lett* **1997,** 79, 241-244.

37. Doi, M.; Edwards, S. F., *The Theory of Polymer Dynamics*. Oxford Science: Oxford, 1986.

38. Green, P. F.; Kramer, E. J. *J. Mater. Res.* **1986,** 1, 202-204.

39. Baljon, A.; Billen, J.; Khare, R. *Phys. Rev. Lett.* **2004,** 93, 255701.

40. Williams, M. L.; Landel, R. F.; Ferry, J. D. *J. Am. Chem. Soc.* **1955,** 77, 3701-3707.

41. Ferry, J. D., *Viscoelastic Properties of Polymers*. 4th ed.; Wiley: New York, 1980.

42. Fakhraai, Z.; Forrest, J. A. *Phys. Rev. Lett.* **2005,** 95, 025701.

Chapter 4: Origin of Dewetting of Polymer Thin Films on Solids

4.1 Introduction

Thermodynamic stability or instability of a polymer film on top of a solid is of vital importance in many technologies (e.g., coating, adhesion, corrosion) as well as new emerging nanotechnologies such as organic photovoltaics, semiconductor chips, and biosensors[1]. A thin polymer film can either wet or dewet from a solid surface, depending on several factors including polymer-substrate interfacial energy (or effective interface potential)[2], polarity[3], film thickness[4, 5] and molecular weight[6]. In case of wetting, the thin polymer film remained homogeneous and flat with a zero contact angle with the substrate at equilibrium situation. Otherwise, the film would encounter a dewetting process from the initial rupture and growth of holes, coalescence into polygonal network, to the formation of dewetting droplets with clear three phase contact lines and a non-zero contact angle respect to the solid substrate.[7-9]

In the thermodynamic point of view, two key factors determine whether a thin polymer film would wet or dewet from the solid substrate: effective interface potential (ϕ) and film thickness (h). The effective interface potential is consisted of both short-range repulsion and long-range Van der Waals interactions and describes the total excess free energy of the film system. Based on the curve of the effective interface potential (ϕ) as a function of film thickness (h), one can tell whether the system is stable, metastable or unstable.[10] Spin coated polystyrene (PS) thin films on silicon substrates covered by a natural silicon oxide thin layer are the most commonly used for dewetting study. The effective interface potential, which determines the film stability, can be greatly changed depending on the thickness of the oxide layer on Si.[9, 10] It has been found that the thin PS films are generally in metastable state when prepared on SiO_x/Si substrates when the

thickness of the oxide layer is around 2 – 4 nm. However, even in the metastable case, the as-prepared spin cast PS film may still exhibits a homogeneous flat surface since the fast evaporation of organic solvents during the spin-casting process would force the glassy chains stay far from equilibrium. Hence, thermally annealing at T > Tg of the polymer is necessary to equilibrate the film and therefore induce dewetting. There are mainly two different dewetting mechanism which result in different patterns: (1) spinodal dewetting and (2) nucleation and growth, depending on the thicknesses of both PS film and silicon oxide layer.[11, 12] In case of thin, native SiO_x layers (2 – 4 nm in thickness), dewetting via nucleation and growth is dominate over spinodal dewetting unless the thickness of PS film is extremely thin (i.e. h < 2 nm).[12] Recently studies have shown that the residual stress which generated from film spin coating and fast solvent evaporation process plays a vital role in nucleation and early growth of dewetting holes.[9, 13] However, it seems high molecular weight PS films are more robust against such residual stress due to their higher viscosity.

On the other hand, it has been found solid surfaces can be programed from non-slippery (wettable) to slippery (nonwettable) by controlling the "topmost" surface chemically or structurally. For example, monolayers composed of small molecules or macromolecules are coated on solids to improve surface wettability[14]. On the other hand, in the case of polymer chains grafted to a solid, they repel chemically identical polymer molecules, depending on the grafting density and the ratio of molecular weights of the non-grafted free chains to end-grafted polymer chains (the so-called "autophobic dewetting"[15-20]. It has been proposed that this type of dewetting is originated from the loss of configurational entropy of the grafted polymer chains[15, 21, 22]. As a result, free chains, which penetrate end-grafted polymer chains, cause stretching of the end-grafted chains, resulting in excess interfacial entropy with a negative value between grafted and non-grafted chains[16].

However, despite a large amount of dewetting studies, the understanding of thin polymer film is still puzzling and there are many issues remained unsolved: for instance, how the chain conformations affects the thin film wet or dewet from a substrate interface and what is the difference in mechanism between dewetting from a solid and autophobic dewetting from its own polymer layer. Moreover, aside from inducing dewetting, it is also known that the thermal annealing process could facilitate the irreversible physisorption of polymer chains from the melt to the solid substrate,[23-28] even when the polymer-substrate interaction is weak.[24] It has also been found that the local segmental dynamics near the substrate interface is greatly hindered due to the pinning of the chains.[29, 30]These adsorbed chains can also act as "connectors" that cause a resistance force against the driving capillary forces for dewetting[17, 31]. However, the relation between dewetting of a thin film and the adsorption of polymer chains is still not yet fully understood. In this paper, we show that low molecular weight polystyrene (PS) thin film dewet on both the native silicon oxide (SiO_x/Si) and hydrogen passivated silicon (H-Si) substrate via autophobic dewetting: a ~2 nm-thick flattened interfacial PS nanolayer wets the solid substrate upon annealing while the rest of the same PS molecules is not further wetted by such flattened nanolayer leading to the formation of droplets. However, the dewetting can be effectively prevented by forming a loosely attached interfacial sublayer at the substrate interface. Besides may other factors responsible for the origin of dewetting in the literature, our presented findings evident that the conformation of adsorbed chains at the solid-polymer interface should be considered as an important factor which causes the dewetting of the thin polymer films.

4.2 Materials and Methods

4.2.1 Sample Preparation

Monodisperse PS with eight different molecular weights (M_w = 3.7 kDa, 13.1 kDa, 50 kDa, 123 kDa, 170 kDa, 290 kDa and 650 kDa, $M_w/M_n < 1.2$, Scientific Polymer Products Inc. or Pressure Chemical CO.) were used to study the dewetting behavior on silicon substrates. The bulk glass transition temperature (T_g) of PS was determined to be T_g = 100 °C by differential scanning calorimetry. Native oxide silicon wafers (~ 2 cm × 2 cm squares) (hereafter denoted as SiO_x/Si substrates) were pre-cleaned using a piranha solution (i.e., a mixture of H_2SO_4 and H_2O_2, *caution: a* piranha solution *is highly corrosive upon contact with skin or eyes and is an explosion hazard when mixed with organic chemicals/materials; Extreme care should be taken when handing it*) for 30 min, subsequently rinsed with deionized water thoroughly. By using x-ray reflectivity, we confirmed that the SiO_x layer after piranha solution cleaning is about 2.4 nm thick on the Si with a surface roughness less than 0.5 nm. The water contact angle of such SiO_x/Si substrate is estimated to be less than 5º, an indication of the hydrophilic nature of the surface. Hereafter, we assign the Si substrates cleaned with piranha solution as B-Si substrates. For the hydrogen passivated silicon wafers (hereafter denoted as H-Si substrates), the cleaned native oxide silicon (SiOx/Si) wafers (or B-Si substrates) were further immersed in an aqueous solution of hydrogen fluoride (HF) for 30s to remove the native oxide (SiO_x) layer. However, as will be discussed later, we confirmed that a SiO_x layer of about 1.3 nm in thickness was reproduced after HF etching due to atmospheric oxygen and moisture, as reported previously[32]. All the silicon cleaning were precisely controlled with the same procedure to avoid the possible difference in the chemistry of the oxide layer on the dewetting behavior of the spin coated PS films.[33] PS thin films with average thicknesses ranging from 8 nm to 40 nm were prepared by spin coating PS/toluene solutions onto both B-Si substrates and H-Si substrates with a rotation speed of 2500 rpm. The thicknesses of the spin-cast PS thin films were measured by an ellipsometer (Rudolf Auto EL-II) with a fixed refractive index of 1.589.

On the other hand, the PS flattened layer and interfacial sublayer on B-Si substrates or H-Si substrates were prepared by the established protocol reported previously[34]: Firstly, PS thin films (~ 50 nm in thickness) were annealed at T = 150 °C for prolonged times (up to 150 h) in an oil-free vacuum oven (below 10^{-3} Torr). As reported previously, the "quasiequilibrium" flattened layer and interfacial sublayer[34] were formed prolong annealing (several hours to days) at T = 150 °C, depending on the molecular weight of PS. The annealed films were then solvent leached in baths of fresh chloroform for the flattened layer and toluene for the interfacial sublayer at room temperature, respectively. This selective extraction of the two different adsorbed nanolayers is possible due to the large difference in the desorption energy between the outer loosely adsorbed chains and the flattened chains, which is proportional to the number of segment-surface contacts[35]. The resultant interfacial sublayers and flattened layers were post-annealed at 150 °C under vacuum overnight to remove any excess solvent molecules trapped in the films.

The polymer used was poly (2-vinylpyridine) (P2VP, M_w = 9 kDa, 36 kDa, 219 kDa, M_w/M_n < 1.11, Scientific Polymer Products Inc.). The bulk glass transition temperature (T_g) of P2VP was determined to be T_g = 98 °C by differential scanning calorimetry. The P2VP flattened layer and interfacial sublayer on B-Si substrates were prepared by the established protocol reported previously[34]: Firstly, P2VP thin films (~ 50 nm in thickness) were spun cast from a dimethylformamide (DMF) solution onto Si substrates which were pretreated with a hot piranha solution (i.e., a mixture of H_2SO_4 and H_2O_2) for 30 min and subsequently rinsed with deionized water thoroughly; Secondly, Spin cast films were annealed at T = 190 °C for prolonged times (up to 200 h) in an oil-free vacuum oven (below 10^{-3} Torr). As reported previously, the "quasiequilibrium" flattened layer and interfacial sublayer[34] are formed after 100 h annealing under the isothermal condition. Finally, the films were solvent leached in baths of fresh DMF for

the flattened layer and cholorobenzene for the interfacial sublayer at room temperature, respectively. This selective extraction of the two different adsorbed nanolayers is possible due to the large difference in the desorption energy between the outer loosely adsorbed chains and the flattened chains, which is proportional to the number of segment-surface contacts[35]. The resultant interfacial sublayers and flattened layers were post-annealed at 190°C under vacuum overnight to remove any excess solvent molecules trapped in the films.

4.2.2 X-ray Reflectivity (XR)

X-ray Reflectivity (XR) experiments were performed under vacuum (approximately 10^{-4} - 10^{-5} Torr) at the X10B and X20A beam lines of the National Synchrotron Light Source, Brookhaven National Laboratory. The specular reflectivity was measured as a function of the scattering vector in the direction perpendicular to the surface, $q_z = 4\pi sin\theta/\lambda$, where θ is the incident angle and λ is the X-ray wavelength (λ = 0.087 nm at X10B and λ = 0.118 nm at X20A, which are equivalent to the X-ray energy of 14.2 keV and 10.5 keV, respectively). The XR data was fit by using a standard multilayer fitting routine for a dispersion value (δ in the X-ray refractive index) in conjunction with a Fourier transformation (FT) method, a powerful tool to obtain detailed structures for low X-ray contrast polymer multilayers[36, 37]. In order to study the thermal stability of the flattened layers, we also performed high temperature XR under vacuum by using a custom-built vacuum furnace with Kapton windows. The films were first heated to high temperature (150 °C - 200 °C), and XR measurements were initiated from the cooling process at a temperature interval of 10 °C. Heating and re-cooling experiments were also performed to ensure reproducibility. At given temperatures, we stabilized the films for approximately 1 h before data collection.

4.2.3 Atomic Force Microscopy (AFM) measurements.

Surface morphologies of the adsorbed layers and thin polymer films were studied by using atomic force microscopy (AFM) (Bruker Bioscope Catalyst and Digital Nanoscope III). A standard tapping mode was conducted in air by using a cantilever with a spring constant of about 40 N/m and a resonant frequency of about 300 kHz. The scan rate was 1.0 Hz with a scanning density of 256 or 512 lines per frame.

4.2.4 Polarized Optical Microscope (POM) Measurements.

Polarized optical microscope (POM) measurements were conducted by using reflective light under an Olympus BHT Microscope equipped with differential interference contrast attachment for incident light after Nomarski (NIC Model). POM images were captured by a digital camera under polarized light at room temperature.

4.3 Results and Discussions

Figure 4-1 (a-f) shows representative optical microscopy images for PS (M_w=30kDa, 50 kDa and 123 kDa) 20 nm-thick spin cast films on hydrogen passivated H-Si and B-Si substrates with the annealing time of 120 h. Note that the thickness of SiO_x layer for H-Si and B-Si substrates was 1.3 and 2.4 nm, respectively. The PS thin films composed of M_w = 30kDa and 50 kDa broke up into droplet-based cellular patterns on both two silicon substrate after the course of annealing, indicating the polymers completely dewet from the substrate and aggregated into spherical droplets[7, 38]. However, the degree of dewetting on H-Si substrate slightly reduced compared to B-Si substrates with some non-dewetted regions in between the droplets. Similar dewetting patterns were also observed in 20 nm-thick films with lower molecular weight PS 3.7 kDa and 13.2 kDa.

However, no sign of dewetting was observed in the PS (M_w = 123 kDa) thin films and the same is true for 20 nm-thick PS thin films composed of M_w larger than 123 kDa. To explore the dewetted film structures at the microscopic scale, AFM measurements were performed. Besides the macroscopic droplets observed from optical microscope, as shown in Figure 4-1(g), we found that on H-Si substrate, the dewetted areas (holes) have microscopic "textures" with the characteristic length of about several tenth of nanometer. In addition, the average height of these "textures" from the SiO_x surface was estimated to be about 2 nm based on the cross sectional analysis of Figure 4-1(g). Based on bearing area analysis using the NanoScope Analysis software (version 1.40, Bruker), the surface coverage was estimated to be about 70% (Supporting information). The thickness and the surface morphology of this texture layer remind us of the formation of the "flattened layer" in which the PS chains strongly adsorb on a H-Si substrate, resulting in a higher density monolayer relative to the bulk density[26, 27]. To clarify whether there is chain adsorption occur on the silicon substrate, we leached the dewetted film with toluene at room temperature. The details of the leaching process have been described elsewhere[27]. As we have found, the surface morphology of the 2 nm-thick residue layer are nearly identical to those of the layer underneath the dewetting holes. Similar surface morphology was also found in 30 kDa dewetted PS films. Hence, the experimental data evidences that for lower molecular weight PS (30kDa and 50kDa) thin films on the H-Si substrate, there is a 2 nm-thick flattened layer formed at the solid-polymer melt interface while the rest of the film completely dewetted into macroscopic droplets. Similar results were also observed by Müller-Buschbaum and coworkers, who show that the nano-droplets with average size of 100 nm could be formed simultaneously with the macroscopic droplets, while they never realize the formation of nano-droplets correspond to the irreversible adsorption of polymer chains on the solid substrate with a flattened chain conformation.

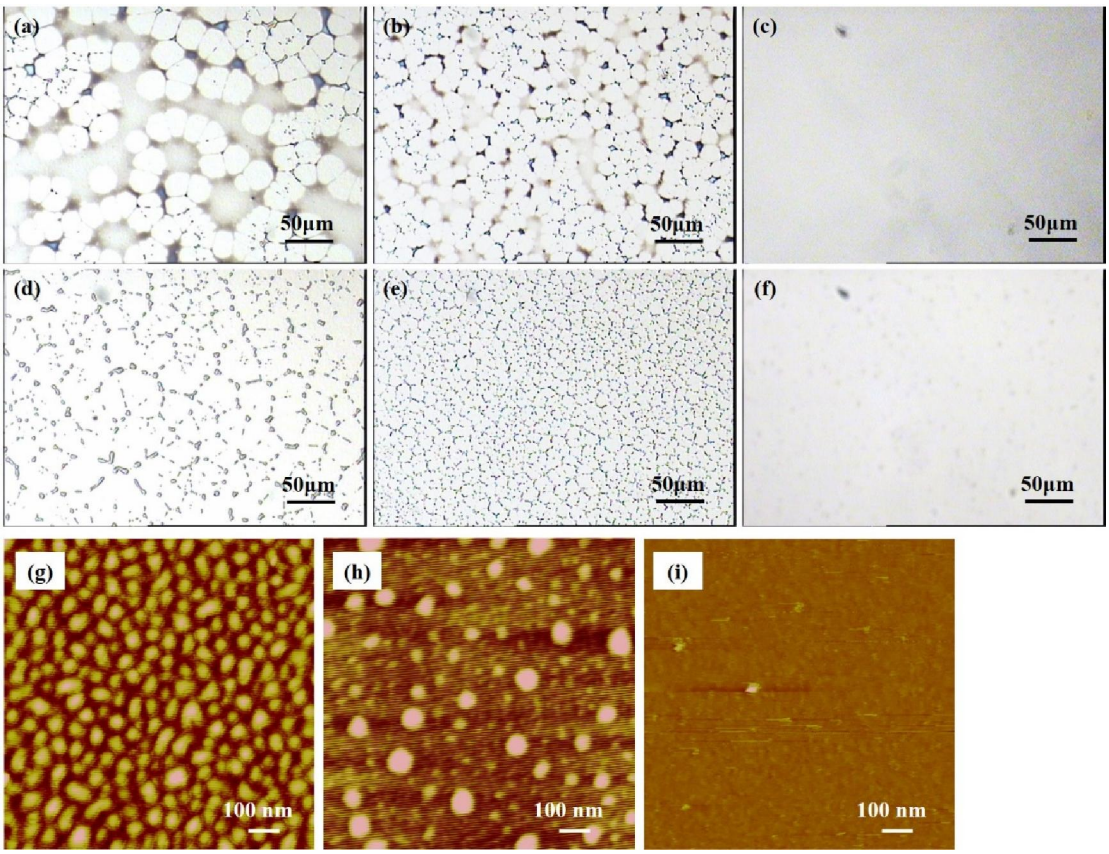

Figure 4 - 1. (a) – (f) shows the POM images of 20 nm-thick PS films on H-Si substrates after thermally annealed at 170 ºC for 120 hours with three different M_w of PS, 30 kDa (a), 50 kDa (b) and 123 kDa (c). (d) – (f) shows the POM images of 20 nm-thick PS films on B-Si substrates after thermally annealed at 170 ºC for 120 hours with three different M_w of PS, 30 kDa (d), 50 kDa (e) and 123 kDa (f). The nanoscale surface morphologies (AFM images) of the dewetted regions in (b) and (e) were shown in (g) and (h), respectively. (i) shows the surface morphologies of a bare Si substrates as a comparison. The height scale for the AFM images is 0 – 10 nm.

In contrast to the H-Si substrate, when the 50 kDa PS film were dewetted on B-Si substrate, the dewetted regions did not appear with dimple-like structures. Instead, as shown in Figure 4-1 (h), large micelles with low surface coverage were observed at the surface with an average height of 12 nm, which corresponds to $2R_g$ of the polymer ($R_{g,\ 50kDa}$ = 6 nm). Since PS is less stable on B-Si substrate, it is reasonable to deduce that polymer chains tend to stay away from the substrate surface with a random chain conformation instead of adsorbed on substrate with a flattened

conformation. On the other hand, in case of the high molecular weight PS thin films, the system appear to be thermally stable and dewetting is not observed even the interaction is very weak. It should be noted that for high M_w PS thin films, there exist the interfacial sublayer at the substrate interface that is composed of the inner flattened layer and outer bulk-like density layer whose thickness increases with increasing M_w[24, 26] (Figure 4-5). As we will show later, the formation of the interfacial sublayer at the substrate interface plays a key role in stabilizing the film.

In order to unveil the correlation between the film stability and interfacial structures, we prepared a series of bilayers composed of the bottom flattened layer or interfacial sublayer and a top overlayer (22 nm in thickness). Since the PS flattened layer is not homogeneous even on the H-Si substrate, we alternatively used poly (2-vinylpyridine) (P2VP, M_w = 219 kDa, M_w/M_n = 1.11, Polysciences Inc.) which enables us to prepare homogenous flattened layers on B-Si substrates[27]. The bottom P2VP flattened layers (~ 3 nm in thickness) were first prepared on the H-Si substrate and the 22 nm-thick overlayers were prepared on the flattened layers by directly spin-coating of a dimethylformamide (DMF) solution. The resultant bilayers were then annealed under vacuum at T=190 °C with different annealing times to study the film stability. Note that the 22 nm-thick P2VP film is stable on the B-Si substrate for at least 192 h under the isothermal condition. Figure 4-2 (a) - (c) show surface morphologies of the 22 nm-thick film on top of the flattened layer at three different t_{an}. We can see that a high number density of dewetting holes were formed within 1 h and the holes grow and coalescent. On the other hand, the 22 nm-thick P2VP film is stable onto the interfacial sublayer (Figure 4-2 (d)) at least t_{an} = 192 h under the isothermal condition. These results reveal that the two different adsorbed nanolayers play opposite roles in controlling the stability of polymer thin films. The dewetting is similar to "autophobic dewetting"[15-20] where polymer chains dewet its own chemically identical grafted chains mainly due to the excess

interfacial entropy generated at the interface between free chains and end-grafted chains. Figure 4-3 summarizes the time evolution of the radius of the hole (r_h) for the bilayer of the layer and flattened layer. From the figure we can see that the growth process is classified into the three-stages: (i) at $t_{an} < 10$ h where the radii of the holes remain nearly constant; (ii) at $10 < t_{an} < 118$ h, the power-law growth ($r_h \sim t_{an}^{0.5}$); (iii) the hole growth saturates at around $r_h = 450$ nm and shows the plateau at $t_{an} > 118$ h. In addition, it should be mentioned that there are no visible rims, characteristic dewetting structures associated with highly elastic nature of a polymer against the driving capillary force[39]. This can be explained by the fact that the radius of the hole is smaller than the critical size ($R_c = hb$, where h and b are the film thickness of the overlayer and the hydrodynamic extrapolation length, respectively) above which the onset of rims is triggered[40]. (notes) The theoretical value of b is given by $b=a(N^3/N_e^2)$, where a is the segment length, N is the degree of polymerization, N_e is the threshold for entanglements) [41]. For the present case with the b value of 156 μm, R_e is estimated to be 1768 nm, which is much lager than the radii of the holes observed in this study. Besides, the depth of the holes from the polymer/air interface is at most 8 nm even at $t_{an} = 150$ h (i.e., the plateau regime), which is still far away from the substrate surface. We also found the thickness dependence of the dewetting, indicating that the dewetting process is governed by slippage[42], while the overall dewetting process (the sizes of the holes and the exponent of the power-law growth) was significantly retarded compared to typical polymer dewetting on non-wettable solid substrates[40, 42-45].

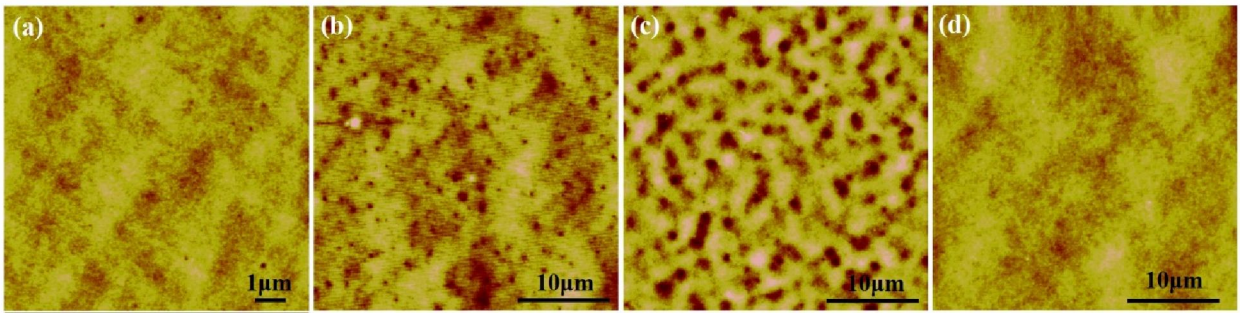

Figure 4 - 2. (a) - (c) The surface morphology (AMF height image) of 22 nm thick P2VP film deposited on P2VP 3 nm-thick equilibrium flattened layer after annealed at 190 ºC for 1 h (a), 60 h (b) and 168 h (c). Dewetting holes are P2V appeared as dark circular regions from the AFM images. (d) The surface morphology of 22 nm thick P film deposited on the P2VP 8 nm-thick interfacial sublayer layer after annealed at 190 ºC for 192 h. The height scale of the AMF images is 0 – 8 nm.

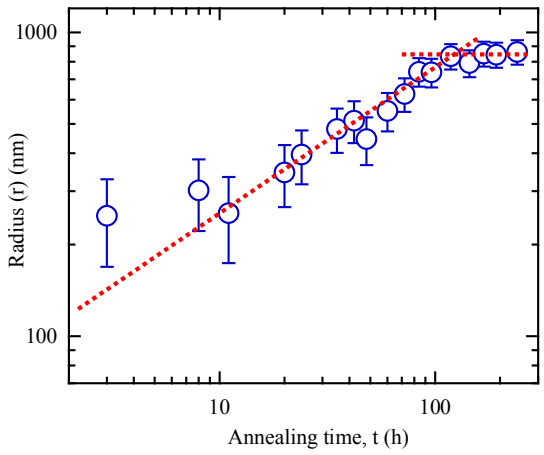

Figure 4 - 3. The change in radius of holes (r_h) as a function of annealing time (t_{an}) at 190 ºC.

Reiter and co-workers demonstrated that autophobicity disappears when long polymer chains are added to a brush (i.e., bimodal brushes): The long polymer chains play a role as "connectors" that cause a resistance force against the driving capillary forces for dewetting[17, 31]. In addition, Composto and co-workers indicated that the dewetting kinetics of polystyrene (PS) thin films can be essentially suppressed when a small amount of PS-*b*-PMMA block copolymer is added[46, 47]. In

order to further discuss the chemically identical polymer/polymer interface, we rinsed the dewetted P2VP bilayers with chlorobenzene which enables us to extract the P2VP interfacial sublayer composed of the bottom flattened chains and the top loosely adsorbed chains. Figure 4-4 shows the thickness of the residue layers after the solvent leaching determined by x-ray reflectivity (XR). From the figure we can see that the thickness of the residual layer remain nearly constant (~ 3 nm) at the early stage ($t_{an} < 10$ h). This corresponds to the thickness of the original flattened layer. On the other hand, at $t_{an} > 10$ h, the thickness of the residual layer increases with increasing t_{an}, demonstrating that the free chains in the top P2VP film start to "reel-in" the empty space of the P2VP flattened layer (less than 10% of the entire film surface)[34], developing the formation of the loosely adsorbed chains that form bridges jointing up nearby empty sites (see, the inset of Figure 4-4)[48]. The comparison with Figure 4-3 illuminates the evidence that the hindrance of the dewetting is correlated with the growth of the loosely adsorbed chains. Hence, we postulate that the loosely adsorbed chains act as connector molecules, in analogue to the autophobicity of end-grafted polymers. It should be emphasized that the chain conformation of the connector is polymer loops. As noted previously[49, 50], polymer loops at the interface can efficiently entangle with free polymer chains when the grafting density is small enough, while resulting in favorable adhesion properties. Furthermore, we can approximate that the loop size of the flattened chains correspond to R_g^{loop} where R_g^{loop} is the radius of polymer gyration of the loop[26]. Based on the critical molecular weight for entanglement (N_e=173 for P2VP)[51], the critical R_g^{loop} is estimated to be 3.6 nm (with the segment length (a) of 0.68 nm[52]) from $R_g=(N/6)^{1/2}a$. Although the chain conformation in the direction normal to the surface is strongly collapsed compared to the bulk R_g for polymer monolayer films[53], it is reasonable to suggest that the flattened layer, whose thickness is less than 4 nm, is not thick enough for entanglements with free chains in the top layer.

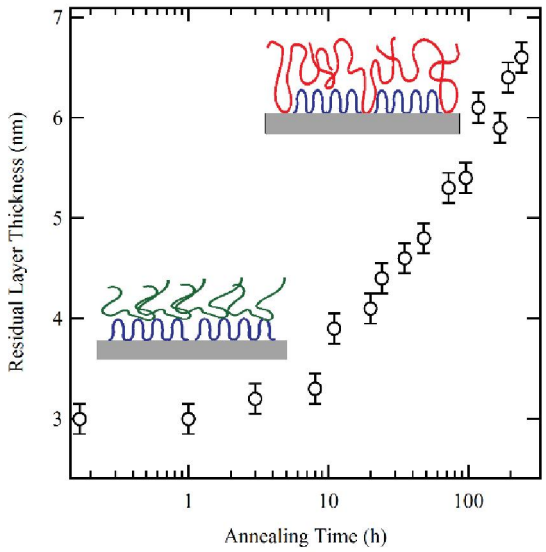

Figure 4 - 4. The change in the residual thickness of the 22 nm thick P2VP film deposited on P2VP 3 nm-thick equilibrium flattened layer after leaching by chlorobenzene as a function of annealing time. The "reel-in" process of loosely adsorbed chains as a function of annealing time is depicted in the inset.

According to Fujii and co-workers, PS films on H-Si substrates should be stable regardless of film thickness (h) since the second derivative of the interfacial energy with respect to h and the spreading coefficient are positive for all values of h[24]. By evidencing the different roles of the flattened chains (slippery) and the loosely adsorbed chains (non-slippery), we now rationalize the mechanism of dewetting of the low M_w PS thin films on H-Si. When the polymer is spun cast onto H-Si substrates, the chains are trapped in a non-equilibrium state due to the rapid solvent evaporation[54]. It was also found that the initial (non-equilibrium) flattened chains on the substrate surface emerge during the spin-casting process[23, 27]. We reported that subsequent thermal annealing at $T>>T_g$ induces accelerates polymer adsorption onto the substrate surface, resulting in the equilibrated flattened layer having many loops[26, 27]. When the polymer chains are short ($Mw\leq$

50 kDa), the formation of the flattened layer on the substrate causes autophobic dewetting at the free polymer chains/flattened layer interface due to the negative excess interfacial entropy and the lack of entanglements there. However, when the molecular weight is large enough (i.e. Mw ≥ 123 kDa in the present case), the loosely adsorbed polymer chains (i.e., loosely loops) are developed at the substrate interface along with the flattened chains (Figure 4-5), acting as connectors to stabilize the interface through the entanglements with free chains. It is known that irreversibly adsorbed polymer chains form three types of segment sequences, "trains" (adsorbed segments), "loops" (sequences of free segments connecting successive trains), and "tails" (non-adsorbed chain ends)[55]. According to previous computational results on chain conformations of adsorbed chains at the polymer melt/solid interface[56], the average number of segments belonging to loops increases (up to ~ 30 %) with increasing N (up to N = 10,000), while that belonging to tails is more dominant (~ 65%). Dadmun and co-workers reported that such loop conformation at the interface plays an important role in improving the interfacial adhesion between different phases.[57-59] Hence, it this reasonable to deduce that the formation of the loops in the loosely adsorbed polymer layers provide structures to which free or unbound polymer chains can entangle, effectively improving the film stability at the solid-polymer melt interfaces.

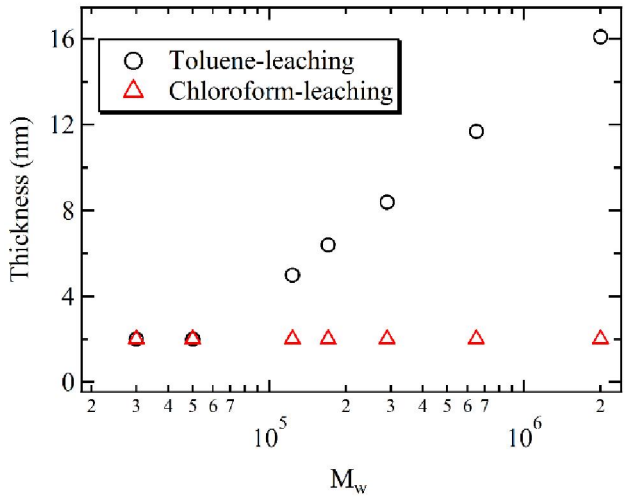

Figure 4 - 5. Thicknesses of the residual PS layers after leaching with toluene (lower desorption energy) or chloroform (higher desorption energy). The original PS films were thermally annealed at 150 ºC for at least 48 h before the leaching process.

4.4 Conclusion

In summary, we have found that when a low M_w PS film dewets on a hydrogen passivated silicon (H-Si) substrate and break into droplet-based cellular patterns, a very thin flattened layer (~ 2 nm in thickness) in which chains are strongly adsorbed on the solid substrate still wets the solid substrate upon annealing. This suggest that the dewetting front of PS film is located at the interface between the matrix chains and the flattened chains and the dewetting mechanism is similar to that of autophobic dewetting. On the other hand, high M_w PS films were stable against dewetting because of the ability to form a loosely adsorbed interfacial sublayer in which chains act as connector molecules to stabilize the film. The wetting/dewetting of P2VP bilayers on native SiOx/Si substrate further suggest that the two different types of interfacial layers, i.e. flattened layer and loosely adsorbed layer, have contrasting roles in thermodynamic stability of polymer films on solid substrate. These unique features enable us to tune the adhesion property of a solid

surface selectively by depositing the the flattened layer or loosely adsorbed layer, which has great potential in the development of coating and antifouling techniques.

4.5 References

1. Geoghegan, M.; Krausch, G. *Prog. Polym. Sci.* **2003,** 28, (2), 261-302.

2. Reiter, G.; Sharma, A.; Casoli, A.; David, M. O.; Khanna, R.; Auroy, P. *Langmuir* **1999,** 15, (7), 2551-2558.

3. Sharma, A. *Langmuir* **1993,** 9, (3), 861-869.

4. Reiter, G. *Phys Rev Lett* **1992,** 68, (1), 75-78.

5. Reiter, G. *Europhys Lett* **1993,** 23, (8), 579-584.

6. Reiter, G. *Phys Rev Lett* **2001,** 87, (18).

7. Reiter, G. *Langmuir* **1993,** 9, (5), 1344-1351.

8. Zhai, X. W.; Weiss, R. A. *Langmuir* **2008,** 24, (22), 12928-12935.

9. Seemann, R.; Herminghaus, S.; Neto, C.; Schlagowski, S.; Podzimek, D.; Konrad, R.; Mantz, H.; Jacobs, K. *J Phys-Condens Mat* **2005,** 17, (9), S267-S290.

10. Seemann, R.; Herminghaus, S.; Jacobs, K. *Phys Rev Lett* **2001,** 86, (24), 5534-5537.

11. Xie, R.; Karim, A.; Douglas, J. F.; Han, C. C.; Weiss, R. A. *Phys Rev Lett* **1998,** 81, (6), 1251-1254.

12. Seemann, R.; Herminghaus, S.; Jacobs, K. *Journal of Physics: Condensed Matter* **2001,** 13, (21), 4925.

13. Reiter, G.; Hamieh, M.; Damman, P.; Sclavons, S.; Gabriele, S.; Vilmin, T.; Raphael, E. *Nat Mater* **2005,** 4, (10), 754-758.

14. Israelachvili, J. N., *Intermolecular and surface forces*. 3rd ed.; Academic Press: San Diego, USA, 2011.

15. Reiter, G.; Auroy, P.; Auvray, L. *Macromolecules* **1996,** 29, (6), 2150-2157.

16. Reiter, G.; Khanna, R. *Phys Rev Lett* **2000,** 85, (26), 5599-5602.

17. Reiter, G.; Khanna, R. *Phys Rev Lett* **2000,** 85, (13), 2753-2756.

18. Voronov, A.; Shafranska, O. *Langmuir* **2002,** 18, (11), 4471-4477.

19. Matsen, M. W.; Gardiner, J. M. *The Journal of Chemical Physics* **2001,** 115, (6), 2794-2804.

20. Zhang, X.; Lee, F. K.; Tsui, O. K. C. *Macromolecules* **2008,** 41, (21), 8148-8151.

21. Leibler, L.; Ajdari, A.; Mourran, A.; Coulon, G.; Chatenay, D., Wetting of Grafted Polymer Surfaces by Compatible Chains. In *Ordering in Macromolecular Systems*, Teramoto, A.; Kobayashi, M.; Norisuye, T., Eds. Springer Berlin Heidelberg: 1994; pp 301-311.

22. Shull, K. R. *Faraday Discussions* **1994,** 98, 203-217.

23. Durning, C. J.; O'Shaughness, B.; Sawhney, U.; Nguyen, D.; Majewski, J.; Smith, G. S. *Macromolecules* **1999,** 32, (20), 6772-6781.

24. Fujii, Y.; Yang, Z. H.; Leach, J.; Atarashi, H.; Tanaka, K.; Tsui, O. K. C. *Macromolecules* **2009,** 42, (19), 7418-7422.

25. Napolitano, S.; Wubbenhorst, M. *Nat Commun* **2011,** 2.

26. Gin, P.; Jiang, N.; Liang, C.; Taniguchi, T.; Akgun, B.; Satija, S. K.; Endoh, M. K.; Koga, T. *Phys Rev Lett* **2012,** 109, (26), 265501.

27. Jiang, N.; Shang, J.; Di, X.; Endoh, M. K.; Koga, T. *Macromolecules* **2014,** 47, (8), 2682-2689.

28. Housmans, C.; Sferrazza, M.; Napolitano, S. *Macromolecules* **2014,** 47, (10), 3390-3393.

29. Koga, T.; Jiang, N.; Gin, P.; Endoh, M. K.; Narayanan, S.; Lurio, L. B.; Sinha, S. K. *Phys Rev Lett* **2011,** 107, (22).

30. Zheng, X.; Rafailovich, M. H.; Sokolov, J.; Strzhemechny, Y.; Schwarz, S. A.; Sauer, B. B.; Rubinstein, M. *Phys Rev Lett* **1997,** 79, (2), 241-244.

31. Reiter, G.; Schultz, J.; Auroy, P.; Auvray, L. *EPL (Europhysics Letters)* **1996,** 33, (1), 29.

32. Shin, K.; Hu, X.; Zheng, X.; Rafailovich, M. H.; Sokolov, J.; Zaitsev, V.; Schwarz, S. A. *Macromolecules* **2001,** 34, 4993-4998.

33. Muller-Buschbaum, P. *Eur Phys J E* **2003,** 12, (3), 443-448.

34. Jiang, N.; Shang, J.; Di, X.; Endoh, M. K.; Koga, T. *Macromolecules* **2014**, in press.

35. O'Shaughnessy, B.; Vavylonis, D. *Phys. Rev. Lett.* **2003,** 90, (5).

36. Seeck, O. H.; Kaendler, I. D.; Tolan, M.; Shin, K.; Rafailovich, M. H.; Sokolov, J.; Kolb, R. *Appl. Phys. Lett.* **2000,** 76, (19), 2713-2715.

37. Koga, T.; Seo, Y. S.; Jerome, J. L.; Ge, S.; Rafailovich, M. H.; Sokolov, J. C.; Chu, B.; Seeck, O. H.; Tolan, M.; Kolb, R. *Appl. Phys. Lett.* **2003,** 83, (21), 4309-4311.

38. Zhai, X.; Weiss, R. A. *Langmuir* **2008,** 24, (22), 12928-12935.

39. Reiter, G. *Phys Rev Lett* **2001,** 87, (18), 186101.

40. Brochard-Wyart, F.; Debregeas, G.; Fondecave, R.; Martin, P. *Macromolecules* **1997,** 30, (4), 1211-1213.

41. de Gennes, P. G. *C. R. Acad. Sci.* **1979,** 288B, 219-222.

42. Reiter, G.; Khanna, R. *Langmuir* **2000,** 16, (15), 6351-6357.

43. Jacobs, K.; Seemann, R.; Schatz, G.; Herminghaus, S. *Langmuir* **1998,** 14, (18), 4961-4963.

44. Becker, J.; Grun, G.; Seemann, R.; Mantz, H.; Jacobs, K.; Mecke, K. R.; Blossey, R. *Nat Mater* **2003,** 2, (1), 59-63.

45. Reiter, G., Visualizing Properties of Polymers at Interfaces. In *Soft Matter Characterization*, Borsali, R.; Pecora, R., Eds. Springer Netherlands: 2008; pp 1243-1292.

46. Costa, A. C.; Composto, R. J.; Vlcek, P. *Macromolecules* **2003,** 36, (9), 3254-3260.

47. Oslanec, R.; Costa, A. C.; Composto, R. J.; Vlcek, P. *Macromolecules* **2000,** 33, (15), 5505-5512.

48. O'Shaughnessy, B.; Vavylonis, D. *Eur Phys J E* **2003,** 11, (3), 213-230.

49. Huang, Z.; Ji, H.; Mays, J. W.; Dadmun, M. D. *Macromolecules* **2008,** 41, (3), 1009-1018.

50. Patton, D.; Knoll, W.; Advincula, R. C. *Macromol Chem Phys* **2011,** 212, (5), 485-497.

51. Creton, C.; Kramer, E. J.; Hadziioannou, G. *Macromolecules* **1991,** 24, 1846-1853.

52. Park, C.-H.; Kim, J.-H.; Ree, M.; Sohn, B.-H.; Jung, J.-C.; Zin, W.-C. *Polymer* **2004,** 45, 4507-4513.

53. Soles, C. L.; Ding, Y. *Science* **2008,** 322, 689-690.

54. Thomas, K. R.; Chenneviere, A.; Reiter, G.; Steiner, U. *Phys Rev E* **2011,** 83, (2), 021804.

55. De Gennes, P.-G., *Scaling concepts in polymer physics*. Cornell university press: 1979.

56. Daoulas, K. C.; Theodorou, D. N.; Harmandaris, V. A.; Karayiannis, N. C.; Mavrantzas, V. G. *Macromolecules* **2005,** 38, (16), 7134-7149.

57. Dadmun, M. *Macromolecules* **1996,** 29, (11), 3868-3874.

58. Eastwood, E. A.; Dadmun, M. D. *Polymer* **2002,** 43, (25), 6707-6717.

59. Eastwood, E. A.; Dadmun, M. D. *Macromolecules* **2002,** 35, (13), 5069-5077.

Chapter 5: Polymer interdiffusion between free chains and interlocking loops in CO_2

5.1 Introduction

Recently, there has been growing interest in the irreversibly adsorbed polymer layer on planar solids due to their strong influence on the physical and mechanical properties of polymeric materials confined at the nanometer scale[1-12], such as organic photovoltaics[13], organic transistors[14], and organic light-emitting diodes[15]. The unique feature of the adsorbed chains that is differentiate from end-grafted polymer chains is loop configurations with $N^{1/2}$ solid-segment contacts[16]. It is expected that the loop conformations at the interface can effectively entangle with matrix polymer chains[17, 18], resulting in improved surface properties[19-23]. For example, Dadmun and co-workers have shown that the adhesion between polymer phases can be improved by introducing polymer loops at the interfaces[20-22]. In addition, due to the physical contacts of polymer repeating units with the solid surface, it has been believed that the adsorbed chains are nearly immobile in air, i.e., no thermal expansion itself[9, 12, 24, 25] and no interdiffusion[8] with the free chains even at a temperature far above the bulk glass transition temperature (T_g) of a polymer. Moreover, many studies have shown the long-range perturbations associated with the "immobile" adsorbed layer in viscosity[8], chain diffusion[26-29], crystalline structures[10] within thin films, which compete against the opposite effect associated with a surface mobile layer at the air/polymer interface[30-33]. It is postulated that chain entanglements between the loop and free polymer chains in a matrix is responsible for the long-range perturbations through the so-called "reduced mobility interface (RMI) layer"[34, 35] where the unadsorbed polymer chains are entropically bound to the loop of the IRA layer via chain entanglements[36, 37] and acts as a "transition zone" to ensure continuity in the mobility profile from the adsorbed layer to the bulk. However, the detailed mechanism behind such a mobility gradient

within a polymer thin film remains unclear due to experimental difficulties to identify such an "interphase" within a single polymer thin film.

In this chapter, we aim to understand a mobility gradient associated with the adsorbed layer within a single polystyrene (PS) thin film by using interdiffusion experiments at the chemically identical (but labeled) polymer/polymer interface in conjunction with solvent annealing. As mentioned above, the mobility of the adsorbed layer is nearly null in air (or vacuum) such that time domains for interdiffusion experimental restricts experimental designs the According to a previous report by Durning et al.[1], irreversibly adsorbed poly(methyl methacrylate) PMMA chains on quartz substrates swell in a good solvent, resulting in a highly stretched chain structure at the substrate interface. Here, we utilize CO_2 as a plasticization agent for PS thin films on planar silicon (Si) substrates since the swelling behavior and dynamics of supported PS thin films in CO_2 have been reported previously[38-44]. It is known that sorption of CO_2 molecules into polymers plays a role as a diluent or plasticizer for glassy polymers by significantly lowering the glass transition temperature (T_g) and hence enhancing the chain mobility[45-48]. Especially, several research groups have shown that the excess sorption of CO_2 molecules takes place within the narrow temperature and pressure regimes near the critical point of CO_2, known as the "density fluctuation ridge"[49], resulting in the anomalous swelling of supported polymer thin films regardless of a choice of polymers[38-41, 43, 50-53]. In addition, it has been shown that the excess sorption of CO_2 molecules leads to the excess interdiffusion at the miscible polymer interface[39]. To monitor the in-situ swelling behavior of the adsorbed PS layer and the interdiffusion between the adsorbed h-PS chains and free d-PS chains in an overlayer, we used a high-pressure neutron reflectivity technique with a custom-built high-pressure cell[40]. As a result, we found that the adsorbed PS layer (12-nm in thickness) swells and interdiffuse (at least at the ridge condition) to some extent in CO_2. At the

same time, we also prepared spin cast h-PS bottom layers with thicknesses of 0.6 R_g, 1R_g, and 2 R_g in place of the adsorbed layer (0.6 R_g thick) and performed similar interdiffusion experiments in CO_2 at the ridge condition. The result is intriguing to illuminate the fact that the diffusion coefficient for the bottom h-PS spin cast 0.6 Rg thick is identical to that for the adsorbed layer, while the interdiffusion is significantly suppressed compared to previous results on bilayers of the top deuterated PS (d-PS) 3Rg thick/bottom h-PS 3 Rg thick film top 3Rg thick film (R_g is the radius of polymer gyration). in CO_2[39]. The NR data reveals that (i) the entire swelling behavior of the 0.6 Rg thick film and interdiffusion of the there is a transition of the interdiffusion dynamics at the polymer/polymer interfaces: The interdiffusion for the bilayers composed of the bottom layers with less than or equal to 2Rg thick is significantly retarded, compared to that composed of the bottom 3Rg thick h-PS layer. As a comparison, we also prepared bilayers of the same d-PS 3R_g thick overlayer on top of the bottom h-PS adsorbed layer (0.6 Rg thick). The NR results indicate that This indicates that at the polymer-polymer interface can be categorized as the three different types: (i) overlayer and the free chains which neither adsorb nor entangle with the adsorbed chains within the bottom spin-cast film; (ii) overlayer and the RMI layer within the bottom spin-cast film; (iii) overlayer and the bottom spin-cast film that is the adsorbed layer.

5.2 Materials and Methods

5.2.1 Sample Preparation

Si wafers were pre-cleaned using a piranha solution (i.e., a mixture of H_2SO_4 and H_2O_2, *caution: a piranha solution is highly corrosive upon contact with skin or eyes and is an explosion hazard when mixed with organic chemicals/materials; Extreme care should be taken when handing it*) for

at least 15 min, subsequently rinsed with deionized water thoroughly, and followed by submersion in an aqueous solution of hydrogen fluoride (HF) to remove a native oxide (SiO_2) layer. However, as will be discussed later, we confirmed that a SiO_2 layer of about 1.3 nm in thickness was reproduced even just after hydrofluoric acid etching due to atmospheric oxygen and moisture, as reported previously[54]. For the *in situ* swelling experiments by using NR, a deuterated polystyrene (d-PS, M_w = 676 kDa, M_w / M_n = 1.1, Polymer Source Inc.) adsorbed monolayer was prepared on hydrogen passivated silicon (H-Si) surfaces (3-inch in diameter). To prepare the adsorbed layer, we reproduced the established protocol[9, 12]: Approximately a 50 nm-thick spin cast film prepared on a H-Si substrate as annealed at 150 ºC (~ T_g + 50 °C) for long time (typically several days) under vacuum below 10^{-3} Torr; the films were then leached in baths of a fresh good solvent (toluene) at room temperature until the resultant film thickness remained constant. According to our recent findings[9, 12], tuning the leaching conditions allows us to prepare two kinds of PS adsorbed monolayers on H-Si substrates as the "quasiequilibrium" state[55]: (i) the "flattened layer" with high-density and (ii) the "interfacial sublayer" composed of the inner flattened layer and outer "loosely adsorbed layer" with bulk like density. In this study, we used only the interfacial sublayers to prevent any artificial effects due to the incomplete surface coverage (~ 70%) of the PS flattened layer[12]. Hereafter we assign the interfacial sublayers as irreversibly adsorbed (IRA) layers unless otherwise stated. After the leaching process, the adsorbed PS IRA layers were dried in a vacuum oven to remove any excess solvent trapped in the films and the thickness was measured at room temperature by using X-ray reflectivity or AutoEL-II ellipsometry (Rudolf Research) before the NR experiments. The film thickness of the d-PS IRA layer was 12 nm, which corresponds to 0.6 Rg (R_g is the radius of polymer gyration). For purposes of comparison, a spin cast d-PS (Mw=676

kDa) film with the same thickness (12 nm) as the IRA layer was also prepared for the *in situ* swelling experiments.

For the interdiffusion NR experiments, hydrogenated PS (h-PS, 650 kDa, $M_w/M_n = 1.1$, Pressure Chemical CO.) and five different molecular weights of d-PS (M_w = 90 kDa, 120 kDa, 334 kDa, 676 kDa, 1323 kDa, $M_w/M_n < 1.2$, Polymer Source Inc.) were used to prepare bilayer films. Bottom h-PS IRA layers were prepared using the same protocol described above. The d-PS overlayers, whose thicknesses were fixed to $3R_g$, were then floated onto the bottom h-PS adsorbed layers from a bath of deionized water. The resultant bilayer films were dried at 60 ºC under vacuum for 24 h to remove residual solvent and water molecules trapped before the interdiffusion experiments. At the same time, interdiffusion process for bilayers of top 3Rg-thick d-PS (with different M_w) films/bottom spin-cast h-PS (Mw=650 kDa) with different film thicknesses (0.6 Rg, 1 Rg, and 2 Rg-thick) were prepared to focus on the long-range propagation of the IRA layer effect at the polymer/polymer interface.

5.2.2 In-situ Neutron Reflectivity (NR)

Specular NR measurements were performed on the NG-7 horizontal reflectometer at the National Institute of Standards and Technology, Center for Neutron Research. The wavelength (λ_N) of the neutron beams was 0.47 nm with $\Delta\lambda_N/\lambda_N$ = 2.5 %. The details of the high-pressure NR experiments including the high-pressure cell have been described elsewhere[40]. The *in situ* swelling experiments were conducted under the isothermal condition (T = 36 °C) with elevated pressures up to P = 17.5 MPa. The temperature and pressure stabilities during the NR measurements were within an accuracy of ± 0.1°C and ± 0.2 %, respectively. The d-PS IRA layer or spin-cast thin films were exposed to CO_2 for up to 4 h prior to data acquisition to ensure the equilibrium swelling. The scattering length density (SLD) of CO_2, which varies from 0.0004×10^{-4} to 2.5×10^{-4} nm^{-2} in

the pressure range of $0.1 < P < 17.5$ MPa at $T = 36$ °C, were calculated based on the density of CO_2 obtained by the equation of state[56]. The NR data was obtained by successively increasing pressure and then slowly decreasing pressure. Since the background scattering from a pure CO_2 phase increases dramatically near the critical point[38, 40], we measured the scattering from the pure fluid phase (i.e., the long-range density fluctuations) for each pressure condition. The NR data corrected for the background scattering was analyzed by comparing the observed reflectivity curves with the calculated ones based on model SLD profiles with three fitting parameters for each layer: film thickness, SLD, and roughness between the layers represented as a Gaussian function[57]. The SLD profiles were subsequently converted into the corresponding polymer volume fraction profiles. Assuming that the concentration of the mixture is homogenous through the entire film, the SLD value of the polymer/CO_2 system is defined by

$$SLD_{mix}(z) = SLD_{polymer} \times \phi(z) + SLD_{SCF} \times (1 - \phi(z)), \quad (1)$$

where SLD_{mix} is the *SLD* value of the mixture at a distance z from the substrate, SLD_{polymer} and SLD_{SCF} are the pure component *SLDs* of the polymer and CO_2, respectively, and $\phi(z)$ is the volume fraction of the polymer at a distance z from the substrate. The density of CO_2 dissolved in the polymer was taken to be 0.956 g/cm^3 since the molar volume of CO_2 within the polymer can be much different from the molar volume of the bulk CO_2[58]. To ensure conservation of mass, the volume fraction profiles were calculated such that the same amount of the polymer chains remained at all solvent concentrations including in the dry state. The interdiffusion experiments were conducted at the CO_2 density fluctuation ridge condition (i.e., $P = 8.2$ MPa at $T = 36$ °C) where the interdiffusion process is maximized due to the excess absorption of CO_2 molecules[39]. We confirmed that the interdiffusion process is much slower than the acquisition time (~ 80 min)

for each NR run. The exposure times used in this study represent the accumulation of the middle time of the respective experiment after we set the CO_2 conditions to the ridge.

5.2.3 X-ray Reflectivity (XR)

To characterize the IRA layers, XR experiments at room temperature were performed at the X10B and X20A beam lines of the National Synchrotron Light Source, Brookhaven National Laboratory. The specular reflectivity was measured as a function of the scattering vector in the perpendicular direction, $q_z = 4\pi sin\theta/\lambda$, where θ is the incident angle and λ is the x-ray wavelength (λ = 0.087 nm at X10B and λ = 0.118 nm at X20A, which are equivalent to the x-ray energy of 14.2 keV and 10.5 keV, respectively). The XR data were fit by using a standard multilayer fitting routine for a dispersion value (δ in the x-ray refractive index) in conjunction with a Fourier transformation method, a powerful tool to obtain detailed structures for low x-ray contrast polymer multilayers[59, 60].

5.2.4 Atomic Force Microscopy (AFM) measurements

The surface morphology of IRA layers were studied by using atomic force microscopy (AFM) (Digital Nanoscope III). A standard tapping mode was conducted in air by using a cantilever with a spring constant of about 40 N/m and a resonant frequency of about 300 kHz. The scan rate was 1.0 Hz with a scanning density of 256 or 512 lines per frame.

5.3 Results and Discussion

5.3.1 Swelling experiments.

Figure 5-1 (a) shows representative NR profiles for the d-PS (M_w=676 kDa) IRA layer (12 nm in thickness) in CO_2 at four different pressures under the isothermal condition (T = 36 °C): P = 0.1 MPa (air), P = 5.5 MPa, P = 8.2 MP, and P = 10 MPa. The thickness of the IRA layer, which was initially 12 nm, slightly increases and reaches to the maximum value of 13 nm at around P = 8.2 MPa, which corresponds to the density fluctuation ridge condition. The linear dilation (S_f) of the IRA layer in the direction normal to the surface was then calculated by the equation, $S_f = (L-L_0)/L_0$, where L and L_0 are the measured thicknesses of the swollen and unswollen IRA layer, respectively. Figure 5-1 (b) summarizes the pressure dependence of the S_f values. We confirmed that the repeated pressurization and depressurization processes exhibit the same swelling behavior. As a comparison, the isothermal swelling curve for the 12-nm thick d-PS (M_w = 676 kDa) spin cast film is also plotted in the figure. Hence it is clear that the entire swelling curve including the anomalous swelling is nearly identical each other, implying that the 0.6 Rg spin-cast film is transformed into the IRA layer via the CO_2 annealing. We previously reported that the anomalous swelling of supported d-PS thin films with the thickness of 1.2 $R_g < L_0 < 8\ R_g$ at the density fluctuation ridge is approximated by the exponential function[38],

$$S_f(T = 36°C, P = 8.2MPa) = 0.11 + 0.37\exp[-0.53L_0/R_g]\ , (2)$$

However, the observed swelling maximum (S_f = 0.08) for the 0.6 R_g thick spin-cast film does not follow the master curve and the excess swelling of the 0.6 R_g spin-cast film is significantly suppressed. While the excess absorption of CO_2 molecules at the CO_2/polymer interface[38-41, 43, 50-53] and polymer/substrate interfaces[51, 61, 62] is expected, the polymer chains strongly confined on the substrate ($L_0 < R_g$) may further increase the segment-solid contacts so as to overcome the conformational entropy loss in the total free energy[63]. According to a previous report by Jia and McCarthy[64], CO_2 interacts with a hydroxyl group on a Si substrate, screening polymer-substrate

interactions. This would be the case for a weakly interacting system such as polycarbonate (PC)/CO_2 system[65]. However, as they also pointed out, when a strong interaction between a polymer and Si substrate is present, the screening effect of CO_2 is not fully achieved. Based on the Owens-Wendt-Kaelble equation[66], the interfacial energy (γ) for PS/H-Si is estimated to be 5.5 mJ/m^2, which is lower than that for PC/bare Si (γ=6.5 mJ/m^2) used in Ref. [65]. Hence, it may be reasonable to suppose that the interaction between PS and H-Si is attractive enough to partially terminate the screening effect of CO_2. We are currently performing NR experiments using different polymer-substrate systems to provide further insight into the screening effect of CO_2. We hence postulate that the excess absorption of CO_2 molecules facilitates polymer adsorption on the solid surface, resulting in the stable polymeric loops on the substrate and inhibiting the chain extension in the direction normal to the substrate surface.

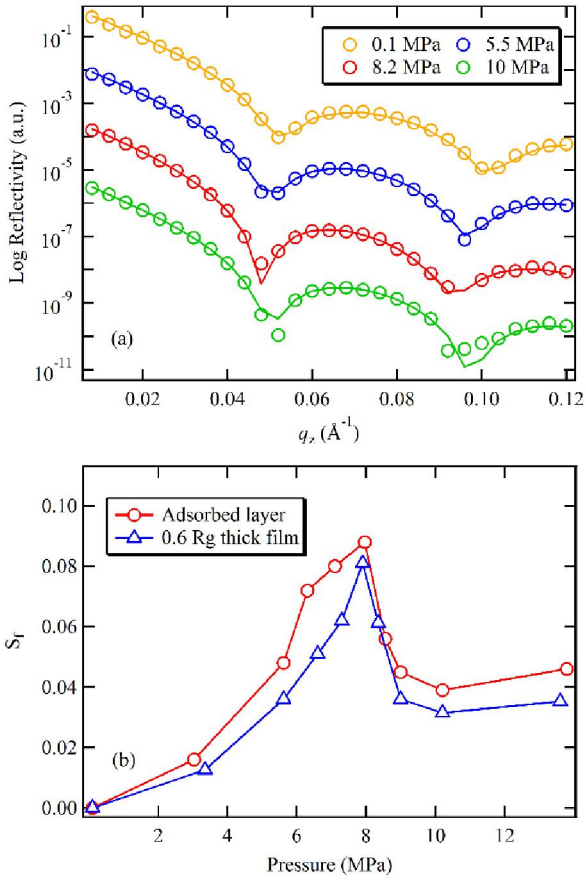

Figure 5 - 1. (a) Representative NR profiles for the d-PS (M_w = 676 kDa) adsorbed layer at the four different pressures at T = 36 °C. The solid lines correspond to the best-fits to the data. Comparison between the pressure dependence of the swelling ratio (S_f) of 0.6 *R*g-thick adsorbed layer and 0.6 *R*g-thick spin cast film is shown in (b).

The present swelling data is different from in-situ XR experiments of PS thin films in CO_2 reported by Gibaud and co-workers. They measured the swelling behavior of about 0.5 Rg and 1.1 Rg thick spin-cast h-PS films on H-Si substrates at $P < P_c$ and T=32 °C[67]. They showed the magnitude of the overall swelling of the 0.5 Rg thick film is much larger than that of the 1.1 Rg thick film. However, it should be also noted that their linear dilation is more than $S_f > 1$ even at around P ~ 6MPa, which is way beyond other experimental reports ($S_f \sim 0.1$) on PS thin films by using in-situ NR[38-41, 52] or in-situ ellipsometry[43] or the bulk behavior[68, 69]. Motivated by their report,

we performed ex-situ XR experiments for the 0.6 Rg thick film after the CO_2 annealing at the ridge and subsequent rapid quench to air pressure (that allows us to preserve the swollen structure via vitrification of the PS chains[39]). As a result, we found the swelling ratio of S_f=0.07, which is in good agreement with the in-situ NR data.

5.3.2 Interdiffusion experiments.

We next focus on the interdiffusion process at the interface between the IRA layer and the overlayer in CO_2. We chose the ridge condition of T = 36 °C and P = 8.2 MPa for the interdiffusion experiments to maximize the plasticization effect of CO_2. Figure 5-2 (a) shows representative NR results for the bilayer composed of the top 3 Rg thick (L_0 = 28 nm) d-PS (M_w = 120 kDa) film and bottom h-PS (M_w = 650 kDa) IRA layer at two different exposure times. From the figure we can see significant changes in the higher order fringes of the NR profiles, indicating the broadening of the interfacial width between the two layers. It should be emphasized that no-interdiffusion takes place for a bilayer of the top d-PS bottom and bottom h-PS IRA layer annealed at 170 ºC for at least 3 days[8]. Based on the best-fits to the data shown in Figure 5-2 (a), the root-mean-square (RMS) roughness (σ) between the two layers were estimated to be 28 ± 4 Å for 1 h exposure and 41 ± 4 Å for 15 h exposure, respectively. Figure 5-2 (b) summarizes σ vs. the CO_2 exposure time for different Mw of the top dPS films. Hence, we find that σ scales linearly with $t^{0.5}$, indicating that diffusion between the two layers follows the Fickian diffusion[70] with an diffusion coefficient (D), $D = \sigma^2/2t$. Hence, we suppose that the observed time domain corresponds to the time after a reputation time[70].

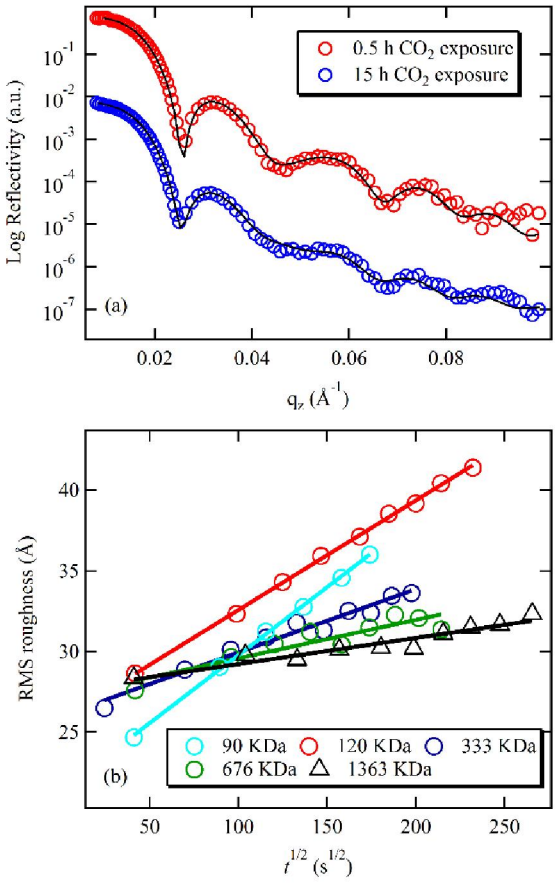

Figure 5 - 2. (a) Observed (circles) and calculated (solid lines) NR profiles of the h-PS (Mw = 650 kDa) adsorbed layer / 3 Rg-thick d-PS (M_w = 120 kDa) bilayer system after CO_2 exposure for 1 h (red) and 15 h (blue) at the density fluctuation ridge condition (P = 8.2 MPa and T =36 °C). (b) Root mean square roughness obtained from the best fits of the NR profiles for the h-PS (M_w = 650 kDa) adsorbed layer / 3 Rg-thick d-PS bilayer systems with five different M_w of d-PS were plotted as a function of exposure time. The solid lines corresponds to the best fits based on the Fickian law, $D = \sigma_{RMS}^2/2t$.

Figure 5-3 plots the D values as a function of M_w of the top d-PS layer on a log-log scale. Compared to our previous interdiffusion experiments for the bilayers of top $3R_g$-thick d-PS films (composed of 94 kDa $\leq M_w \leq$ 699 kDa)/bottom 3 R_g-thick h-PS (M_w = 650 kDa) films[39], the D values are almost 2 orders of magnitude smaller. In addition, we can see the power law behavior ($D \sim M_w^{\alpha}$) with $\alpha \sim -1.1 \pm 0.1$ for the bilayers of the top 3 R_g -thick d-PS films/bottom h-PS IRA

layers. This behavior is quite different from the previous results, exhibiting $\alpha \sim -2.0 \pm 0.1$ which is in agreement with that for entangled polymer melts above T_g[70], while the stronger dependence on molecule weight $\alpha = -2.38$ has been reported in the self-diffusivity of PS chains in CO_2 at the off-ridge condition[71]. Intriguingly, we also found that the bilayers of top 3 R_g-thick d-PS films (with the five different M_w) /bottom 0.6 R_g-thick h-PS (M_w = 650 kDa) spin-cast films exhibit the nearly same D values as those of the bilayers of the 3 R_g-thick d-PS film/h-PS IRA layer (M_w = 650 kDa) in CO_2 (Fig. 3). Thus, these experimental results support that the bottom 0.6 R_g-thick h-PS spin-cast film transforms into the IRA layer via the CO_2 annealing and retarded the interdiffusion of the chemically identical bilayer systems.

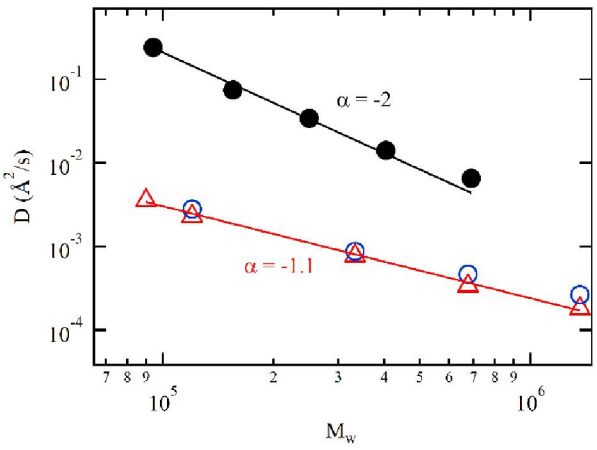

Figure 5 - 3. Molecular weight dependence of the diffusion coefficients, D, obtained from the best fits based on the time dependent root mean square roughness between the bilayer systems. Here, the plotted M_w corresponds to the molecular weight of the top 3 R_g-thick d-PS layers. Three different bottom h-PS layers with the fixed molecular weight (M_w = 650 kDa) were used: 1) 0.6 R_g-thick adsorbed layer (red circles), 2) 0.6 R_g-thick spin cast film (blue circles) and 3) 3 R_g-thick spin cast film (black dots). The data of 3 R_g-thick h-PS / 3 R_g-thick d-PS bilayer systems are reproduced from Ref. 40.

To further clarify the formation process of the IRA layer via the CO_2 annealing, we prepared h-PS (M_w = 650 kDa) spin cast films with the original thicknesses of 2.3 R_g (i.e., 50 nm)-thick on H-Si substrates. The spin-cast films were exposed to CO_2 at the ridge condition with different exposure times and subsequently leached with fresh toluene to remove the unadsorbed chains. Figure 5-4 shows the thickness of the residual layer (h_{ad}) measured by XR as a function of the CO_2 annealing time (t_{CO2}). From the figure we can see the residual layer exhibits a power-law growth ($h_{ad} \propto t_{CO2}^{\beta}$) with β = 0.7 ± 0.1 at the early stage of the adsorption kinetics before the crossover time ($t_C = 2\ h$), when the substrate surface is fully covered [12], and then transfers into a sluggish growth during the late stage. At this point, it is not clear whether this sluggish kinetics follows a logarithmic growth, as seen in the polymer adsorption from the melt [12]. We also confirmed that the overall adsorption kinetics in CO_2 including t_c is almost independent of original film thickness, implying that the plasticization effect of CO_2 at the polymer/substrate interface takes place regardless of the original film thickness, as reported previously[62]. In addition, the resultant residual layer on the H-Si substrate is featureless (i.e., homogenous) after t_c based on AFM measurements (data not shown). Furthermore, as a comparison, we also prepared the adsorbed layers from the same h-PS (M_w = 650 kDa) spin cast films (2.3 Rg thick) via thermal annealing (under vacuum) at T=150 °C. The details of the IRA layer preparation via the thermal annealing has been described elsewhere[12]. The comparison with the thermal annealing process highlights the following characteristics of the adsorption via the CO_2 annealing: (i) the much faster power-law growth at $t < t_c$ for the CO_2 annealing (α = 0.30 ± 0.05 for the thermal annealing); (ii) the weaker logarithmic growth for the CO_2 annealing at $t > t_c$; (iii) the much thinner thickness of the "quasiequilibrium" state at t_{CO2} > 72h (8.0 ± 0.3 nm) compared to that formed via the thermal annealing (12.5 ± 0.3 nm). These differences are related to the combined plasticization effect of

CO_2[42, 62, 64] and screening effect[64] at the polymer/CO_2 interface: The CO_2 molecules would not only enhance the chain mobility but prompts some detachments of the surface-segment contacts. As a result, the desorption energy of the adsorbed chains, which is proportional to the number of segment-solid contacts[72], decreases after the CO_2 annealing, resulting in further reduced film thickness of the CO_2 annealed IRA layer even with the same toluene leaching. Consequently, the CO_2 annealing also induces a similar mobility gradient within the spin-cast film to that reported in thermally annealed films[8, 27]: the long-range perturbations within PS thin films on H-Si substrates persists up to 6-10 R_g from the substrate interface under vacuum.

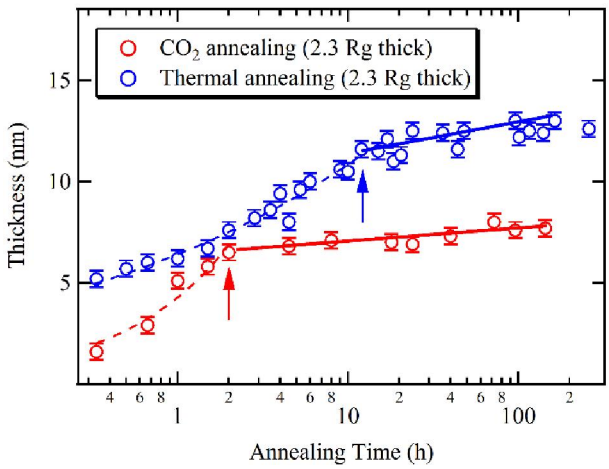

Figure 5 - 4. Comparison of the growth of PS (M_w = 650 kDa) adsorbed layer as a function of time via CO_2 annealing at density fluctuation ridge condition (P = 8.2 MPa and T = 36 °C) (red circle) and thermal annealing at T = 150 °C (blue circle). The dotted lines and the solid lines correspond to the best-fits of the first stage power-law growth and the second stage logarithmic growth, respectively. The crossover times from the power-law growth to logarithmic growth for the adsorbed layers are indicated in the arrows.

In order to determine the critical threshold below which the long-range perturbations exist in the swollen PS/CO_2 film, we also prepared two additional bilayers composed of the same top 3

R_g-thick d-PS (M_w = 333 kDa) overlayers on top of the bottom h-PS (M_w = 650 kDa) spin-cast films with thickness ranging from 1 to 4 R_g-thick. The D values for these bilayers determined by NR are plotted in Figure 5-5 as a function of the scaled original film thickness of the bottom films by R_g. From the figure we can see that the D values gradually increase with increasing the scaled film thickness and a sharp transition occurs between $2R_g$ and $3R_g$. Hence, it is clear that the long-range perturbations is significantly "diluted" by the presence of CO_2 compared to those in air/vacuum such that the results at the polymer/polymer interface distanced the 3 R_g from the substrate surface more closely approximated by the behavior expected for reptating polymer chains. This may be explained by the present finding that the chain entanglements between the loop and entropically bound chains (the reduced mobility interface) is weakened or loosened by the presence of CO_2. At this point, we cannot conclude that this phenomenon is specific to the CO_2 annealing at the ridge condition. Further interdiffusion experiments at off-ridge CO_2 conditions or using different supercritical fluids such as ethane, where similar anomalous swelling related to the density fluctuations occurs[52], or organic solvent vapors[73] need to be done. In addition, high-pressure CO_2 NR studies on other factors (including solid-segment interactions, chain stiffness, molecular weights, polymer-CO_2 interactions) contributing to the long-range perturbations will deserve future work.

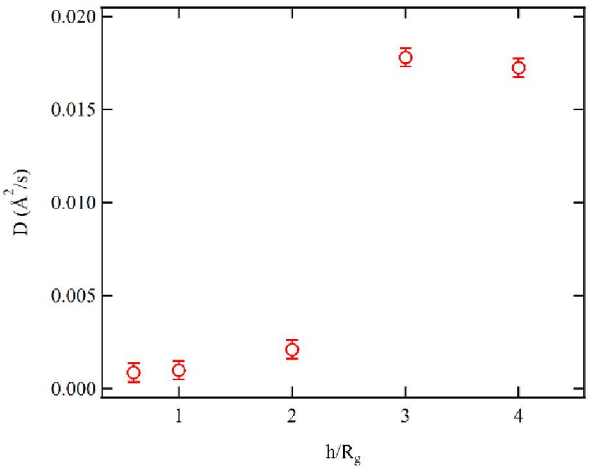

Figure 5 - 5. Estimated diffusion coefficient, D, as a function of the bottom h-PS ((M_w = 650 kDa) layer thickness normalized on the radius of gyration, R_g, of the polymer. The top d-PS (M_w = 333 kDa) layers were fixed with a thickness in the order of 3 R_g.

As discussed above, the diffusion coefficient of d-PS chains across the h-PS IRA layer appeared to approximately scale with inverse molecular weight, in contrast to the well-known scaling in the bulk ($D \propto N^{-2}$) or reported self-diffusivity of PS chains in concentrated solutions of organic solvents[74, 75] or CO_2[71]. While the power law exponent is comparable to that of the bead-friction controlled Rouse behavior[76], the facts that (i) all of the polymer systems examined here exceed the entanglement molecular weight of PS swollen by a low molecular weight solvent (i.e., M_e = 18,000/c, where c is the PS concentration (~ 90%) in the present study based on the NR) and (ii) Fickian diffusion behavior is observed within the experimental time domains (Fig. 2(b)) may rule out the possibility[77]. At the same time, it should be emphasized that the loop conformations of the adsorbed chains are quite different from what they would be in the melt of two miscible polymers. To the best of our knowledge, there are no reports on interdiffusion between polymeric loops and free polymer chains under a mutual enthalpic attraction is involved in the presence of a third component. Zheng and co-workers has previously reported similar significant suppression in D

(about 2 orders of magnitude smaller than the bulk) and a deviation of the power law from the bulk ($D \sim M_w^{-3/2}$) near an attractive substrate interface without solvent molecules[26, 27]. They proposed that this unusual scaling behavior can be still explained by the reptation theory[70] by considering monomer-solid contacts ($\sim N^{1/2}$ per chain) that restrict the chain mobility near the interface and modify the friction force from the bulk. This model may be applicable here with the fact that $N^{1/2}$ contacts are characteristic of the PS IRA layers prepared on H-Si[5]. However, there is still a slight discrepancy in the exponent. It is also interesting to point out that simulation results showed the lateral diffusion coefficient ($D_{//}$) of isolated polymer chains adsorbed on a surface is scaled as $D_{//} \sim N^{-1}$ with and without the presence of solvent molecules[78-80]. Experimentally, adsorbed DNA diffusion on cationic phospholipid bilayers in the fluid phase showed the same N^{-1} dependences[81]. Since the film thickness of the IRA layer is less than Rg, further interdiffusion experiments under other solvent vapors are needed to clarify whether the $N^{1.1}$ dependence is rather general for interdiffusion between the polymeric loops and free chains.

5.4 Conclusion

We have revealed the effect of CO_2 annealing on not only the swelling and interdiffusion of irreversibly adsorbed PS chains on Si substrates but also the polymer adsorption in the solvent. In-situ neutron reflectivity experiments have elucidated that the PS adsorbed layer with 0.6 Rg in thickness swell, but the magnitude of the swelling is strongly suppressed compared to the thicker (3 Rg-thick) films. The swollen adsorbed chains allow interdiffusion with the free chains in CO_2, but the diffusion coefficient is much smaller than the bulk and the power law of D vs. M_w shows the unusual exponent of -1.1. We also found that the spin-cast film with the same film thickness (0.6 Rg) as the adsorbed layer have the nearly identical swelling and interdiffusion behavior. On

the other hand, the CO_2 induced plasticization effect facilitates the formation of the adsorbed layer at the solid-polymer interface. We also found the long-range pertubation of the adsorbed layer can propagate towards the film interior with a distance of at least 2 Rg from the substrate in the presence of CO_2, resulting in a heterogeneous diffusion rate near the substrate interface. Considering the thickness of the adsorbed layer is only 0.6 Rg in CO_2, the long range propagation clearly demonstrate that there is a reduced mobility interface (RMI) layer in which the chains are not in direct contact with the substrate but are connected with the adsorbed chains through entanglement. As a result, the mobility of these "indirect adsorbed" chains is gradually increased as getting father from the substrate, but is still about 10 times slower that the free chains. These findings of the adsorbed layer in the presence of CO_2 are of great importance to gain more direct insight into the heterogeneous dynamics of thin polymer films on a solid substrate. Furthermore, the CO_2–induced plasticization effect on the polymer adsorption from the melt can be used an alternative and more effective method to replace the energy consuming thermal annealing treatment.

5.5 References

1. Durning, C. J.; O'Shaughness, B.; Sawhney, U.; Nguyen, D.; Majewski, J.; Smith, G. S. *Macromolecules* **1999,** 32, (20), 6772-6781.

2. Napolitano, S.; Wübbenhorst, M. *J. Phys. Chem. B* **2007,** 111, 9197-9199.

3. Napolitano, S.; Prevosto, D.; Lucchesi, M.; Pingue, P.; D'Acunto, M.; Rolla, P. *Langmuir* **2007,** 23, 2103-2109.

4. Napolitano, S.; Lupascu, V.; Wubbenhorst, M. *Macromolecules* **2008,** 41, 1061-1063.

5. Fujii, Y.; Yang, Z. H.; Leach, J.; Atarashi, H.; Tanaka, K.; Tsui, O. K. C. *Macromolecules* **2009,** 42, 7418.

6. Napolitano, S.; Pilleri, A.; Rolla, P.; Wübbenhorst, M. *Acs Nano* **2010,** 4, (2), 841-848.

7. Napolitano, S.; Wübbenhorst, M. *Nat Commun* **2011,** 2, 260.

8. Koga, T.; Jiang, N.; Gin, P.; Endoh, M. K.; Narayanan, S.; Lurio, L. B.; Sinha, S. K. *Phys. Rev. Lett.* **2011,** 107, 225901.

9. Gin, P.; Jiang, N.; Liang, C.; Taniguchi, T.; Akgun, B.; Satija, S. K.; Endoh, M. K.; Koga, T. *Phys. Rev. Lett.* **2012,** 109, 265501.

10. Asada, M.; Jiang, N.; Sendogdular, L.; Gin, P.; Wang, Y.; Endoh, M. K.; Koga, T.; Fukuto, M.; Schultz, D.; Lee, M.; Li, X.; Wang, J.; Kikuchi, M.; Takahara, A. *Macromolecules* **2012,** 45, 7098-7106.

11. Asada, M.; Jiang, N.; Sendogdular, L.; Sokolov, J.; Endoh, M. K.; Koga, T.; Fukuto, M.; Yang, L.; Akgun, B.; Dimitriou, M.; Satija, S. K. *Soft Matter* **2014**.

12. Jiang, N.; Shang, J.; Di, X.; Endoh, M. K.; Koga, T. *Macromolecules* **2014,** 47, 2682-2689.

13. Nelson, J. *Mater. Today* **2011,** 14, 462-470.

14. Klauk, H., *Organic Electronics: Materials, Manufacturing and Applications* Wiley-VCH: 2006.

15. Friend, R. H.; Gymer, R. W.; Holmes, A. B.; Burroughes, J. H.; Marks, R. N.; Taliani, C.; Bradley, D. D. C.; Santos, D. A. D.; Brédas, J. L.; Lögdlund, M.; Salaneck, W. R. *Nature* **1999,** 397, 121-128.

16. Guiselin, O. *Europhys. Lett.* **1992,** 17, (3), 225-230.

17. Huang, Z. Y.; Ji, H. N.; Mays, J. W.; Dadmun, M. D. *Macromolecules* **2008,** 41, (3), 1009-1018.

18. Patton, D.; Knoll, W.; Advincula, R. C. *Macromol. Chem. Phys.* **2011,** 212, (5), 485-497.

19. Shull, K. R. *Faraday Discuss.* **1994,** 98, 203-217.

20. Dadmun, M. *Macromolecules* **1996,** 29, (11), 3868-3874.

21. Eastwood, E. A.; Dadmun, M. D. *Polymer* **2002,** 43, (25), 6707-6717.

22. Eastwood, E. A.; Dadmun, M. D. *Macromolecules* **2002,** 35, (13), 5069-5077.

23. Irvine, D. J.; Mayes, A. M.; GriffithCima, L. *Macromolecules* **1996,** 29, (18), 6037-6043.

24. Inoue, R.; Kawashima, K.; Matsui, K.; Kanaya, T.; Nishida, K.; Matsuba, G.; Hino, M. *Phys Rev E* **2011,** 83, (2), 7.

25. Inoue, R.; Nakamura, M.; Matsui, K.; Kanaya, T.; Nishida, K.; Hino, M. *Physical Review E* **2013,** 88, (3), 6.

26. Zheng, X.; Sauer, B. B.; Vanalsten, J. G.; Schwarz, S. A.; Rafailovich, M. H.; Sokolov, J.; Rubinstein, M. *Phys Rev Lett* **1995,** 74, (3), 407-410.

27. Zheng, X.; Rafailovich, M. H.; Sokolov, J.; Strzhemechny, Y.; Schwarz, S. A.; Sauer, B. B.; Rubinstein, M. *Phys Rev Lett* **1997,** 79, (2), 241-244.

28. Lin, E. K.; Wu, W. I.; Satija, S. K. *Macromolecules* **1997,** 30, (23), 7224-7231.

29. Lin, E. K.; Kolb, R.; Satija, S. K.; Wu, W.-l. *Macromolecules* **1999,** 32, (11), 3753-3757.

30. Fakhraai, Z.; Forrest, J. A. *Science* **2008,** 319, 600.

31. Ilton, M.; Qi, D.; Forrest, J. A. *Macromolecules* **2009,** 42, 6851-6854.

32. Yang, Z.; Fujii, Y.; Lee, F. K.; Lam, C.-H.; Tsui, O. *Science* **2010,** 328, 1676.

33. Koga, T.; Li, C.; Endoh, M. K.; Koo, L.; Rafailovich, M. H.; Narayanan, S.; Lee, D. R.; Lurio, L.; Sinha, S. K. *Phys. Rev. Lett.* **2010,** 104, 066101.

34. Wallace, W. E.; Zanten, J. H. c.; Wu, W. L. *Phys. Rev. E* **1995,** 52, R3329.

35. van Zanten, J. H.; Wallace, W. E.; Wu, W. L. *Phys. Rev. E* **1996,** 53, R2053-2056.

36. Bruinsma, R. *Macromolecules* **1990,** 23, 276-280.

37. Zhang, Y.; Ge, S.; Tang, B.; Koga, T.; Rafailovich, M. H.; Sokolov, J. C.; Peiffer, D. G.; Li, Z.; Dias, A. J.; McElrath, K. O.; Lin, M. Y.; Satija, S. K.; Urquhart, S. G.; Ade, H.; Nguyen, D. *Macromolecules* **2001,** 34, (20), 7056-7065.

38. Koga, T.; Seo, Y. S.; Zhang, Y.; Sin, K.; Kusano, K.; Nishikawa, K.; Rafailovich, M. H.; Sokolov, J. C.; Chu, B.; Peiffer, D.; Occhiogrosso, R.; Satija, S. K. *Phys. Rev. Lett.* **2002,** 89, 125506.

39. Koga, T.; Seo, Y. S.; Hu, X.; Kwanwoo, S.; Zhang, Y.; Rafailovich, M. H.; Sokolov, J. C.; Chu, B.; Satija, S. K. *Europhys. Lett.* **2002,** 60, 559.

40. Koga, T.; Seo, Y. S.; Shin, K.; Zhang, Y.; Rafailovich, M. H.; Sokolov, J. C.; Chu, B.; Peiffeer, D.; Satija, S. K. *Macromolecules* **2003,** 36, 5236.

41. Koga, T.; Ji, Y.; Seo, Y. S.; Rafailovich, M. H.; Sokolov, J. C.; Satija, S. K. *J. Polym. Sci., Part B:Polym. Phys.* **2004,** 42, 3282.

42. Meli, L.; Pham, J. Q.; Johnston, K. P.; Green, P. F. *Phys Rev E* **2004,** 69, (5), 8.

43. Li, Y.; park, E.; Lim, K.; Johnston, K. P.; Green, P. F. *J. Polym. Sci., Part B:Polym. Phys.* **2007,** 45, 1313-1324.

44. Chebil, M. S.; Vignaud, G.; Grohens, Y.; Konovalov, O.; Sanyal, M. K.; Beuvier, T.; Gibaud, A. *Macromolecules* **2012,** 45, (16), 6611-6617.

45. Wissinger, R. G.; Paulaitis, M. E. *J. Poly. Sci. Polym. Phys. Ed.* **1987,** 25, 2497-2510.

46. Goel, S. K.; Beckman, E. J. *Polymer* **1993,** 34, 1410-1417.

47. McHugh, M. A.; Krukonis, V., *Supercritical Fluids Extraction Principles and Practice*. Woburn, MA: 1994.

48. Condo, P. D.; Paul, D. R.; Johnston, K. P. *Macromolecules* **1994,** 27, 365-371.

49. Nishikawa, K.; Tanaka, I.; Amemiya, Y. *J. Phys. Chem.* **1996,** 100, 418-421.

50. Sirard, S. M.; J., Z. K.; Sanchez, L. C.; Green, P. F.; Johnston, K. P. *Macromolecules* **2002,** 35, 1928.

51. Li, X. X.; Vogt, B. D. *Polymer* **2009,** 50, (17), 4182-4188.

52. Koga, T.; Gin, P.; Yamaguchi, H.; Endoh, M.; Sendogdular, L.; Kobayashi, M.; Takahara, A.; Akgun, B.; Satija, S. K.; Sumi, T. *Polymer* **2011,** 52, 4331-4336.

53. Mendoza-Galvan, A.; Trejo-Cruz, C.; Solis-Canto, O.; Luna-Barcenas, G. *J. Supercrit. Fluids* **2012,** 64, 25-31.

54. Shin, K.; Hu, X.; Zheng, X.; Rafailovich, M. H.; Sokolov, J.; Zaitsev, V.; Schwarz, S. A. *Macromolecules* **2001,** 34, 4993-4998.

55. Zajac, R.; Chakrabarti, A. *Physical Review E* **1995,** 52, (6), 6536-6549.

56. Huang, F. H.; Li, M. H.; Lee, L. L.; Starling, K. E.; Chung, F. T. H. *J. Chem. Eng. Jpn.* **1985,** 18, 490-496.

57. Russell, T. P. *Mater. Sci. Rep.* **1990,** 5, (4), 171-271.

58. Fleming, G. K.; Koros, W. J. *Macromolecules* **1986,** 19, 2285-2291.

59. Seeck, O. H.; Kaendler, I. D.; Tolan, M.; Shin, K.; Rafailovich, M. H.; Sokolov, J.; Kolb, R. *Appl Phys Lett* **2000,** 76, (19), 2713-2715.

60. Koga, T.; Seo, Y. S.; Jerome, J.; Ge, S.; Rafailovich, M. H.; Sokolov, J. C.; Chu, B.; Seeck, O. H.; Tolan, M.; Kolb, R. *Appl. Phys. Lett.* **2003,** 83, 4309.

61. Li, X. X.; Vogt, B. D. *Macromolecules* **2008,** 41, (23), 9306-9311.

62. Li, X. X.; Vogt, B. D. *J Supercrit Fluid* **2009,** 51, (2), 256-263.

63. Scheutjens, J. M. H. M.; Fleer, G. J. *The Journal of Physical Chemistry* **1980,** 84, (2), 178-190.

64. Jia, X. Q.; McCarthy, T. J. *Langmuir* **2002,** 18, (3), 683-687.

65. Lan, Q.; Yu, J.; Zhang, J.; He, J. *Macromolecules* **2011,** 44, 5743.

66. Kwok, D. Y.; Neumann, A. W. *Colloids Surfaces A: Physicochem. Eng. Aspects* **1999,** 161, (1), 31-48.

67. Chebil, M. S.; Vignaud, G.; Grohens, Y.; Konovalov, O.; Sanyal, M. K.; Beuvier, T.; Gibaud, A. *Macromolecules* **2012,** 45, 6611-6617.

68. Zhang, Y.; Gangwani, K. K.; Lemert, R. M. *J. Supercrit. Fluids* **1997,** 11, 115-134.

69. Chang, S. H.; Park, S. C.; Shim, J. J. *J. Supercrit. Fluids* **1998,** 13, 113-119.

70. Doi, M.; Edwards, S. F., *The Theory of Polymer Dynamics*. Oxford Science: Oxford, 1986.

71. Gupta, R. R.; Lavery, K. A.; Francis, T. J.; Webster, J. R. P.; Smith, G. S.; Russell, T. P.; Watkins, J. J. *Macromolecules* **2002,** 36, (2), 346-352.

72. O'Shaughnessy, B.; Vavylonis, D. *Phys Rev Lett* **2003,** 90, (5), 056103.

73. Thompson, R. L.; McDonald, M. T.; Lenthall, J. T.; Hutchings, L. R. *Macromolecules* **2005,** 38, (10), 4339-4344.

74. Nemoto, N.; Kishine, M.; Inoue, T.; Osaki, K. *Macromolecules* **1990,** 23, (2), 659-664.

75. Nemoto, N.; Kishine, M.; Inoue, T.; Osaki, K. *Macromolecules* **1991,** 24, (7), 1648-1654.

76. Rouse, P. E. *J. Chem. Phys.* **1953,** 21, 1272.

77. Karim, A.; Mansour, A.; Felcher, G. P.; Russell, T. P. *Phys. Rev. B* **1990,** 42, (10), 6846-6849.

78. Lai, P. Y. *Phys. Rev. E* **1994,** 49, 5420.

79. Milchev, A.; Binder, K. *Macromolecules* **1996,** 29, (1), 343-354.

80. Desai, T. G.; Keblinski, P.; Kumar, S. K.; Granick, S. *Phys. Rev. Lett.* **2007,** 98, 218301.

81. Maier, B.; Radler, J. O. *Phys Rev Lett* **1999,** 82, (9), 1911-1914.

Chapter 6: New insight into the architectures and dynamics of macromolecules bound to nanoparticles

6.1 Introduction

Polymer nanocomposites have been of great interest to the broad materials community for at least the last three decades[1]. The addition of nanoparticles (to polymers affects the overall rheological and mechanical properties mainly due to the creation of the nanometer-size "bound polymer layer (BPL)" at the particle surface[2-4]. The most thorough experimental and theoretical studies on BPLs have been carried out for carbon black (CB)-filled rubber systems[5-10]. A few nanometer-thick bound layer (BPL) is typically formed on the CB surface due to a complex combination of physical adsorption, chemi-adsorption and mechanical interlocking and is thus resistant to dissolution even in a good solvent [11]. There seems to be consensus that the thickness of BPL in various polymer nanocomposites is between 1−4 nm[12-16]. In theory, the interactions of polymer chains with the particle surfaces restrict the molecular motion, which correlates with increased resistance to the mechanical deformation (i.e., stiffening), as compared to free polymers that locates away from the particle interface [17]. This was indicated by previous Nuclear Magnetic Resonance (NMR) spectroscopy experiments [18-21] and the particle-particle and the particle-matrix interactions further control the properties of the BPL. In spite of their importance, the formation and optimization of the BPL is still based on empirical know-how strategies [22], since the actual mechanism remain unsolved [21, 23], mainly due to experimental difficulties to gain the chain statistics of bound polymer chains separately from those of free chains in bulk. Furthermore, not all polymer-filler mixtures show m echanical enhancements, raising questions about the length scale over which bound polymer chains interact (entangle) with free chains in a matrix, propagating the structural and dynamical perturbations of the BPL into the film interior.

In this chapter, we report the unique nano-architectures and nanosecond dynamics of the polymer chains bound to CB fillers that would be the origin of the bulk reinforcement property. While the CB fillers typically have large size distributions and fused, aggregated structures[24-26], a modern methodology of neutron scattering techniques with the use of deuterated labeling enables us to highlight the BPL alone. The small-angle neutron scattering (SANS) experiments have revealed that the BPL is composed of the two different density regions with the solvent in the direction normal to the filler surface: the inner unswollen region (~1 nm in thickness) even in a good solvent, and the outer mobile region, which swells to a great extent, show a parabolic concentration profile, as seen in an end-grafted polymer brush in a good solvent [27]. Furthermore, the neutron spin echo (NSE) experiments, which has the highest energy contrast resolution in quasi-elastic neutron scattering and allows us to study the dynamics of mesoscopic objects[28], have shown the collective dynamics of the swollen bound chains on the nanosecond time scale, the so-called the breathing mode [29]. We also found that the collective dynamics of the BPL becomes much faster when the BPL is composed of the same polymer, but larger M_w. This is attributed to an increase in the fraction of polymer loops in the BPL, resulting in more rigid nature of the chains. Hence, the experimental evidences provide new insight into the (microscopic) structure- (reinforcement) property relationship, leading to a great impact to the practical uses as industry relevant materials.

6.2 Materials and Methods

6.2.1 Sample Preparation

The mean radius of the CB filler (R_{TEM}) used in this study was determined to be 40 nm from transmission electron microscopy (TEM) experiments. The density of the CB filler was 1.8 g/cm^3.

The polymer used in this study was monodisperse hydrogenated polybutadiene (h-PB) (weight-average molecular weight (M_w) =39,500, polydispersity (M_w/M_n) =1.04, Polymer Sources). The BPL on the CB filler was prepared as follows: The CB filler was compounded into the h-PB by using a Banbury mixer, heated to T = 150 ºC for 10 min. The CB/h-PB compound was then cut into small pieces and loosely packed in a cage with 200 mesh size. The cage was immersed in a sufficiently large amount of toluene to remove soluble polymer components. The solvent leaching was carried out at room temperature for 72 h until the weight of the CB filler coated with the insoluble rubber (i.e., BPL) remain unchanged. The insoluble rubber component including CB was dried at room temperature for 3 days under vacuum. Based on the TEM data, as shown in Figure 6-1, we confirmed the presence of the BRL with the thickness of 4.5 nm ± 0.5 on the CB filler surfaces. Hereafter we assign the CB fillers with the BPL layer as "BRL-coated CB". To label the BPL for SANS and NSE experiments, deuterated toluene (d-toluene, degree of deuteration of 99.8%, Cambridge Isotope Laboratories, Inc., MA), whose scattering length density ($SLD_{\text{d-toluene}} = 5.7\times10^{-4}\,\text{nm}^{-2}$) is nearly identical to that of CB ($SLD_{\text{CB}} = 6.0\times10^{-4}\,\text{nm}^{-2}$), was used. The BPL-coated CB fillers were then dispersed in d-toluene (the volume fraction of the CB fillers (ϕ) was fixed to 1.8 %) using an ultrasonic cleaner. The concentration was chosen to prevent further aggregation of the CB fillers and increase the scattering intensity. We confirmed that the BPL-coated CB fillers were stable in d-toluene for at least 30 days (i.e., no precipitation).

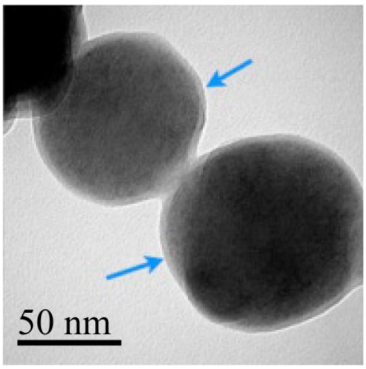

Figure 6 - 1**.** Transmission electron microscope image of the bound hydrogenated polybutadiene (h-PB) layers on carbon black (CB) fillers in a dry state.

6.2.2 Small Angle Neutron Scattering (SANS) and Neutron Spin Echo (NSE)

Small angle neutron scattering (SANS) and neutron spin echo (NSE) experiments were performed at the National Institute of Standards and Technology (NIST) Center for Neutron Research (NCNR). The details of the SANS and NSE experiments have been described elsewhere[30]. The BPL-coated CB/d-toluene solutions were filled in custom-made titanium cells with quartz windows available at NCNR for SANS and NSE experiments. The temperature was controlled by using a water circulation bath system at 25, 50, and 70 °C with accuracy better than 0.1°C. To insure the equilibrium of the systems at the given temperatures, we waited for 1 h prior to the SANS and NSE measurements.

6.3 Results and Discussions

Figure 6-2 (a) shows representative SANS profile from the BPL-coated CB in d-toluene at t = 25 °C. SANS profiles were measured as a function of the scattering vector, $q = (4\pi\sin\theta)/\lambda$, where θ is the incident angle and λ is the neutron wavelength ($\lambda = 0.47$ nm). Since distinct scattering

maxima from a core-shell type form factor were not clearly observed, we instead utilized the Beaucage unified equation[31] for hierarchical structural analysis of nanoparticles by further considering an interfacial width (σ) between the BPL-coated CB and d-toluene[32]:

$$I(q) = Aq^{-\alpha} + B\exp(-q^2 R_{g,BR}/3) + C[\{erf(qR_{g,BR}/\sqrt{6}\}^3/q]^{\beta}\exp(-\sigma^2 q^2), \qquad (1)$$

where $R_{g,BR}$ is the radius of gyration of the entire BPL-coated CB fillers, and α, β, A, B, C are numerical constants. The σ value of 5.3 nm was used based on a previous experimental result on the poly(styrene-*ran*-butadiene) (SBS) BPL formed on CB fillers in toluene[32]. The best-fit to the data (the dotted line in Figure 6-2(a)) at the low-q region gave us the $R_{g,BR}$ value of 57 ± 1 nm. At the same time, the bare CB fillers (without the BPL) dispersed into d-toluene was characterized by using small-angle x-ray scattering (SAXS) at the beamline x27C, National Synchrotron Light Source (Upton). The same analysis using eq. (1) (without the interfacial contribution) demonstrated that the radius of gyration ($R_{g,CB}$) of the pure CB fillers was determined to be 49 ±1 nm, which is 1.6 times larger than that of the primary CB particles ($R_{g,TEM} = \sqrt{(3/5)}R_{TEM}$=31 nm). Based on the volume consideration, it is reasonable to deduce that about 4 ($=(R_{g,CB}/R_{g,TEM})^3$) CB primary particles are fused together into the "dispersible unit" that are the fundamental unit of the CB fillers [24, 25]. The total thickness of the bound rubber layer (l_{BR}) is therefore estimated to be 8 nm from $l_{BR} = R_{g,BR} - R_{g,CB}$. This result indicates that the BPL (the thickness in the dry state is about 5 nm) swells in the good solvent, as previous reported[32]. Note that no significant temperature dependence of the structures was observed.

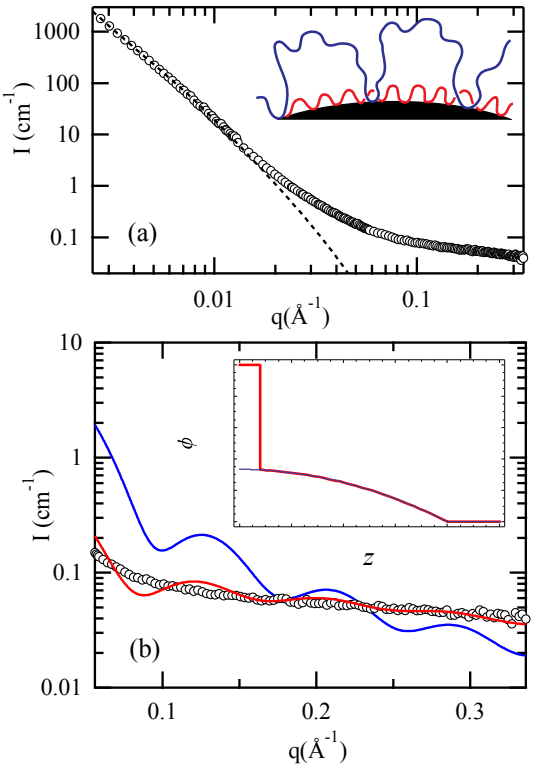

Figure 6 - 2**.** (a): SANS profile of the BPL (Mw = 39.5kDa)-coated CB in d-toluene at 25 °C. In the inset, the schematic view of the two different chain conformations is shown. (b): SANS profile after subtraction of the filler scattering expressed by eq. (1). The solid lines correspond to the calculated scattering profiles based on the volume fraction profile shown in the inset.

Another important feature of the SANS profile is the excess scattering at the high q region (i.e., the deviation from eq. 1). This implies the presence of a shorter length scale concentration fluctuation in the BPL. Figure 6-2 (b) shows the excess scattering (indicated in circles) after subtraction of the scattering component expressed by eq. (1) from the observed SANS data. In order to further analyze the data, two assumptions were made: (i) the CB fillers were approximated as a "planar" geometry since the size of the CB dispersible unit by far exceeds the BPL thickness; (ii) the swollen PBL has the following volume fraction profile $\phi(z)$, as predicted by the self-consistent mean-field theory for a end-grafted polymer chain in a good solvent [33]:

$$\phi(z) = \begin{cases} \phi_0[1-(z/L)^2], & z < L \\ 0, & z > L \end{cases} \quad (2)$$

where ϕ_0 is the polymer volume fraction at $z = 0$ (i.e., the substrate surface), L is the cut-off thickness of the swollen BPL layer. The static scattering function $S(q)$ from the BPL is then given by

$$S(q) = F(q)^2 = \left\{ \int_0^L \phi(z)\exp(iqz)\,dz \right\}, \quad (3)$$

where $F(q)$ is the scattering amplitude of the BPL. In addition, a tail was also introduced to fit the data by convoluting eq. (3) with a normalized Gaussian function [27]. As shown in Figure 6-2 (b), the calculated scattering function (indicated in blue) based on the volume fraction model (the blue line shown in the inset of Figure 6-2 (b)) is inappropriate to describe the experimental result. Instead, motivated by previous experimental [15] and computational [34] results, a two-layer structural model (shown in the inset of Figure 6-2 (a)) with the inclusion of a very thin less swollen adsorbed layer next to the filler surface was examined. As a result, it was found that the fitting result based on the two-layer model (the red line shown in the inset of Figure 6-2 (b) could fit the experimental data satisfactorily (the red line in Figure 6-2 (b)), while further consideration of a polydispersity of the BPL thickness is needed to explain the absence of fringes of the observed excess scattering profile. The fitting results indicate that the inner region of 0.7 nm in thickness does not contain the solvent, while the polymer chains in the outer region are expanded parabolically (the inset of Figure 6-2 (b)). In addition, this picture is reminiscent of the picture developed for polymer adsorption from melts onto planer substrates [35, 36], as schematically shown in the inset of Figure 6-2(a): polymer molecules arriving first on the surface are adsorbed with a flat conformation,

forming the inner high-density region, while late-coming chains, which find less free surface areas, adsorb loosely onto the substrate, developing the outer bulk-like density region. It should be noted that it is not straightforward for the presence study to quantify the density of the inner flattened layer since the neutron scattering contrast between the two layers is also developed due to the difference in the swelling ratio.

Next, we aim to investigate the dynamics of the bound polymer chains by using NSE. Figure 6-3 shows representative NSE data for the BPL-coated CB in d-toluene at 50 °C. $I(q,t)/I(q,0)$ corresponds to the normalized intermediate scattering function, i.e., the dynamic structure factor. From the figure we can see that even at the largest q value (q=1.52 nm^{-1}), the scattering functions are not fully relaxed at the Fourier times of up to 20 ns. This plateau-like behavior might suggest the presence of an immobile polymer layer near the CB surface, as reported by NMR experiments[18-20]. However, the NSE data clearly shows that the plateau depends on q, indicating that the polymer chains are still mobile in the solvent[37]. Hence, the overall dynamic structure factor including the tail at long decay times can't be explained by the polymer (segmental) chain dynamics in a solvent, such as the Zimm model [38] and Rouse model [39]. Rather, we postulate that the dynamics is attributed to collective motions of the adsorbed polymer chains[40-42]. On the theoretical side, de Gennes elucidated the collective relaxation processes of physically adsorbed polymer chains in a good solvent, i.e., the breathing longitudinal mode [29]. From the experimental point of view, collective dynamics of end-grafted polymer chains in a good solvent has been observed by using scattering techniques[40-42]. The typical feature of the collective motions is the fast and slow decays in the dynamic structure factor, as observed in Figure 6-3. Motivated by these results, we analyzed the NSE data.

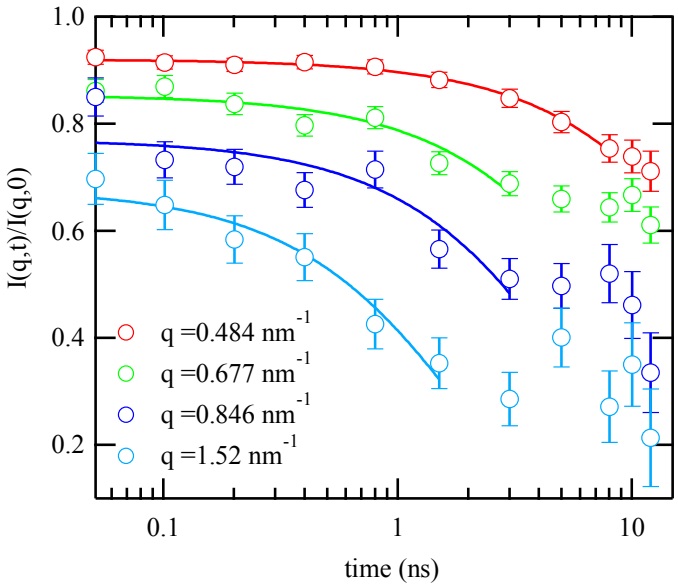

Figure 6 - 3**.** Dynamic structure factor from the BPL (Mw=39.5 kDa)-coated CB in d-toluene at 50°C. The solid lines correspond to the best-fits of the single exponential function (eq.4) with $D=1.6\times10^{-6}$ (cm^2/s) to the data.

Firstly, Fytas and co-workers analyzed the fast-mode of the dynamic structure factor as an isotropic diffusive component[42]:

$$\frac{I(q,t)}{I(q,0)} = \exp[-\Gamma(q)t] = \exp[-Dq^2t] \quad (4)$$

where $\Gamma(q)$ is the relaxation rate and D is a diffusion constant. Based on the best-fits to the data (solid lines in Figure 6-3), we obtained $D = 1.6 \times 10^{-6}$ cm^2/s at 50 °C. This value is the same order of magnitude of the one reported for a PS brush (M_w=160 kDa) on a planar glass substrate in toluene ($D = 1.3 \times 10^{-6}$ cm^2/s at 20 °C)[42]. Hence, as for end-grafted chains in a solvent [43, 44], we can see the intrinsic property of the collective dynamics in the BPL as well. Note that the D value of the CB dispersible unit in toluene (ϕ=1.8 %) was estimated to be 0.1×10^{-6} cm^2/s based on dynamic light scattering experiments such that the contribution can be negligible within the time

domain used in this study. To further provide insight into the collective dynamics, we prepared BPL with a higher M_w h-PB (M_w=436 kDa, M_w/M_n=2.5) on the same CB filler. Based on TEM and SANS experiments, we found that the thicknesses of the BPL were determined to be 7.0 ± 0.5 nm in air and 11.0 ± 0.5 nm in toluene, respectively. As shown in supplementary information[45], $I(q,t)/I(q,0)$ for the BPL (M_w=436 kDa)-coated CB in d-toluene also display a fast cooperative diffusion component and a slow contribution with a non-exponential shape. Using eq. (4), the D value is determined to be 27.6 × 10^{-6} cm^2/s at 50 °C, which is more than one of magnitude larger than that of the BPL (M_w=39.5 kDa) coated CB at 50 °C. This trend is opposed to the theoretical scaling (including the hydrodynamic interactions) for end-grafted polymer brushes [46]:

$$\Gamma(q) \propto \sigma^{-1} N^{-3} , \qquad (5)$$

where σ is the grafting density that increases with increasing N for an adsorbed layer since the number of the chain/segment contact points scale as $N^{1/2}$ [47]. We postulate that this unusual dynamics is attributed to the formation of "loops" in the bound chains. It is known that irreversibly adsorbed polymer chains form three types of segment sequences, "trains" (adsorbed segments), "loops" (sequences of free segments connecting successive trains), and "tails" (non-adsorbed chain ends) [48]. According to previous computational results on chain conformations of adsorbed chains at the polymer melt/solid interface [49], the average number of segments belonging to loops increases (up to ~ 30 %) with increasing N (up to N = 10,000), while that belonging to tails is more dominant (~ 65%). Patton and co-workers studied the formation process of polymer loops by using telechelic polystyrene prepared on planar surfaces[50]. They reported that the loops (i.e., doubly-bound chains) are less stretched and occupy more lateral space compared to end-grafted polymer brushes (i.e., singly-bound chains). Moreover, they evidenced that the presence of the polymer loops on the film surface imparts a more rigid structure to the adsorbed layer, while a polymer brush behaves more

viscoelastic nature owing to a large number of flexible and random tails. As described above, the swelling ratio (in the direction normal to the surface, S_f) of the BPL composed of the lower M_w PB (M_w=38 kDa) is slightly larger (S_f=1.75) than that of the BPL composed of the higher M_w PB (M_w=436 kDa, S_f=1.57). This suggests an increase in the fraction of the loop components in the BPL composed of the high M_w PB, as the theoretical calculation was predicted[49]. Hence, we may conclude that the faster collective dynamics of the BPL composed of the higher M_w PB is attributed to the more rigid nature compared to the BPL composed of the lower M_w PB.

Finally, we also discuss the slower decays in the dynamic structure factor. By using NSE, Richer and co-workers demonstrated a collective dynamic response (i.e., breathing mode) of end-grafted polymers on the surface of a spherical polymer core in a good solvent [40]. We hence simulated the dynamic structure factor originated from the breathing mode based on the de Gennes's theory[29]. In the original theory, the equation of local displacement u of tethered chains along the normal direction z of the surface (i.e., for the breathing mode) is given by

$$\frac{\partial}{\partial Z}\left(E(z)\frac{\partial u}{\partial z}\right)=\frac{\eta}{\xi^2}\frac{\partial u}{\partial t} \tag{6}$$

where E, η and ξ are the osmotic compressibility, the viscosity, and the correlation length that is related to the concentration through $\xi \propto c^{-3/4}$ [51], respectively. Using the concentration profile[52] as well as the scaling relation[51] for semidilute solutions, one gets the following relations; $\xi \propto z$ and $E(z) \propto k_B T / z^3$. As for the time decay, Eq. (9) has a solution of a simple exponential:

$$u(t) = u_n(z)\exp(-t/\tau_n). \tag{7}$$

In addition, due to the boundary conditions, Eq. (9) is a Sturm–Liouville boundary value problem

with eigenvalues $1/\tau_p$ and eigen functions $u_n(z)$ for the displacement. Furthermore, according to Richter et al.[40], the influence of the plane parallel modulation is considered only for the eigenvalue such that the intermediate scattering function is finally given by

$$I(q,t)/I(q,0) \propto \sum_{n.l}\left[\left\langle a_{n.l}^2\right\rangle 4\pi(2l+1)\left|\int_0^\infty j_l(qr)\left[2u_{r,n}cr+(u_{r,n}c)'r^2\right]dr\right|^2 \exp(-t/\lambda_n)\right] \quad (8)$$

with $\left\langle a_{n.l}^2\right\rangle = \gamma k_B T/\eta\lambda_{n.l}$, where γ is a numerical constant and $j_i(qr)$ is a spherical Bessel function of order l.

S(q) obtained from the SANS results and the following parameters (E_0, γ) were used to calculate I(q,t)/I(q,0). As shown in Figure 6-4, a reasonable fit to the data including the slower decay was obtained with the following parameters $E_0 = 0.75$, $\gamma = 0.016$. It should be noted that the breathing dynamics is attributed to the average dynamics of the swollen tail and loop parts of the outer loosely adsorbed chains in the BPL, while the dynamics of the unswollen flattened chains would be too slow to see within the time resolution windows of the NSE. At this point, it is not straightforward to extract the dynamics of the loops from the NSE data. Further NSE experiments using telechelic polymer chains on nanoparticles surface in solvents as well as polymer melts deserve future work.

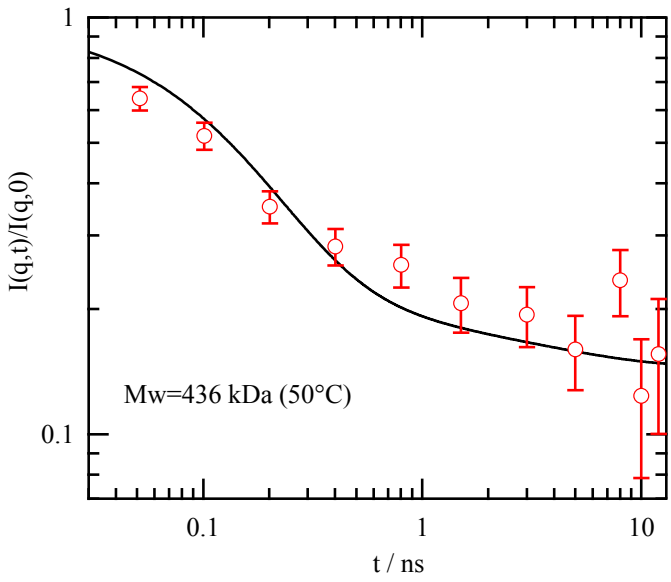

Figure 6 - 4**.** Dynamic structure factor from the BPL (Mw=436 kDa)-coated CB in d-toluene at 50°C. The solid lines correspond to the best-fits based on eq. (8) with $E_0 = 0.75$, $\gamma = 0.016$ to the data.

6.4 Conclusion

In summary, we have revealed the unique nano-architectures and corresponding dynamics of the polymer chains strongly adsorbed on nanofiller surfaces. The SANS experiments in toluene demonstrate the presence of the two different chain conformations on the CB surface. In addition, the NSE results reveal the collective dynamics of the outer loosely adsorbed chains, while the dynamics of the inner unswollen flattened chains are too slow to detect the dynamics within the experimental resolution. Furthermore, we found that the collective dynamics is accelerated when the chain lengths increase, in contrast to the theoretical prediction for end-grafted polymer chain [46]. We postulate that this unique characteristic is originated from the presence of loops in the adsorbed chains, which imparts more rigid nature to the adsorbed layer compared to end-grafted polymer chains composed of a large number of flexible and random tails[50]. The present

experimental results indicate that the preparation of polymeric systems capable of binding to a solid surface at multiple sites are crucial in the new design and development of polymer nanocomposites superior to traditional singly-bound polymeric structures.

6.5 References

1. Balazs, A. C.; Emrick, T.; Russell, T. P. *Science* **2006,** 314, 1107-1110.

2. Ebbesen, T. W.; Lezec, H. J.; Hiura, H.; Bennett, J. W.; Ghaemi, H. F.; Thio, T. *Nature* **1996,** 382, (6586), 54-56.

3. Ajayan, P. M.; Schadler, L. S.; Braum, P. V., *Nanocomposite Science and Technology*. Wiley-VCH: Weinheim, Germany, 2003.

4. Oberdisse, J. *Soft Matter* **2006,** 2, (1), 29-36.

5. Villars, D. S. *Journal of Polymer Science* **1956,** 21, 257-271.

6. Medalia, A. I. *J. Colloid Interface Sci.* **1970,** 32, 115.

7. Blow, C. M. *Polymer* **1973,** 14, 309.

8. Dannenberg, E. M. *Rubber Chem. Technol.* **1986,** 59, 512.

9. Kenny, J. C.; McBrietry, V. J.; Rigbi, Z.; Douglass, D. C. *Macromolecules* **1991,** 24, 436.

10. Karasek, L.; Sumita, M. *Journal of Materials Science* **1996,** 31, (2), 281-289.

11. Heinrich, G.; Vilgis, T. A. *Rub. Chem. Technol.* **1995,** 6.

12. Brown, D.; Marcadon, V.; Mele, P.; Alberola, N. D. *Macromolecules* **2008,** 41, (4), 1499-1511.

13. Harton, S. E.; Kumar, S. K.; Yang, H. C.; Koga, T.; Hicks, K.; Lee, E.; Mijovic, J.; Liu, M.; Vallery, R. S.; Gidley, D. W. *Macromolecules* **2010,** 43, (7), 3415-3421.

14. Kim, S. Y.; Schweizer, K. S.; Zukoski, C. F. *Phys. Rev. Lett.* **2011,** 107, (22).

15. Papon, A.; Montes, H.; Hanafi, M.; Lequeux, F. *Phys. Rev. Lett.* **2012,** 108, 065702.

16. Jouault, N.; Moll, J. F.; Meng, D.; Windsor, K.; Ramcharan, S.; Kearney, C.; Kumar, S. K. *ACS Macro Lett.* **2013,** 2, (5), 371-374.

17. Stickney, P. B.; Falb, R. D. *Rubber Chem. Technol.* **1964,** 37, 1299–1340.

18. Blum, F. D.; Xu, G.; Liang, M.; Wade, C. G. *Macromolecules* **1996,** 29, 8740.

19. Lin, W.; Blum, F. D. *Macromolecules* **1997,** 30, 5331-5338.

20. Lin, W. Y.; Blum, F. D. *Macromolecules* **1998,** 31, (13), 4135-4142.

21. Litvinov, V. M.; Steeman, P. A. M. *Macromolecules* **1999,** 32, (25), 8476-8490.

22. Donnet, J. B.; Bansal, R. C.; Wang, M. J., *Carbon Black: Science and Technology*. Marcel Dekker Inc.: New York, Basel, Hong Kong, 1993.

23. Goritz, D.; Raab, H.; Frohlich, J.; Maier, P. G. *Rub. Chem.Technol.* **1999,** 72, 929–945.

24. Koga, T.; Takenaka, M.; Aizawa, K.; Nakamura, M.; Hashimoto, T. *Langmuir* **2005,** 21, (24), 11409-11413.

25. Koga, T.; Hashimoto, T.; Takenaka, M.; Aizawa, K.; Amino, N.; Nakamura, M.; Yamaguchi, D.; Koizumi, S. *Macromolecules* **2008,** 41, (2), 453-464.

26. Baeza, G. P.; Genix, A. C.; Degrandcourt, C.; Petitjean, L.; Gummel, J.; Schweins, R.; Couty, M.; Oberdisse, J. *Macromolecules* **2013,** 46, (16), 6621-6633.

27. Karim, A.; Satija, S. K.; Douglas, J. F.; Ankner, J. F.; Fetters, L. J. *Phy. Rev. Lett.* **1994,** 73, 3407.

28. Richter, D.; Monkenbusch, M.; Arbe, A.; Colmenero, J. *Adv. Polym. Sci.* **2005,** 174, 1-221.

29. de Gennes, P. G. *C. R. Acad. Sci. Paris Ser. II* **1986,** 302, 765.

30. Woodka, A. C.; Butler, P. D.; Porcar, L.; Farago, B.; Nagao, M. *Phys. Rev. Lett.* **2012,** 109, (5), 5.

31. Beaucage, G. *J. Appl. Cryst.* **1995,** 28, 717-728.

32. Takenaka, M.; Nishitsuji, S.; Amino, N.; Ishikawa, Y.; Yamaguchi, D.; Koizumi, S. *Rubber Chem. Technol.* **2012,** 85, 157-164.

33. Milner, S. T.; Witten, T. A.; Cates, M. E. *Macromolecules* **1988,** 21, 2610.

34. Kritikos, G.; Terzis, A. F. *Eur. Polym. J.* **2013,** 49, (3), 613-629.

35. Gin, P.; Jiang, N. S.; Liang, C.; Taniguchi, T.; Akgun, B.; Satija, S. K.; Endoh, M. K.; Koga, T. *Phys. Rev. Lett.* **2012,** 109, (26), 265501.

36. Jiang, N.; Shang, J.; Di, X.; Endoh, M. K.; Koga, T. *Macromolecules* **2014,** 47, 2682-2689.

37. Krutyeva, M.; Wischnewski, A.; Monkenbusch, M.; Willner, L.; Maiz, J.; Mijangos, C.; Arbe, A.; Colmenero, J.; Radulescu, A.; Holderer, O.; Ohl, M.; Richter, D. *Phys Rev Lett* **2013,** 110, (10).

38. Zimm, B. H. *J. Chem. Phys.* **1956,** 24, 269.

39. Rouse, P. E. *J. Chem. Phys.* **1953,** 21, 1272.

40. Farago, B.; Monkenbusch, M.; Richter, D.; Huang, J. S.; Fetters, L. J.; Gast, A. P. *Phys. Rev. Lett.* **1993,** 71, (7), 1015-1018.

41. Fytas, G.; Anastasiadis, S. H.; Seghrouchni, R.; Vlassopoulos, D.; Li, J. B.; Factor, B. J.; Theobald, W.; Toprakcioglu, C. *Science* **1996,** 274, (5295), 2041-2044.

42. Yakubov, G. E.; Loppinet, B.; Zhang, H.; Ruhe, J.; Sigel, R.; Fytas, G. *Phys. Rev. Lett.* **2004,** 92, (11), 4.

43. de Gennes, P. G. *Adv. Colloid Interface Sci.* **1987,** 27, 189.

44. Milner, S. T. *Science* **1991,** 251, 905.

45. information, S.

46. Klushin, L. I.; Skvortsov, A. M. *Macromolecules* **1991,** 24, (7), 1549-1553.

47. Guiselin, O. *Europhys. Lett.* **1992,** 17, (3), 225-230.

48. de Gennes, P.-G., *Scaling Concepts in Polymer Physics*. Cornell University Press: 1979.

49. Daoulas, K. C.; Theodorou, D. N.; Harmandaris, V. A.; Karayiannis, N. C.; Mavrantzas, V. G. *Macromolecules* **2005,** 38, (16), 7134-7149.

50. Patton, D.; Knoll, W.; Advincula, R. C. *Macromol. Chem. Phys.* **2011,** 212, (5), 485-497.

51. de Gennes, P. G., *Scaling Concepts in Polymer Physics* Cornell University Press: Ithaca, 1979.

52. Bouchaud, E.; Auvray, L.; Cotton, J. P.; Daoud, M.; Farnoux, B.; Jannink, G. *Prog. Surf. Sci.* **1988,** 27, 5.

Bibliography

Chapter 1

1. Tsui, O. K. C.; Russell, T. P., *Polymer thin films.* World Scientific: Singapore; Hackensack, NJ, 2008.

2. Gin, P.; Jiang, N.; Liang, C.; Taniguchi, T.; Akgun, B.; Satija, S. K.; Endoh, M. K.; Koga, T. *Phys Rev Lett* **2012,** 109, (26), 265501.

3. Fujii, Y.; Yang, Z. H.; Leach, J.; Atarashi, H.; Tanaka, K.; Tsui, O. K. C. *Macromolecules* **2009,** 42, (19), 7418-7422.

4. Rotella, C.; Napolitano, S.; Vandendriessche, S.; Valev, V. K.; Verbiest, T.; Larkowska, M.; Kucharski, S.; Wubbenhorst, M. *Langmuir* **2011,** 27, (22), 13533-13538.

5. Napolitano, S.; Wubbenhorst, M. *Nat Commun* **2011,** 2.

6. *Polymer Handbook 4th Ed.* John Wiley & Sons, Inc.: NY, 1999.

7. Reiter, G.; Sharma, A.; Casoli, A.; David, M. O.; Khanna, R.; Auroy, P. *Langmuir* **1999,** 15, (7), 2551-2558.

8. Seemann, R.; Herminghaus, S.; Jacobs, K. *Phys Rev Lett* **2001,** 86, (24), 5534-5537.

9. Sharma, A. *Langmuir* **1993,** 9, (3), 861-869.

10. Reiter, G. *Phys Rev Lett* **1992,** 68, (1), 75-78.

11. Reiter, G. *Europhys Lett* **1993,** 23, (8), 579-584.

12. Reiter, G.; Hamieh, M.; Damman, P.; Sclavons, S.; Gabriele, S.; Vilmin, T.; Raphael, E. *Nat Mater* **2005,** 4, (10), 754-758.

13. Koga, T.; Seo, Y. S.; Zhang, Y.; Sin, K.; Kusano, K.; Nishikawa, K.; Rafailovich, M. H.; Sokolov, J. C.; Chu, B.; Peiffer, D.; Occhiogrosso, R.; Satija, S. K. *Phys. Rev. Lett.* **2002,** 89, 125506.

14. Koga, T.; Seo, Y. S.; Hu, X.; Kwanwoo, S.; Zhang, Y.; Rafailovich, M. H.; Sokolov, J. C.; Chu, B.; Satija, S. K. *Europhys. Lett.* **2002,** 60, 559.

15. Koga, T.; Seo, Y. S.; Shin, K.; Zhang, Y.; Rafailovich, M. H.; Sokolov, J. C.; Chu, B.; Peiffeer, D.; Satija, S. K. *Macromolecules* **2003,** 36, 5236.

16. Koga, T.; Ji, Y.; Seo, Y. S.; Rafailovich, M. H.; Sokolov, J. C.; Satija, S. K. *J. Polym. Sci., Part B:Polym. Phys.* **2004,** 42, 3282.

17. Meli, L.; Pham, J. Q.; Johnston, K. P.; Green, P. F. *Physical Review E* **2004,** 69, (5), 8.

18. Li, Y.; park, E.; Lim, K.; Johnston, K. P.; Green, P. F. *J. Polym. Sci., Part B:Polym. Phys.* **2007,** 45, 1313-1324.

19. Chebil, M. S.; Vignaud, G.; Grohens, Y.; Konovalov, O.; Sanyal, M. K.; Beuvier, T.; Gibaud, A. *Macromolecules* **2012,** 45, (16), 6611-6617.

20. Nishikawa, K.; Tanaka, I.; Amemiya, Y. *J. Phys. Chem.* **1996,** 100, 418-421.

21. Sirard, S. M.; J., Z. K.; Sanchez, L. C.; Green, P. F.; Johnston, K. P. *Macromolecules* **2002,** 35, 1928.

22. Li, X. X.; Vogt, B. D. *Polymer* **2009,** 50, (17), 4182-4188.

23. Koga, T.; Gin, P.; Yamaguchi, H.; Endoh, M.; Sendogdular, L.; Kobayashi, M.; Takahara, A.; Akgun, B.; Satija, S. K.; Sumi, T. *Polymer* **2011,** 52, 4331-4336.

24. Mendoza-Galvan, A.; Trejo-Cruz, C.; Solis-Canto, O.; Luna-Barcenas, G. *J. Supercrit. Fluids* **2012,** 64, 25-31.

25. Geoghegan, M.; Krausch, G. *Prog. Polym. Sci.* **2003,** 28, (2), 261-302.

26. Keddie, J. L.; Jones, R. A. L.; Cory, R. A. *Faraday Discussions* **1994,** 98, 219-230.

27. Keddie, J. L.; Jones, R. A. L.; Cory, R. A. *Europhys Lett* **1994,** 27, (1), 59-64.

28. Kim, J. H.; Jang, J.; Zin, W. C. *Langmuir* **2000,** 16, (9), 4064-4067.

29. Kawana, S.; Jones, R. A. L. *Phys Rev E* **2001,** 63, (2).

30. Xie, F. C.; Zhang, H. F.; Lee, F. K.; Du, B. Y.; Tsui, O. K. C.; Yokoe, Y.; Tanaka, K.; Takahara, A.; Kajiyama, T.; He, T. B. *Macromolecules* **2002,** 35, (5), 1491-1492.

31. Fakhraai, Z.; Valadkhan, S.; Forrest, J. A. *Eur Phys J E* **2005,** 18, (2), 143-148.

32. Fakhraai, Z.; Forrest, J. A. *Phys Rev Lett* **2005,** 95, (2).

33. Kajiyama, T.; Tanaka, K.; Takahara, A. *Macromolecules* **1995,** 28, (9), 3482-3484.

34. Mattsson, J.; Forrest, J. A.; Borjesson, L. *Phys Rev E* **2000,** 62, (4), 5187-5200.

35. Forrest, J. A.; DalnokiVeress, K.; Dutcher, J. R. *Phys Rev E* **1997,** 56, (5), 5705-5716.

36. Forrest, J. A.; DalnokiVeress, K.; Stevens, J. R.; Dutcher, J. R. *Phys Rev Lett* **1996,** 77, (10), 2002-2005.

37. Teichroeb, J. H.; Forrest, J. A. *Phys Rev Lett* **2003,** 91, (1).

38. Qi, D.; Ilton, M.; Forrest, J. A. *Eur Phys J E* **2011,** 34, (6).

39. Ilton, M.; Qi, D.; Forrest, J. A. *Macromolecules* **2009,** 42, (18), 6851-6854.

40. Qi, D.; Fakhraai, Z.; Forrest, J. A. *Phys Rev Lett* **2008,** 101, (9).

41. Fakhraai, Z.; Forrest, J. A. *Science* **2008,** 319, (5863), 600-604.

42. Sharp, J. S.; Teichroeb, J. H.; Forrest, J. A. *Eur Phys J E* **2004,** 15, (4), 473-487.

43. Tanaka, K.; Takahara, A.; Kajiyama, T. *Macromolecules* **1997,** 30, (21), 6626-6632.

44. DeMaggio, G. B.; Frieze, W. E.; Gidley, D. W.; Zhu, M.; Hristov, H. A.; Yee, A. F. *Phys Rev Lett* **1997,** 78, (8), 1524-1527.

45. Roth, C. B.; McNerny, K. L.; Jager, W. F.; Torkelson, J. M. *Macromolecules* **2007,** 40, (7), 2568-2574.

46. Priestley, R. D.; Ellison, C. J.; Broadbelt, L. J.; Torkelson, J. M. *Science* **2005,** 309, (5733), 456-459.

47. Ellison, C. J.; Torkelson, J. M. *Nat Mater* **2003,** 2, (10), 695-700.

48. Rotella, C.; Wubbenhorst, M.; Napolitano, S. *Soft Matter* **2011,** 7, (11), 5260-5266.

49. Rotella, C.; Napolitano, S.; De Cremer, L.; Koeckelberghs, G.; Wubbenhorst, M. *Macromolecules* **2010,** 43, (20), 8686-8691.

50. Napolitano, S.; Wubbenhorst, M. *Polymer* **2010,** 51, (23), 5309-5312.

51. Rotella, C.; Napolitano, S.; Wuebbenhorst, M. *Macromolecules* **2009,** 42, (5), 1415-1417.

52. Peter, S.; Napolitano, S.; Meyer, H.; Wubbenhorst, M.; Baschnagel, J. *Macromolecules* **2008,** 41, (20), 7729-7743.

53. Napolitano, S.; Lupascu, V.; Wubbenhorst, M. *Macromolecules* **2008,** 41, (4), 1061-1063.

54. Napolitano, S.; Wubbenhorst, M. *J Phys Chem B* **2007,** 111, (21), 5775-5780.

55. Napolitano, S.; Prevosto, D.; Lucchesi, M.; Pingue, P.; D'Acunto, M.; Rolla, P. *Langmuir* **2007,** 23, (4), 2103-2109.

56. Kessairi, K.; Napolitano, S.; Capaccioli, S.; Rolla, P.; Wubbenhorst, M. *Macromolecules* **2007,** 40, (6), 1786-1788.

57. Wallace, W. E.; Vanzanten, J. H.; Wu, W. L. *Phys Rev E* **1995,** 52, (4), R3329-R3332.

58. vanZanten, J. H.; Wallace, W. E.; Wu, W. L. *Phys Rev E* **1996,** 53, (3), R2053-R2056.

59. Fryer, D. S.; Peters, R. D.; Kim, E. J.; Tomaszewski, J. E.; de Pablo, J. J.; Nealey, P. F.; White, C. C.; Wu, W. L. *Macromolecules* **2001,** 34, (16), 5627-5634.

60. Kim, H.; Ruhm, A.; Lurio, L. B.; Basu, J. K.; Lal, J.; Lumma, D.; Mochrie, S. G. J.; Sinha, S. K. *Phys Rev Lett* **2003,** 90, (6).

61. Kim, H.; Ruhm, A.; Lurio, L. B.; Basu, J. K.; Lal, J.; Mochrie, S. G. J.; Sinha, S. K. *Physica B* **2003,** 336, (1-2), 211-215.

62. Li, C. H.; Koga, T.; Jiang, J.; Sharma, S.; Narayanan, S.; Lurio, L. B.; Hu, Y.; Jiao, X.; Sinha, S. K.; Billet, S.; Sosnowik, D.; Kim, H.; Sokolov, J. C.; Rafailovich, M. H. *Macromolecules* **2005,** 38, (12), 5144-5151.

63. Ellison, C. J.; Torkelson, J. M. *Nature Mater.* **2003,** 2, 695-700.

64. Fakhraai, Z.; Forrest, J. A. *Phys. Rev. Lett.* **2005,** 95, 025701.

65. Yang, Z. H.; Fujii, Y.; Lee, F. K.; Lam, C. H.; Tsui, O. K. C. *Science* **2010,** 328, (5986), 1676-1679.

66. Bodiguel, H.; Fretigny, C. *Macromolecules* **2007,** 40, (20), 7291-7298.

67. Li, C. H.; Kim, H. J.; Jiang, J.; Li, C.; Koga, T.; Lurio, L.; Schwarz, S.; Narayanan, S.; Lee, H. J.; Lee, Y. J.; Jiang, Z.; Sinha, S.; Rafailovich, M. H.; Sokolov, J. C. *Europhys Lett* **2006,** 73, (6), 899-905.

68. Bodiguel, H.; Fretigny, C. *Phys Rev Lett* **2006,** 97, (26).

69. O'Connell, P. A.; McKenna, G. B. *Science* **2005,** 307, (5716), 1760-1763.

70. Masson, J. L.; Green, P. F. *Phys Rev E* **2002,** 65, (3).

71. Zheng, X.; Sauer, B. B.; Vanalsten, J. G.; Schwarz, S. A.; Rafailovich, M. H.; Sokolov, J.; Rubinstein, M. *Phys Rev Lett* **1995,** 74, (3), 407-410.

72. Zheng, X.; Rafailovich, M. H.; Sokolov, J.; Strzhemechny, Y.; Schwarz, S. A.; Sauer, B., B.; Rubinstein, M. *Phys Rev Lett* **1997,** 79, 241-244.

73. Priestley, R. D.; Ellison, C.; Broadbelt, L. J.; Torkelson, J. M. *Science* **2005,** 309, 456-459.

74. Herminghaus, S. *Eur Phys J E* **2002,** 8, (2), 237-243.

75. Long, D.; Lequeux, F. *Eur Phys J E* **2001,** 4, (3), 371-387.

76. Kim, J. H.; Jang, J.; Zin, W. C. *Langmuir* **2001,** 17, (9), 2703-2710.

77. Sharp, J. S.; Forrest, J. A. *Phys Rev Lett* **2003,** 91, (23).

78. Forrest, J. A.; Dalnoki-Veress, K. *Adv Colloid Interfac* **2001,** 94, (1-3), 167-196.

79. Forrest, J. A.; Dalnoki-Veress, K.; Dutcher, J. R. *Phys Rev E* **1998,** 58, (5), 6109-6114.

80. Forrest, J. A.; DalnokiVeress, K.; Stevens, J. R.; Dutcher, J. R. *Phys Rev Lett* **1996,** 77, (19), 4108-4108.

81. Tsui, O. K. C.; Russell, T. P.; Hawker, C. J. *Macromolecules* **2001,** 34, (16), 5535-5539.

82. Frank, C. W.; Rao, V.; Despotopoulou, M. M.; Pease, R. F. W.; Hinsberg, W. D.; Miller, R. D.; Rabolt, J. F. *Science* **1996,** 273, (5277), 912-915.

83. Sharp, J. S.; Forrest, J. A. *Phys Rev E* **2003,** 67, (3).

84. Priestley, R. D.; Mundra, M. K.; Barnett, N. J.; Broadbelt, L. J.; Torkelson, J. M. *Aust J Chem* **2007,** 60, (10), 765-771.

85. Durning, C. J.; O'Shaughness, B.; Sawhney, U.; Nguyen, D.; Majewski, J.; Smith, G. S. *Macromolecules* **1999,** 32, (20), 6772-6781.

86. Ediger, M. D.; Forrest, J. A. *Macromolecules* **2014,** 47, (2), 471-478.

87. Frank, B.; Gast, A. P.; Russell, T. P.; Brown, H. R.; Hawker, C. J. *Macromolecules* **1996,** 29, (20), 6531-6534.

88. Zheng, X.; Rafailovich, M. H.; Sokolov, J.; Strzhemechny, Y.; Schwarz, S. A.; Sauer, B. B.; Rubinstein, M. *Phys Rev Lett* **1997,** 79, (2), 241-244.

89. Scheutjens, J. M. H. M.; Fleer, G. J. *The Journal of Physical Chemistry* **1980,** 84, (2), 178-190.

90. Schneider, H. M.; Frantz, P.; Granick, S. *Langmuir* **1996,** 12, (4), 994-996.

91. Douglas, J. F.; Schneider, H. M.; Frantz, P.; Lipman, R.; Granick, S. *Journal of Physics: Condensed Matter* **1997,** 9, (37), 7699.

92. O'Shaughnessy, B.; Vavylonis, D. *J Phys-Condens Mat* **2005,** 17, (2), R63-R99.

93. O'Shaughnessy, B.; Vavylonis, D. *Eur Phys J E* **2003,** 11, (3), 213-230.

94. Simha, R.; Frisch, H. L.; Eirich, F. R. *The Journal of Physical Chemistry* **1953,** 57, (6), 584-589.

95. Scheutjens, J. M. H. M.; Fleer, G. J. *Macromolecules* **1985,** 18, (10), 1882-1900.

96. Scheutjens, J. M. H. M.; Fleer, G. J. *The Journal of Physical Chemistry* **1979,** 83, (12), 1619-1635.

97. Papirer, E., *Adsorption on silica surfaces*. CRC Press: 2000.

98. Granick, S. *Eur. Phys. J. E* **2002,** 9, (1), 421-424.

99. Santore, M. M. *Curr Opin Colloid In* **2005,** 10, (3–4), 176-183.

100. Sommer, J.-U. *Eur. Phys. J. E* **2002,** 9, (1), 417-419.

101. Fu, Z.; Santore, M. *Macromolecules* **1999,** 32, (6), 1939-1948.

102. Fu, Z.; Santore, M. M. *Langmuir* **1997,** 13, (21), 5779-5781.

103. Ligoure, C.; Leibler, L. *J. Phys. France* **1990,** 51, (12), 1313-1328.

104. Linse, P. *Soft Matter* **2012,** 8, (19), 5140-5150.

105. Linse, P.; Källrot, N. *Macromolecules* **2010,** 43, (4), 2054-2068.

106. Housmans, C.; Sferrazza, M.; Napolitano, S. *Macromolecules* **2014,** 47, (10), 3390-3393.

107. Napolitano, S.; Capponi, S.; Vanroy, B. *Eur. Phys. J. E* **2013,** 36, (6), 1-37.

108. Napolitano, S.; Rotella, C.; Wübbenhorst, M. *Acs Macro Lett* **2012,** 1, (10), 1189-1193.

109. Ramanathan, M.; Darling, S. B. *Progress in Polymer Science* **2011,** 36, (6), 793-812.

110. Reiter, G. *Langmuir* **1993,** 9, (5), 1344-1351.

111. Zhai, X. W.; Weiss, R. A. *Langmuir* **2008,** 24, (22), 12928-12935.

112. Seemann, R.; Herminghaus, S.; Neto, C.; Schlagowski, S.; Podzimek, D.; Konrad, R.; Mantz, H.; Jacobs, K. *J Phys-Condens Mat* **2005,** 17, (9), S267-S290.

113. Muller-Buschbaum, P. *Eur Phys J E* **2003,** 12, (3), 443-448.

114. Suh, H. S.; Kang, H. M.; Liu, C. C.; Nealey, P. F.; Char, K. *Macromolecules* **2010,** 43, (1), 461-466.

115. Kargupta, K.; Sharma, A. *Langmuir* **2003,** 19, (12), 5153-5163.

116. Renger, C.; Muller-Buschbaum, P.; Stamm, M.; Hinrichsen, G. *Macromolecules* **2000,** 33, (22), 8388-8398.

117. Mansky, P.; Liu, Y.; Huang, E.; Russell, T. P.; Hawker, C. J. *Science* **1997,** 275, (5305), 1458-1460.

118. Yerushalmi-Rozen, R.; Klein, J.; Fetters, L. J. *Science-AAAS-Weekly Paper Edition-including Guide to Scientific Information* **1994,** 263, (5148), 793-795.

119. Costa, A. C.; Composto, R. J.; Vlcek, P.; Morera, S. *J Adhesion* **2005,** 81, (7-8), 683-698.

120. Costa, A. C.; Composto, R. J.; Vlcek, P. *Macromolecules* **2003,** 36, (9), 3254-3260.

121. Oslanec, R.; Costa, A. C.; Composto, R. J.; Vlcek, P. *Macromolecules* **2000,** 33, (15), 5505-5512.

122. Krishnan, R. S.; Mackay, M. E.; Duxbury, P. M.; Hawker, C. J.; Asokan, S.; Wong, M. S.; Goyette, R.; Thiyagarajan, P. *J Phys-Condens Mat* **2007,** 19, (35).

123. Henn, G.; Bucknall, D. G.; Stamm, M.; Vanhoorne, P.; Jerome, R. *Macromolecules* **1996,** 29, (12), 4305-4313.

124. Reiter, G.; Schultz, J.; Auroy, P.; Auvray, L. *Europhys Lett* **1996,** 33, (1), 29-34.

125. Chu, B., *Dynamic Light Scattering, 2nd Ed.* Academic Press: New York, 1991.

126. Leheny, R. L. *Curr Opin Colloid In* **2012,** 17, (1), 3-12.

127. Sutton, M. *Cr Phys* **2008,** 9, (5-6), 657-667.

128. Livet, F. *Acta Crystallogr A* **2007,** 63, 87-107.

129. Mochrie, S. G. J.; Lurio, L. B.; Ruhm, A.; Lumma, D.; Borthwick, M.; Falus, P.; Kim, H. J.; Basu, J. K.; Lal, J.; Sinha, S. K. *Physica B* **2003,** 336, (1-2), 173-180.

130. Kim, H.; Ruhm, A.; Lurio, L. B.; Basu, J. K.; Lal, J.; Mochrie, S. G. J.; Sinha, S. K. *J Phys-Condens Mat* **2004,** 16, (33), S3491-S3497.

131. Jiang, Z.; Kim, H.; Jiao, X.; Lee, H.; Lee, Y. J.; Byun, Y.; Song, S.; Eom, D.; Li, C.; Rafailovich, M. H.; Lurio, L. B.; Sinha, S. K. *Phys Rev Lett* **2007,** 98, (22).

132. Kim, H.; Jiang, Z.; Lee, H.; Lee, Y. J.; Jiao, X. S.; Li, C. H.; Lurio, L.; Rafailovich, M.; Sinha, S. K. *Thin Solid Films* **2007,** 515, (14), 5536-5540.

133. Jiang, Z.; Mukhopadhyay, M. K.; Song, S.; Narayanan, S.; Lurio, L. B.; Kim, H.; Sinha, S. K. *Phys Rev Lett* **2008,** 101, (24).

134. Dierker, S. B.; Pindak, R.; Fleming, R. M.; Robinson, I. K.; Berman, L. *Phys Rev Lett* **1995,** 75, (3), 449-452.

135. Koga, T.; Li, C.; Endoh, M. K.; Koo, J.; Rafailovich, M.; Narayanan, S.; Lee, D. R.; Lurio, L. B.; Sinha, S. K. *Phys Rev Lett* **2010,** 104, (6).

136. Russell, T. P. *Materials Science Reports* **1990,** 5, (4), 171-271.

137. Seeck, O. H.; Kaendler, I. D.; Tolan, M.; Shin, K.; Rafailovich, M. H.; Sokolov, J.; Kolb, R. *Appl Phys Lett* **2000,** 76, (19), 2713-2715.

138. Koga, T.; Seo, Y. S.; Zhang, Y. M.; Shin, K.; Kusano, K.; Nishikawa, K.; Rafailovich, M. H.; Sokolov, J. C.; Chu, B.; Peiffer, D.; Occhiogrosso, R.; Satija, S. K. *Physical Review Letters* **2002,** 89, (12).

139. Koga, T.; Seo, Y.-S.; Hu, X.; Shin, K.; Zhang, Y.; Rafailovich, M. H.; Sokolov, J. C.; Chu, B.; Satija, S. K. *EPL (Europhysics Letters)* **2002,** 60, (4), 559.

140. Koga, T.; Seo, Y. S.; Shin, K.; Zhang, Y.; Rafailovich, M. H.; Sokolov, J. C.; Chu, B.; Satija, S. K. *Macromolecules* **2003,** 36, (14), 5236-5243.

141. Koga, T.; Ji, Y.; Seo, Y. S.; Gordon, C.; Qu, F.; Rafailovich, M. H.; Sokolov, J. C.; Satija, S. K. *J Polym Sci Pol Phys* **2004,** 42, (17), 3282-3289.

142. Koga, T.; Jerome, J. L.; Seo, Y. S.; Rafailovich, M. H.; Sokolov, J. C.; Satija, S. K. *Langmuir* **2005,** 21, (14), 6157-6160.

143. Koga, T.; Li, C.; Sun, Y.; Brazin, A.; Rafailovich, M. H.; Sokolov, J. C.; Douglas, J. F.; Mahajan, D. *Top Catal* **2005,** 32, (3-4), 257-262.

144. Koga, T.; Kugler, B.; Loewenstein, J.; Jerome, J.; Rafailovich, M. H. *J Appl Crystallogr* **2007,** 40, S684-S686.

145. Richter, D.; Fetters, L. J.; Huang, J. S.; Farago, B.; Ewen, B. *J Non-Cryst Solids* **1991,** 131, 604-611.

146. Imae, T.; Kanaya, T.; Furusaka, M.; Torikai, N., *Neutrons in soft matter*. John Wiley & Sons: 2011.

147. Richter, D.; Monkenbusch, M.; Arbe, A.; Colmenero, J., Neutron Spin Echo in Polymer Systems. In *Advances in Polymer Science*, Springer Berlin Heidelberg: **2005**; Vol. 174, pp 1-221.

Chapter 2

1. Richardson, H.; Carelli, C.; Keddie, J. L.; Sferrazza, M. *Eur Phys J E* **2003,** 12, (3), 437-440.

2. Reiter, G.; Hamieh, M.; Damman, P.; Sclavons, S.; Gabriele, S.; Vilmin, T.; Raphael, E. *Nat Mater* **2005,** 4, (10), 754-758.

3. Damman, P.; Gabriele, S.; Coppée, S.; Desprez, S.; Villers, D.; Vilmin, T.; Raphaël, E.; Hamieh, M.; Al Akhrass, S.; Reiter, G. *Phys Rev Lett* **2007,** 99, (3), 036101.

4. Ziebert, F.; Raphael, E. *Phys Rev E* **2009,** 79, (3), 10.

5. Thomas, K. R.; Chenneviere, A.; Reiter, G.; Steiner, U. *Phys Rev E* **2011,** 83, (2), 8.

6. Barbero, D. R.; Steiner, U. *Phys Rev Lett* **2009,** 102, (24), 248303.

7. Doi, M.; Edwards, S. F., *The Theory of Polymer Dynamics*. Oxford Science: Oxford, 1986.

8. Thomas, K. R.; Chenneviere, A.; Reiter, G.; Steiner, U. *Phys Rev E* **2011,** 83, (2), 021804.

9. Chung, J. Y.; Chastek, T. Q.; Fasolka, M. J.; Ro, H. W.; Stafford, C. M. *ACS Nano* **2009,** 3, (4), 844-852.

10. Fleer, G. J.; Cohen Stuart, M. A.; Scheutjens, J. M. H. M.; Cosgrove, T.; Vincent, B., *Polymers at Interfaces*. Chapman and Hall: London, 1993.

11. Durning, C. J.; O'Shaughness, B.; Sawhney, U.; Nguyen, D.; Majewski, J.; Smith, G. S. *Macromolecules* **1999,** 32, (20), 6772-6781.

12. Napolitano, S.; Prevosto, D.; Lucchesi, M.; Pingue, P.; D'Acunto, M.; Rolla, P. *Langmuir* **2007,** 23, (4), 2103-2109.

13. Napolitano, S.; Wübbenhorst, M. *J. Phys. Chem. B* **2007,** 111, 9197-9199.

14. Napolitano, S.; Lupascu, V.; Wubbenhorst, M. *Macromolecules* **2008,** 41, (4), 1061-1063.

15. Fujii, Y.; Yang, Z. H.; Leach, J.; Atarashi, H.; Tanaka, K.; Tsui, O. K. C. *Macromolecules* **2009,** 42, (19), 7418-7422.

16. Napolitano, S.; Pilleri, A.; Rolla, P.; Wübbenhorst, M. *Acs Nano* **2010,** 4, (2), 841-848.

17. Napolitano, S.; Wubbenhorst, M. *Nat Commun* **2011,** 2.

18. Koga, T.; Jiang, N.; Gin, P.; Endoh, M. K.; Narayanan, S.; Lurio, L. B.; Sinha, S. K. *Phys Rev Lett* **2011,** 107, (22).

19. Gin, P.; Jiang, N.; Liang, C.; Taniguchi, T.; Akgun, B.; Satija, S. K.; Endoh, M. K.; Koga, T. *Phys Rev Lett* **2012,** 109, (26), 265501.

20. Guiselin, O. *Europhys. Lett.* **1992,** 17, (3), 225-230.

21. Wallace, W. E.; van Zanten, J. H.; Wu, W. L. *Phys. Rev. E* **1995,** 52, R3329-3332.

22. van Zanten, J. H.; Wallace, W. E.; Wu, W. L. *Phys. Rev. E* **1996,** 53, R2053-2056.

23. Zhang, Y.; Ge, S.; Tang, B.; Koga, T.; Rafailovich, M. H.; Sokolov, J. C.; Peiffer, D. G.; Li, Z.; Dias, A. J.; McElrath, K. O.; Lin, M. Y.; Satija, S. K.; Urquhart, S. G.; Ade, H.; Nguyen, D. *Macromolecules* **2001,** 34, (20), 7056-7065.

24. Asada, M.; Jiang, N.; Sendogdular, L.; Gin, P.; Wang, Y.; Endoh, M. K.; Koga, T.; Fukuto, M.; Schultz, D.; Lee, M.; Li, X.; Wang, J.; Kikuchi, M.; Takahara, A. *Macromolecules* **2012,** 45, 7098-7106.

25. Vanroy, B.; Wübbenhorst, M.; Napolitano, S. *ACS Macro Letters* **2013,** 2, (2), 168-172.

26. Zheng, X.; Rafailovich, M. H.; Sokolov, J.; Strzhemechny, Y.; Schwarz, S. A.; Sauer, B. B.; Rubinstein, M. *Phys Rev Lett* **1997,** 79, (2), 241-244.

27. Hu, X.-W.; Granick, S. *Science* **1992,** 258, 1339.

28. Orts, W. J.; Vanzanten, J. H.; Wu, W. L.; Satija, S. K. *Phys Rev Lett* **1993,** 71, (6), 867-870.

29. Zheng, X.; Rafailovich, M. H.; Sokolov, J.; Strzhemechny, Y.; Schwarz, S. A.; Sauer, B., B.; Rubinstein, M. *Phys Rev Lett* **1997,** 79, 241-244.

30. Napolitano, S.; Wubbenhorst, M. *Nat. Commun.* **2011,** 2.

31. Napolitano, S.; Rotella, C.; Wübbenhorst, M. *ACS Macro Letters* **2012,** 1, (10), 1189-1193.

32. Labahn, D.; Mix, R.; Schönhals, A. *Phys Rev E* **2009,** 79, (1), 011801.

33. Johnson, H. E.; Granick, S. *Science* **1992,** 255, (5047), 966-968.

34. Schneider, H. M.; Frantz, P.; Granick, S. *Langmuir* **1996,** 12, (4), 994-996.

35. Soga, I.; Granick, S. *Langmuir* **1998,** 14, (15), 4266-4271.

36. Douglas, J. F.; Johnson, H. E.; Granick, S. *Science* **1993,** 262, (5142), 2010-2012.

37. Linse, P.; Källrot, N. *Macromolecules* **2010,** 43, (4), 2054-2068.

38. Schuetjens, M. H. M.; Fleer, G. J. *J. Phys. Chem.* **1980,** 84, 178.

39. Granick, S. *Eur. Phys. J. E* **2002,** 9, (1), 421-424.

40. Santore, M. M. *Curr Opin Colloid In* **2005,** 10, (3–4), 176-183.

41. Napolitano, S.; Capponi, S.; Vanroy, B. *Eur. Phys. J. E* **2013,** 36, (6), 1-37.

42. Rotella, C.; Napolitano, S.; Vandendriessche, S.; Valev, V. K.; Verbiest, T.; Larkowska, M.; Kucharski, S.; Wubbenhorst, M. *Langmuir* **2011,** 27, (22), 13533-13538.

43. Fu, Z. L.; Santore, M. *Macromolecules* **1999,** 32, (6), 1939-1948.

44. Fu, Z.; Santore, M. M. *Langmuir* **1997,** 13, (21), 5779-5781.

45. Shin, K.; Hu, X.; Zheng, X.; Rafailovich, M. H.; Sokolov, J.; Zaitsev, V.; Schwarz, S. A. *Macromolecules* **2001,** 34, 4993-4998.

46. Wang, Y.; Rafailovich, M.; Sokolov, J.; Gersappe, D.; Araki, T.; Zou, Y.; Kilcoyne, A. D. L.; Ade, H.; Marom, G.; Lustiger, A. *Phys Rev Lett* **2006,** 96, (2), 028303.

47. Kawai, A.; Kawakami, J.; Sasazaki, H. *J Photopolym Sci Tec* **2008,** 21, (6), 739-740.

48. Israelachvili, J. N., *Intermolecular and surface forces: revised third edition*. Academic press: 2011.

49. Kwok, D. Y.; Neumann, A. W. *Adv. Colloid Interface Sci.* **1999,** 81, (3), 167-249.

50. vanZanten, J. H.; Wallace, W. E.; Wu, W. L. *Phys Rev E* **1996,** 53, (3), R2053-R2056.

51. Roth, C. B.; McNerny, K. L.; Jager, W. F.; Torkelson, J. M. *Macromolecules* **2007,** 40, (7), 2568-2574.

52. *Polymer Handbook 4th Ed.* John Wiley & Sons, Inc.: NY, 1999.

53. O'Shaughnessy, B.; Vavylonis, D. *Eur Phys J E* **2003,** 11, (3), 213-230.

54. O'Shaughnessy, B.; Vavylonis, D. *Phys Rev Lett* **2003,** 90, (5), 056103.

55. Seeck, O. H.; Kaendler, I. D.; Tolan, M.; Shin, K.; Rafailovich, M. H.; Sokolov, J.; Kolb, R. *Appl. Phys. Lett.* **2000,** 76, (19), 2713-2715.

56. Koga, T.; Seo, Y. S.; Jerome, J. L.; Ge, S.; Rafailovich, M. H.; Sokolov, J. C.; Chu, B.; Seeck, O. H.; Tolan, M.; Kolb, R. *Appl. Phys. Lett.* **2003,** 83, (21), 4309-4311.

57. Johnson, H. E.; Granick, S. *Macromolecules* **1990,** 23, (13), 3367-3374.

58. Frantz, P.; Granick, S. *Phys Rev Lett* **1991,** 66, (7), 899-902.

59. Frantz, P.; Granick, S. *Macromolecules* **1994,** 27, (9), 2553-2558.

60. Frantz, P.; Granick, S. *Macromolecules* **1995,** 28, (20), 6915-6925.

61. Jack, F. D.; Hildegard, M. S.; Peter, F.; Robert, L.; Steve, G. *Journal of Physics: Condensed Matter* **1997,** 9, (37), 7699.

62. Soga, I.; Granick, S. *Macromolecules* **1998,** 31, (16), 5450-5455.

63. Zhao, J.; Granick, S. *Macromolecules* **2007,** 40, (4), 1243-1247.

64. Zajac, R.; Chakrabarti, A. *Phys Rev E* **1995,** 52, (6), 6536-6549.

65. Buenviaje, C.; Ge, S. R.; Rafailovich, M.; Sokolov, J.; Drake, J. M.; Overney, R. M. *Langmuir* **1999,** 15, (19), 6446-6450.

66. Schneider, H. M.; Granick, S. *Macromolecules* **1992,** 25, (19), 5054-5059.

67. Feder, J.; Giaever, I. *J Colloid Interf Sci* **1980,** 78, (1), 144-154.

68. Onoda, G. Y.; Liniger, E. G. *Phys Rev A* **1986,** 33, (1), 715-716.

69. Adamczyk, Z.; Siwek, B.; Zembala, M. *J Colloid Interf Sci* **1992,** 151, (2), 351-369.

70. Ramsden, J. J. *J Stat Phys* **1993,** 73, (5-6), 853-877.

71. Ramsden, J. J. *Phys Rev Lett* **1993,** 71, (2), 295-298.

72. Adamczyk, Z.; Siwek, B.; Zembala, M.; Belouschek, P. *Adv Colloid Interfac* **1994,** 48, (0), 151-280.

73. Van Tassel, P. R.; Viot, P.; Tarjus, G.; Talbot, J. *The Journal of Chemical Physics* **1994,** 101, (8), 7064-7073.

74. Lai, P. Y.; Binder, K. *The Journal of chemical physics* **1992,** 97, 586.

75. Grest, G. S.; Murat, M. *Macromolecules* **1993,** 26, (12), 3108-3117.

76. O'shea, S.; Welland, M.; Rayment, T. *Langmuir* **1993,** 9, (7), 1826-1835.

77. Yeung, C.; Balazs, A. C.; Jasnow, D. *Macromolecules* **1993,** 26, (8), 1914-1921.

78. Zhao, W.; Krausch, G.; Rafailovich, M.; Sokolov, J. *Macromolecules* **1994,** 27, (11), 2933-2935.

79. Choi, B. C.; Choi, S.; Leckband, D. E. *Langmuir* **2013,** 29, (19), 5841-5850.

80. Ishida, N.; Biggs, S. *Macromolecules* **2010,** 43, (17), 7269-7276.

81. Ishida, N.; Biggs, S. *Langmuir* **2007,** 23, (22), 11083-11088.

82. Carignano, M. A.; Szleifer, I. *The Journal of Chemical Physics* **1994,** 100, (4), 3210-3223.

83. Jones, R. A.; Richards, R. W., *Polymers at Surfaces and Interfaces*. Cambridge University Press: 1999.

84. Aubouy, M.; Fredrickson, G. H.; Pincus, P.; Raphaeel, E. *Macromolecules* **1995,** 28, (8), 2979-2981.

85. Linse, P. *Soft Matter* **2012,** 8, (19), 5140-5150.

86. Källrot, N.; Linse, P. *The Journal of Physical Chemistry B* **2010,** 114, (11), 3741-3753.

87. Källrot, N.; Dahlqvist, M.; Linse, P. *Macromolecules* **2009,** 42, (10), 3641-3649.

88. Källrot, N.; Linse, P. *Macromolecules* **2007,** 40, (13), 4669-4679.

89. Kovacs, A. J. *Adv. Polym. Sci.* **1964,** 3, 394–508.

90. Li, Y.; Ishida, H. *Macromolecules* **2005,** 38, (15), 6513-6519.

Chapter 3

1. Forrest, J. A. *Eur. Phys. J. E* **2002,** 8, 261-266.

2. Ellison, C. J.; Torkelson, J. M. *Nature Mater.* **2003,** 2, 695-700.

3. Ellison, C. J.; Mundra, M. K.; Torkelson, J. M. *Macromolecules* **2005,** 38, 1767-1778.

4. Roth, C. B.; McNerny, K. L.; Jager, W. F.; Torkelson, J. M. *Macromolecules* **2007,** 40, 2568-2574.

5. Napolitano, S.; Pilleri, A.; Rolla, P.; Wubbenhorst, M. *ACS Nano* **2010,** 4, 841-848.

6. Napolitano, S.; Wübbenhorst, M. *Nat. Commun.* **2011,** 2, 1259-1266.

7. Koga, T.; Li, C.; Endoh, M.; Koo, J.; Rafailovich, M. H.; Narayanan, S.; Lee, D. R.; Lurio, L.; Sinha, S. K. *Phys. Rev. Lett.* **2010,** 104, 066101.

8. Rudoy, V. M.; Dement'eva, O. V.; Yaminskii, I. V.; Sukhov, V. M.; Kartseva, M. E.; Ogarev, V. A. *Colloid J.* **2002,** 64, 746-754.

9. Teichroeb, J. H.; Forrest, J., A. *Phys. Rev. Lett.* **2003,** 91, 016104.

10. Gasemjit, P.; Johannsmann, D. *J. Polym. Sci., Polym. Phys.* **2006,** 44, 3031-3036.

11. Papaleo, R. M.; Leal, R.; Carreira, W. H.; Barbosa, L. G.; Bello, I.; Bulla, A. *Phys. Rev. B* **2006,** 74, 094203.

12. Sharp, J. S.; Forrest, J. A.; Fakhraai, Z.; Khomenko, M.; Teichroeb, J. H.; Dalnoki-Veress, K. *Eur. Phys. J. E* **2007,** 22, 287-291.

13. Qi, D.; Fakhraai, Z.; Forrest, J. A. *Phys. Rev. Lett.* **2008,** 101, 096101.

14. Fakhraai, Z.; Forrest, J. A. *Science* **2008,** 319, 600-604.

15. Ilton, M.; Qi, D.; Forrest, J. A. *Macromolecules* **2009,** 42, 6851-6854.

16. Yang, Z.; Fujii, Y.; Lee, F. K.; Lam, C.-H.; Tsui, O. *Science* **2010,** 328, 1676-1679.

17. Napolitano, S.; Wubbenhorst, M. *J. Phys. Chem. B* **2007,** 111, 9197-9199.

18. Napolitano, S.; Prevosto, D.; Lucchesi, M.; Pingue, P.; D'Acunto, M.; Rolla, P. *Langmuir* **2007,** 23, 2103-2109.

19. Napolitano, S.; Lupascu, V.; Wubbenhorst, M. *Macromolecules* **2008,** 41, 1061-1063.

20. Fujii, Y.; Yang, Z.; Leach, J.; Atarashi, H.; Tanaka, K.; Tsui, O. *Macromolecules* **2009,** 42, 7418-7422.

21. Rotella, C.; Napolitano, S.; De Cremer, L.; Koeckelberghs, G.; Wubbenhorst, M. *Macromolecules* **2010,** 43, 8686-8691.

22. Rotella, C.; Wubbenhorst, M.; Napolitano, S. *Soft Matter* **2011,** 7, 5260-5266.

23. Napolitano, S.; Rotella, C.; Wubbenhorst, M. *Macromol. Rapid Commun.* **2011,** 32, 844-848.

24. Yee, C. K.; R., J.; A., U.; H., W.; A., K.; M., R.; J., S. *Langmuir* **1999,** 15, 3486-3491.

25. Koga, T. *See supplementary materials for additional references and the details of the materials, methods, NR results.*

26. Hu, X.; Shin, K.; Rafailovich, M.; Sokolov, J.; Stein, R.; Chan, Y.; Williams, K.; Wu, W.; Kolb, R. *High Perform. Polym.* **2000,** 12, 621-629.

27. Graessley, W. W. *J. Polym. Sci. Part B. Polym. Phys.* **1980,** 18, 27-34.

28. Kim, H.; Ruhm, A.; Lurio, L. B.; Basu, J. K.; Lal, J.; Lumma, D.; Mochrie, S. G. J.; Sinha, S. K. *Phys. Rev. Lett.* **2003,** 90, 068302.

29. Wang, J.; Bedzyk, M.; Caffrey, M. *Science* **1992,** 258, 775-778.

30. Guo, H. Y.; Bourret, G.; Corbierre, M. K.; Rucareanu, S.; Lennox, R. B.; Laaziri, K.; Piche, L.; Sutton, M.; Harden, J. L.; Leheny, R. L. *Phys Rev Lett* **2009,** 102, (7).

31. Narayanan, S.; Lee, D. R.; Hagman, A.; Li, X. F.; Wang, J. *Phys Rev Lett* **2007,** 98, (18).

32. Peter, S.; Meyer, H.; Baschnagel, J.; Seemann, R. *J. Phys. Condens. Matter* **2007,** 19, 205119.

33. Wallace, W. E.; van Zanten, J. H.; Wu, W. L. *Phys. Rev. E* **1995,** 52, R3329-3332.

34. van Zanten, J. H.; Wallace, W. E.; Wu, W. L. *Phys. Rev. E* **1996,** 53, R2053-2056.

35. Bruinsma, R. *Macromolecules* **1990,** 23, 276-280.

36. Zheng, X.; Rafailovich, M. H.; Sokolov, J.; Strzhemechny, Y.; Schwarz, S. A.; Sauer, B., B.; Rubinstein, M. *Phys Rev Lett* **1997,** 79, 241-244.

37. Doi, M.; Edwards, S. F., *The Theory of Polymer Dynamics*. Oxford Science: Oxford, 1986.

38. Green, P. F.; Kramer, E. J. *J. Mater. Res.* **1986,** 1, 202-204.

39. Baljon, A.; Billen, J.; Khare, R. *Phys. Rev. Lett.* **2004,** 93, 255701.

40. Williams, M. L.; Landel, R. F.; Ferry, J. D. *J. Am. Chem. Soc.* **1955,** 77, 3701-3707.

41. Ferry, J. D., *Viscoelastic Properties of Polymers*. 4th ed.; Wiley: New York, 1980.

42. Fakhraai, Z.; Forrest, J. A. *Phys. Rev. Lett.* **2005,** 95, 025701.

Chapter 4

1. Geoghegan, M.; Krausch, G. *Prog. Polym. Sci.* **2003,** 28, (2), 261-302.

2. Reiter, G.; Sharma, A.; Casoli, A.; David, M. O.; Khanna, R.; Auroy, P. *Langmuir* **1999,** 15, (7), 2551-2558.

3. Sharma, A. *Langmuir* **1993,** 9, (3), 861-869.

4. Reiter, G. *Phys Rev Lett* **1992,** 68, (1), 75-78.

5. Reiter, G. *Europhys Lett* **1993,** 23, (8), 579-584.

6. Reiter, G. *Phys Rev Lett* **2001,** 87, (18).

7. Reiter, G. *Langmuir* **1993,** 9, (5), 1344-1351.

8. Zhai, X. W.; Weiss, R. A. *Langmuir* **2008,** 24, (22), 12928-12935.

9. Seemann, R.; Herminghaus, S.; Neto, C.; Schlagowski, S.; Podzimek, D.; Konrad, R.; Mantz, H.; Jacobs, K. *J Phys-Condens Mat* **2005,** 17, (9), S267-S290.

10. Seemann, R.; Herminghaus, S.; Jacobs, K. *Phys Rev Lett* **2001,** 86, (24), 5534-5537.

11. Xie, R.; Karim, A.; Douglas, J. F.; Han, C. C.; Weiss, R. A. *Phys Rev Lett* **1998,** 81, (6), 1251-1254.

12. Seemann, R.; Herminghaus, S.; Jacobs, K. *Journal of Physics: Condensed Matter* **2001,** 13, (21), 4925.

13. Reiter, G.; Hamieh, M.; Damman, P.; Sclavons, S.; Gabriele, S.; Vilmin, T.; Raphael, E. *Nat Mater* **2005,** 4, (10), 754-758.

14. Israelachvili, J. N., *Intermolecular and surface forces*. 3rd ed.; Academic Press: San Diego, USA, 2011.

15. Reiter, G.; Auroy, P.; Auvray, L. *Macromolecules* **1996,** 29, (6), 2150-2157.

16. Reiter, G.; Khanna, R. *Phys Rev Lett* **2000,** 85, (26), 5599-5602.

17. Reiter, G.; Khanna, R. *Phys Rev Lett* **2000,** 85, (13), 2753-2756.

18. Voronov, A.; Shafranska, O. *Langmuir* **2002,** 18, (11), 4471-4477.

19. Matsen, M. W.; Gardiner, J. M. *The Journal of Chemical Physics* **2001,** 115, (6), 2794-2804.

20. Zhang, X.; Lee, F. K.; Tsui, O. K. C. *Macromolecules* **2008,** 41, (21), 8148-8151.

21. Leibler, L.; Ajdari, A.; Mourran, A.; Coulon, G.; Chatenay, D., Wetting of Grafted Polymer Surfaces by Compatible Chains. In *Ordering in Macromolecular Systems*, Teramoto, A.; Kobayashi, M.; Norisuye, T., Eds. Springer Berlin Heidelberg: 1994; pp 301-311.

22. Shull, K. R. *Faraday Discussions* **1994,** 98, 203-217.

23. Durning, C. J.; O'Shaughness, B.; Sawhney, U.; Nguyen, D.; Majewski, J.; Smith, G. S. *Macromolecules* **1999,** 32, (20), 6772-6781.

24. Fujii, Y.; Yang, Z. H.; Leach, J.; Atarashi, H.; Tanaka, K.; Tsui, O. K. C. *Macromolecules* **2009,** 42, (19), 7418-7422.

25. Napolitano, S.; Wubbenhorst, M. *Nat Commun* **2011,** 2.

26. Gin, P.; Jiang, N.; Liang, C.; Taniguchi, T.; Akgun, B.; Satija, S. K.; Endoh, M. K.; Koga, T. *Phys Rev Lett* **2012,** 109, (26), 265501.

27. Jiang, N.; Shang, J.; Di, X.; Endoh, M. K.; Koga, T. *Macromolecules* **2014,** 47, (8), 2682-2689.

28. Housmans, C.; Sferrazza, M.; Napolitano, S. *Macromolecules* **2014,** 47, (10), 3390-3393.

29. Koga, T.; Jiang, N.; Gin, P.; Endoh, M. K.; Narayanan, S.; Lurio, L. B.; Sinha, S. K. *Phys Rev Lett* **2011,** 107, (22).

30. Zheng, X.; Rafailovich, M. H.; Sokolov, J.; Strzhemechny, Y.; Schwarz, S. A.; Sauer, B. B.; Rubinstein, M. *Phys Rev Lett* **1997,** 79, (2), 241-244.

31. Reiter, G.; Schultz, J.; Auroy, P.; Auvray, L. *EPL (Europhysics Letters)* **1996,** 33, (1), 29.

32. Shin, K.; Hu, X.; Zheng, X.; Rafailovich, M. H.; Sokolov, J.; Zaitsev, V.; Schwarz, S. A. *Macromolecules* **2001,** 34, 4993-4998.

33. Muller-Buschbaum, P. *Eur Phys J E* **2003,** 12, (3), 443-448.

34. Jiang, N.; Shang, J.; Di, X.; Endoh, M. K.; Koga, T. *Macromolecules* **2014**, in press.

35. O'Shaughnessy, B.; Vavylonis, D. *Phys. Rev. Lett.* **2003,** 90, (5).

36. Seeck, O. H.; Kaendler, I. D.; Tolan, M.; Shin, K.; Rafailovich, M. H.; Sokolov, J.; Kolb, R. *Appl. Phys. Lett.* **2000,** 76, (19), 2713-2715.

37. Koga, T.; Seo, Y. S.; Jerome, J. L.; Ge, S.; Rafailovich, M. H.; Sokolov, J. C.; Chu, B.; Seeck, O. H.; Tolan, M.; Kolb, R. *Appl. Phys. Lett.* **2003,** 83, (21), 4309-4311.

38. Zhai, X.; Weiss, R. A. *Langmuir* **2008,** 24, (22), 12928-12935.

39. Reiter, G. *Phys Rev Lett* **2001,** 87, (18), 186101.

40. Brochard-Wyart, F.; Debregeas, G.; Fondecave, R.; Martin, P. *Macromolecules* **1997,** 30, (4), 1211-1213.

41. de Gennes, P. G. *C. R. Acad. Sci.* **1979,** 288B, 219-222.

42. Reiter, G.; Khanna, R. *Langmuir* **2000,** 16, (15), 6351-6357.

43. Jacobs, K.; Seemann, R.; Schatz, G.; Herminghaus, S. *Langmuir* **1998,** 14, (18), 4961-4963.

44. Becker, J.; Grun, G.; Seemann, R.; Mantz, H.; Jacobs, K.; Mecke, K. R.; Blossey, R. *Nat Mater* **2003,** 2, (1), 59-63.

45. Reiter, G., Visualizing Properties of Polymers at Interfaces. In *Soft Matter Characterization*, Borsali, R.; Pecora, R., Eds. Springer Netherlands: 2008; pp 1243-1292.

46. Costa, A. C.; Composto, R. J.; Vlcek, P. *Macromolecules* **2003,** 36, (9), 3254-3260.

47. Oslanec, R.; Costa, A. C.; Composto, R. J.; Vlcek, P. *Macromolecules* **2000,** 33, (15), 5505-5512.

48. O'Shaughnessy, B.; Vavylonis, D. *Eur Phys J E* **2003,** 11, (3), 213-230.

49. Huang, Z.; Ji, H.; Mays, J. W.; Dadmun, M. D. *Macromolecules* **2008,** 41, (3), 1009-1018.

50. Patton, D.; Knoll, W.; Advincula, R. C. *Macromol Chem Phys* **2011,** 212, (5), 485-497.

51. Creton, C.; Kramer, E. J.; Hadziioannou, G. *Macromolecules* **1991,** 24, 1846-1853.

52. Park, C.-H.; Kim, J.-H.; Ree, M.; Sohn, B.-H.; Jung, J.-C.; Zin, W.-C. *Polymer* **2004,** 45, 4507-4513.

53. Soles, C. L.; Ding, Y. *Science* **2008,** 322, 689-690.

54. Thomas, K. R.; Chenneviere, A.; Reiter, G.; Steiner, U. *Phys Rev E* **2011,** 83, (2), 021804.

55. De Gennes, P.-G., *Scaling concepts in polymer physics*. Cornell university press: 1979.

56. Daoulas, K. C.; Theodorou, D. N.; Harmandaris, V. A.; Karayiannis, N. C.; Mavrantzas, V. G. *Macromolecules* **2005,** 38, (16), 7134-7149.

57. Dadmun, M. *Macromolecules* **1996,** 29, (11), 3868-3874.

58. Eastwood, E. A.; Dadmun, M. D. *Polymer* **2002,** 43, (25), 6707-6717.

59. Eastwood, E. A.; Dadmun, M. D. *Macromolecules* **2002,** 35, (13), 5069-5077.

Chapter 5

1. Durning, C. J.; O'Shaughness, B.; Sawhney, U.; Nguyen, D.; Majewski, J.; Smith, G. S. *Macromolecules* **1999,** 32, (20), 6772-6781.

2. Napolitano, S.; Wübbenhorst, M. *J. Phys. Chem. B* **2007,** 111, 9197-9199.

3. Napolitano, S.; Prevosto, D.; Lucchesi, M.; Pingue, P.; D'Acunto, M.; Rolla, P. *Langmuir* **2007,** 23, 2103-2109.

4. Napolitano, S.; Lupascu, V.; Wubbenhorst, M. *Macromolecules* **2008,** 41, 1061-1063.

5. Fujii, Y.; Yang, Z. H.; Leach, J.; Atarashi, H.; Tanaka, K.; Tsui, O. K. C. *Macromolecules* **2009,** 42, 7418.

6. Napolitano, S.; Pilleri, A.; Rolla, P.; Wübbenhorst, M. *Acs Nano* **2010,** 4, (2), 841-848.

7. Napolitano, S.; Wübbenhorst, M. *Nat Commun* **2011,** 2, 260.

8. Koga, T.; Jiang, N.; Gin, P.; Endoh, M. K.; Narayanan, S.; Lurio, L. B.; Sinha, S. K. *Phys. Rev. Lett.* **2011,** 107, 225901.

9. Gin, P.; Jiang, N.; Liang, C.; Taniguchi, T.; Akgun, B.; Satija, S. K.; Endoh, M. K.; Koga, T. *Phys. Rev. Lett.* **2012,** 109, 265501.

10. Asada, M.; Jiang, N.; Sendogdular, L.; Gin, P.; Wang, Y.; Endoh, M. K.; Koga, T.; Fukuto, M.; Schultz, D.; Lee, M.; Li, X.; Wang, J.; Kikuchi, M.; Takahara, A. *Macromolecules* **2012,** 45, 7098-7106.

11. Asada, M.; Jiang, N.; Sendogdular, L.; Sokolov, J.; Endoh, M. K.; Koga, T.; Fukuto, M.; Yang, L.; Akgun, B.; Dimitriou, M.; Satija, S. K. *Soft Matter* **2014**.

12. Jiang, N.; Shang, J.; Di, X.; Endoh, M. K.; Koga, T. *Macromolecules* **2014,** 47, 2682-2689.

13. Nelson, J. *Mater. Today* **2011,** 14, 462-470.

14. Klauk, H., *Organic Electronics: Materials, Manufacturing and Applications* Wiley-VCH: 2006.

15. Friend, R. H.; Gymer, R. W.; Holmes, A. B.; Burroughes, J. H.; Marks, R. N.; Taliani, C.; Bradley, D. D. C.; Santos, D. A. D.; Brédas, J. L.; Lögdlund, M.; Salaneck, W. R. *Nature* **1999,** 397, 121-128.

16. Guiselin, O. *Europhys. Lett.* **1992,** 17, (3), 225-230.

17. Huang, Z. Y.; Ji, H. N.; Mays, J. W.; Dadmun, M. D. *Macromolecules* **2008,** 41, (3), 1009-1018.

18. Patton, D.; Knoll, W.; Advincula, R. C. *Macromol. Chem. Phys.* **2011,** 212, (5), 485-497.

19. Shull, K. R. *Faraday Discuss.* **1994,** 98, 203-217.

20. Dadmun, M. *Macromolecules* **1996,** 29, (11), 3868-3874.

21. Eastwood, E. A.; Dadmun, M. D. *Polymer* **2002,** 43, (25), 6707-6717.

22. Eastwood, E. A.; Dadmun, M. D. *Macromolecules* **2002,** 35, (13), 5069-5077.

23. Irvine, D. J.; Mayes, A. M.; GriffithCima, L. *Macromolecules* **1996,** 29, (18), 6037-6043.

24. Inoue, R.; Kawashima, K.; Matsui, K.; Kanaya, T.; Nishida, K.; Matsuba, G.; Hino, M. *Phys Rev E* **2011,** 83, (2), 7.

25. Inoue, R.; Nakamura, M.; Matsui, K.; Kanaya, T.; Nishida, K.; Hino, M. *Physical Review E* **2013,** 88, (3), 6.

26. Zheng, X.; Sauer, B. B.; Vanalsten, J. G.; Schwarz, S. A.; Rafailovich, M. H.; Sokolov, J.; Rubinstein, M. *Phys Rev Lett* **1995,** 74, (3), 407-410.

27. Zheng, X.; Rafailovich, M. H.; Sokolov, J.; Strzhemechny, Y.; Schwarz, S. A.; Sauer, B. B.; Rubinstein, M. *Phys Rev Lett* **1997,** 79, (2), 241-244.

28. Lin, E. K.; Wu, W. I.; Satija, S. K. *Macromolecules* **1997,** 30, (23), 7224-7231.

29. Lin, E. K.; Kolb, R.; Satija, S. K.; Wu, W.-l. *Macromolecules* **1999,** 32, (11), 3753-3757.

30. Fakhraai, Z.; Forrest, J. A. *Science* **2008,** 319, 600.

31. Ilton, M.; Qi, D.; Forrest, J. A. *Macromolecules* **2009,** 42, 6851-6854.

32. Yang, Z.; Fujii, Y.; Lee, F. K.; Lam, C.-H.; Tsui, O. *Science* **2010,** 328, 1676.

33. Koga, T.; Li, C.; Endoh, M. K.; Koo, L.; Rafailovich, M. H.; Narayanan, S.; Lee, D. R.; Lurio, L.; Sinha, S. K. *Phys. Rev. Lett.* **2010,** 104, 066101.

34. Wallace, W. E.; Zanten, J. H. c.; Wu, W. L. *Phys. Rev. E* **1995,** 52, R3329.

35. van Zanten, J. H.; Wallace, W. E.; Wu, W. L. *Phys. Rev. E* **1996,** 53, R2053-2056.

36. Bruinsma, R. *Macromolecules* **1990,** 23, 276-280.

37. Zhang, Y.; Ge, S.; Tang, B.; Koga, T.; Rafailovich, M. H.; Sokolov, J. C.; Peiffer, D. G.; Li, Z.; Dias, A. J.; McElrath, K. O.; Lin, M. Y.; Satija, S. K.; Urquhart, S. G.; Ade, H.; Nguyen, D. *Macromolecules* **2001,** 34, (20), 7056-7065.

38. Koga, T.; Seo, Y. S.; Zhang, Y.; Sin, K.; Kusano, K.; Nishikawa, K.; Rafailovich, M. H.; Sokolov, J. C.; Chu, B.; Peiffer, D.; Occhiogrosso, R.; Satija, S. K. *Phys. Rev. Lett.* **2002,** 89, 125506.

39. Koga, T.; Seo, Y. S.; Hu, X.; Kwanwoo, S.; Zhang, Y.; Rafailovich, M. H.; Sokolov, J. C.; Chu, B.; Satija, S. K. *Europhys. Lett.* **2002,** 60, 559.

40. Koga, T.; Seo, Y. S.; Shin, K.; Zhang, Y.; Rafailovich, M. H.; Sokolov, J. C.; Chu, B.; Peiffeer, D.; Satija, S. K. *Macromolecules* **2003,** 36, 5236.

41. Koga, T.; Ji, Y.; Seo, Y. S.; Rafailovich, M. H.; Sokolov, J. C.; Satija, S. K. *J. Polym. Sci., Part B:Polym. Phys.* **2004,** 42, 3282.

42. Meli, L.; Pham, J. Q.; Johnston, K. P.; Green, P. F. *Phys Rev E* **2004,** 69, (5), 8.

43. Li, Y.; park, E.; Lim, K.; Johnston, K. P.; Green, P. F. *J. Polym. Sci., Part B:Polym. Phys.* **2007,** 45, 1313-1324.

44. Chebil, M. S.; Vignaud, G.; Grohens, Y.; Konovalov, O.; Sanyal, M. K.; Beuvier, T.; Gibaud, A. *Macromolecules* **2012,** 45, (16), 6611-6617.

45. Wissinger, R. G.; Paulaitis, M. E. *J. Poly. Sci. Polym. Phys. Ed.* **1987,** 25, 2497-2510.

46. Goel, S. K.; Beckman, E. J. *Polymer* **1993,** 34, 1410-1417.

47. McHugh, M. A.; Krukonis, V., *Supercritical Fluids Extraction Principles and Practice*. Woburn, MA: 1994.

48. Condo, P. D.; Paul, D. R.; Johnston, K. P. *Macromolecules* **1994,** 27, 365-371.

49. Nishikawa, K.; Tanaka, I.; Amemiya, Y. *J. Phys. Chem.* **1996,** 100, 418-421.

50. Sirard, S. M.; J., Z. K.; Sanchez, L. C.; Green, P. F.; Johnston, K. P. *Macromolecules* **2002,** 35, 1928.

51. Li, X. X.; Vogt, B. D. *Polymer* **2009,** 50, (17), 4182-4188.

52. Koga, T.; Gin, P.; Yamaguchi, H.; Endoh, M.; Sendogdular, L.; Kobayashi, M.; Takahara, A.; Akgun, B.; Satija, S. K.; Sumi, T. *Polymer* **2011,** 52, 4331-4336.

53. Mendoza-Galvan, A.; Trejo-Cruz, C.; Solis-Canto, O.; Luna-Barcenas, G. *J. Supercrit. Fluids* **2012,** 64, 25-31.

54. Shin, K.; Hu, X.; Zheng, X.; Rafailovich, M. H.; Sokolov, J.; Zaitsev, V.; Schwarz, S. A. *Macromolecules* **2001,** 34, 4993-4998.

55. Zajac, R.; Chakrabarti, A. *Physical Review E* **1995,** 52, (6), 6536-6549.

56. Huang, F. H.; Li, M. H.; Lee, L. L.; Starling, K. E.; Chung, F. T. H. *J. Chem. Eng. Jpn.* **1985,** 18, 490-496.

57. Russell, T. P. *Mater. Sci. Rep.* **1990,** 5, (4), 171-271.

58. Fleming, G. K.; Koros, W. J. *Macromolecules* **1986,** 19, 2285-2291.

59. Seeck, O. H.; Kaendler, I. D.; Tolan, M.; Shin, K.; Rafailovich, M. H.; Sokolov, J.; Kolb, R. *Appl Phys Lett* **2000,** 76, (19), 2713-2715.

60. Koga, T.; Seo, Y. S.; Jerome, J.; Ge, S.; Rafailovich, M. H.; Sokolov, J. C.; Chu, B.; Seeck, O. H.; Tolan, M.; Kolb, R. *Appl. Phys. Lett.* **2003,** 83, 4309.

61. Li, X. X.; Vogt, B. D. *Macromolecules* **2008,** 41, (23), 9306-9311.

62. Li, X. X.; Vogt, B. D. *J Supercrit Fluid* **2009,** 51, (2), 256-263.

63. Scheutjens, J. M. H. M.; Fleer, G. J. *The Journal of Physical Chemistry* **1980,** 84, (2), 178-190.

64. Jia, X. Q.; McCarthy, T. J. *Langmuir* **2002,** 18, (3), 683-687.

65. Lan, Q.; Yu, J.; Zhang, J.; He, J. *Macromolecules* **2011,** 44, 5743.

66. Kwok, D. Y.; Neumann, A. W. *Colloids Surfaces A: Physicochem. Eng. Aspects* **1999,** 161, (1), 31-48.

67. Chebil, M. S.; Vignaud, G.; Grohens, Y.; Konovalov, O.; Sanyal, M. K.; Beuvier, T.; Gibaud, A. *Macromolecules* **2012,** 45, 6611-6617.

68. Zhang, Y.; Gangwani, K. K.; Lemert, R. M. *J. Supercrit. Fluids* **1997,** 11, 115-134.

69. Chang, S. H.; Park, S. C.; Shim, J. J. *J. Supercrit. Fluids* **1998,** 13, 113-119.

70. Doi, M.; Edwards, S. F., *The Theory of Polymer Dynamics*. Oxford Science: Oxford, 1986.

71. Gupta, R. R.; Lavery, K. A.; Francis, T. J.; Webster, J. R. P.; Smith, G. S.; Russell, T. P.; Watkins, J. J. *Macromolecules* **2002,** 36, (2), 346-352.

72. O'Shaughnessy, B.; Vavylonis, D. *Phys Rev Lett* **2003,** 90, (5), 056103.

73. Thompson, R. L.; McDonald, M. T.; Lenthall, J. T.; Hutchings, L. R. *Macromolecules* **2005,** 38, (10), 4339-4344.

74. Nemoto, N.; Kishine, M.; Inoue, T.; Osaki, K. *Macromolecules* **1990,** 23, (2), 659-664.

75. Nemoto, N.; Kishine, M.; Inoue, T.; Osaki, K. *Macromolecules* **1991,** 24, (7), 1648-1654.

76. Rouse, P. E. *J. Chem. Phys.* **1953,** 21, 1272.

77. Karim, A.; Mansour, A.; Felcher, G. P.; Russell, T. P. *Phys. Rev. B* **1990,** 42, (10), 6846-6849.

78. Lai, P. Y. *Phys. Rev. E* **1994,** 49, 5420.

79. Milchev, A.; Binder, K. *Macromolecules* **1996,** 29, (1), 343-354.

80. Desai, T. G.; Keblinski, P.; Kumar, S. K.; Granick, S. *Phys. Rev. Lett.* **2007,** 98, 218301.

81. Maier, B.; Radler, J. O. *Phys Rev Lett* **1999,** 82, (9), 1911-1914.

Chapter 6

1. Balazs, A. C.; Emrick, T.; Russell, T. P. *Science* **2006,** 314, 1107-1110.

2. Ebbesen, T. W.; Lezec, H. J.; Hiura, H.; Bennett, J. W.; Ghaemi, H. F.; Thio, T. *Nature* **1996,** 382, (6586), 54-56.

3. Ajayan, P. M.; Schadler, L. S.; Braum, P. V., *Nanocomposite Science and Technology*. Wiley-VCH: Weinheim, Germany, 2003.

4. Oberdisse, J. *Soft Matter* **2006,** 2, (1), 29-36.

5. Villars, D. S. *Journal of Polymer Science* **1956,** 21, 257-271.

6. Medalia, A. I. *J. Colloid Interface Sci.* **1970,** 32, 115.

7. Blow, C. M. *Polymer* **1973,** 14, 309.

8. Dannenberg, E. M. *Rubber Chem. Technol.* **1986,** 59, 512.

9. Kenny, J. C.; McBrietry, V. J.; Rigbi, Z.; Douglass, D. C. *Macromolecules* **1991,** 24, 436.

10. Karasek, L.; Sumita, M. *Journal of Materials Science* **1996,** 31, (2), 281-289.

11. Heinrich, G.; Vilgis, T. A. *Rub. Chem. Technol.* **1995,** 6.

12. Brown, D.; Marcadon, V.; Mele, P.; Alberola, N. D. *Macromolecules* **2008,** 41, (4), 1499-1511.

13. Harton, S. E.; Kumar, S. K.; Yang, H. C.; Koga, T.; Hicks, K.; Lee, E.; Mijovic, J.; Liu, M.; Vallery, R. S.; Gidley, D. W. *Macromolecules* **2010,** 43, (7), 3415-3421.

14. Kim, S. Y.; Schweizer, K. S.; Zukoski, C. F. *Phys. Rev. Lett.* **2011,** 107, (22).

15. Papon, A.; Montes, H.; Hanafi, M.; Lequeux, F. *Phys. Rev. Lett.* **2012,** 108, 065702.

16. Jouault, N.; Moll, J. F.; Meng, D.; Windsor, K.; Ramcharan, S.; Kearney, C.; Kumar, S. K. *ACS Macro Lett.* **2013,** 2, (5), 371-374.

17. Stickney, P. B.; Falb, R. D. *Rubber Chem. Technol.* **1964,** 37, 1299–1340.

18. Blum, F. D.; Xu, G.; Liang, M.; Wade, C. G. *Macromolecules* **1996,** 29, 8740.

19. Lin, W.; Blum, F. D. *Macromolecules* **1997,** 30, 5331-5338.

20. Lin, W. Y.; Blum, F. D. *Macromolecules* **1998,** 31, (13), 4135-4142.

21. Litvinov, V. M.; Steeman, P. A. M. *Macromolecules* **1999,** 32, (25), 8476-8490.

22. Donnet, J. B.; Bansal, R. C.; Wang, M. J., *Carbon Black: Science and Technology*. Marcel Dekker Inc.: New York, Basel, Hong Kong, 1993.

23. Goritz, D.; Raab, H.; Frohlich, J.; Maier, P. G. *Rub. Chem.Technol.* **1999,** 72, 929–945.

24. Koga, T.; Takenaka, M.; Aizawa, K.; Nakamura, M.; Hashimoto, T. *Langmuir* **2005,** 21, (24), 11409-11413.

25. Koga, T.; Hashimoto, T.; Takenaka, M.; Aizawa, K.; Amino, N.; Nakamura, M.; Yamaguchi, D.; Koizumi, S. *Macromolecules* **2008,** 41, (2), 453-464.

26. Baeza, G. P.; Genix, A. C.; Degrandcourt, C.; Petitjean, L.; Gummel, J.; Schweins, R.; Couty, M.; Oberdisse, J. *Macromolecules* **2013,** 46, (16), 6621-6633.

27. Karim, A.; Satija, S. K.; Douglas, J. F.; Ankner, J. F.; Fetters, L. J. *Phy. Rev. Lett.* **1994,** 73, 3407.

28. Richter, D.; Monkenbusch, M.; Arbe, A.; Colmenero, J. *Adv. Polym. Sci.* **2005,** 174, 1-221.

29. de Gennes, P. G. *C. R. Acad. Sci. Paris Ser. II* **1986,** 302, 765.

30. Woodka, A. C.; Butler, P. D.; Porcar, L.; Farago, B.; Nagao, M. *Phys. Rev. Lett.* **2012,** 109, (5), 5.

31. Beaucage, G. *J. Appl. Cryst.* **1995,** 28, 717-728.

32. Takenaka, M.; Nishitsuji, S.; Amino, N.; Ishikawa, Y.; Yamaguchi, D.; Koizumi, S. *Rubber Chem. Technol.* **2012,** 85, 157-164.

33. Milner, S. T.; Witten, T. A.; Cates, M. E. *Macromolecules* **1988,** 21, 2610.

34. Kritikos, G.; Terzis, A. F. *Eur. Polym. J.* **2013,** 49, (3), 613-629.

35. Gin, P.; Jiang, N. S.; Liang, C.; Taniguchi, T.; Akgun, B.; Satija, S. K.; Endoh, M. K.; Koga, T. *Phys. Rev. Lett.* **2012,** 109, (26), 265501.

36. Jiang, N.; Shang, J.; Di, X.; Endoh, M. K.; Koga, T. *Macromolecules* **2014,** 47, 2682-2689.

37. Krutyeva, M.; Wischnewski, A.; Monkenbusch, M.; Willner, L.; Maiz, J.; Mijangos, C.; Arbe, A.; Colmenero, J.; Radulescu, A.; Holderer, O.; Ohl, M.; Richter, D. *Phys Rev Lett* **2013,** 110, (10).

38. Zimm, B. H. *J. Chem. Phys.* **1956,** 24, 269.

39. Rouse, P. E. *J. Chem. Phys.* **1953,** 21, 1272.

40. Farago, B.; Monkenbusch, M.; Richter, D.; Huang, J. S.; Fetters, L. J.; Gast, A. P. *Phys. Rev. Lett.* **1993,** 71, (7), 1015-1018.

41. Fytas, G.; Anastasiadis, S. H.; Seghrouchni, R.; Vlassopoulos, D.; Li, J. B.; Factor, B. J.; Theobald, W.; Toprakcioglu, C. *Science* **1996,** 274, (5295), 2041-2044.

42. Yakubov, G. E.; Loppinet, B.; Zhang, H.; Ruhe, J.; Sigel, R.; Fytas, G. *Phys. Rev. Lett.* **2004,** 92, (11), 4.

43. de Gennes, P. G. *Adv. Colloid Interface Sci.* **1987,** 27, 189.

44. Milner, S. T. *Science* **1991,** 251, 905.

45. information, S.

46. Klushin, L. I.; Skvortsov, A. M. *Macromolecules* **1991,** 24, (7), 1549-1553.

47. Guiselin, O. *Europhys. Lett.* **1992,** 17, (3), 225-230.

48. de Gennes, P.-G., *Scaling Concepts in Polymer Physics*. Cornell University Press: 1979.

49. Daoulas, K. C.; Theodorou, D. N.; Harmandaris, V. A.; Karayiannis, N. C.; Mavrantzas, V. G. *Macromolecules* **2005,** 38, (16), 7134-7149.

50. Patton, D.; Knoll, W.; Advincula, R. C. *Macromol. Chem. Phys.* **2011,** 212, (5), 485-497.

51. de Gennes, P. G., *Scaling Concepts in Polymer Physics* Cornell University Press: Ithaca, 1979.

52. Bouchaud, E.; Auvray, L.; Cotton, J. P.; Daoud, M.; Farnoux, B.; Jannink, G. *Prog. Surf. Sci.* **1988,** 27, 5.